

THE UNIVERSITY OF CALGARY

**Electrochemical Behaviour of Quaternary Pyridinium Compounds
and their Interaction with Electrode Surfaces**

by

Rick P.C. Wong

A THESIS

SUBMITTED TO THE FACULTY OF GRADUATE STUDIES
IN PARTIAL FULFILMENT OF THE REQUIREMENTS FOR THE
DEGREE OF MASTER OF SCIENCE

DEPARTMENT OF CHEMISTRY

CALGARY, ALBERTA

AUGUST, 1998

© Rick P.C. Wong 1998



National Library
of Canada

Acquisitions and
Bibliographic Services

395 Wellington Street
Ottawa ON K1A 0N4
Canada

Bibliothèque nationale
du Canada

Acquisitions et
services bibliographiques

395, rue Wellington
Ottawa ON K1A 0N4
Canada

Your file Votre référence

Our file Notre référence

The author has granted a non-exclusive licence allowing the National Library of Canada to reproduce, loan, distribute or sell copies of this thesis in microform, paper or electronic formats.

The author retains ownership of the copyright in this thesis. Neither the thesis nor substantial extracts from it may be printed or otherwise reproduced without the author's permission.

L'auteur a accordé une licence non exclusive permettant à la Bibliothèque nationale du Canada de reproduire, prêter, distribuer ou vendre des copies de cette thèse sous la forme de microfiche/film, de reproduction sur papier ou sur format électronique.

L'auteur conserve la propriété du droit d'auteur qui protège cette thèse. Ni la thèse ni des extraits substantiels de celle-ci ne doivent être imprimés ou autrement reproduits sans son autorisation.

0-612-35008-8

ABSTRACT

A series of newly synthesized quaternary pyridinium compounds (Quats) were studied electrochemically (pH 1 – 13) at several different electrodes in order to determine their adsorption and redox chemistry, and to predict their efficacy as corrosion inhibitors. Those Quats having a relatively long side chain completely blocked the Pt electrochemical response in neutral and basic solutions. *In situ* mass measurements showed that ca. one monolayer of Quat was sufficient to achieve this, but that additional layers of Quat were deposited with longer exposure times. All Quats undergo a two-electron reduction at ca. -1.1 V vs. SSCE, leading to the deposition of a surface film (up to ca. 25 monolayers), likely the neutral amine and possibly some dimers. Most of this surface product redissolves upon oxidation at ca. -0.2 V, with some residue retained with time. Impedance measurements at carbon steel electrodes showed that these Quats, when mixed with commercially used surfactants, were very effective in inhibiting corrosion in brine solutions.

ACKNOWLEDGEMENTS

I would like to acknowledge the assistance of the following individuals:

Dr. Viola I. Birss, my supervisor, for her endless support and guidance throughout this project. Dr. Birss spent a lot of time clarifying concepts which I did not understand, in correcting written reports, and in discussing alternative research pathways;

Dr. Scott Hinman, Dr. David Cramb and Dr. Bill Shaw, my committee members, for their helpful input to this thesis;

Dr. Neil Warrender (Travis Chemicals Inc), for his planning and input during this project. I thank him also for giving me the opportunity to be part of the IRAP project and working at the Travis Chemicals Inc facility;

Dr. Petr Vanýsek (NIU), for his useful discussions regarding the ac impedance and QCMB techniques, Dr. Jean Lessard (Univ. de Sherbrooke), for his input in terms of organic mechanisms and John Cossar (Travis Chemicals Inc), for his help in clarifying many organic questions/problems;

All of the present and recent past members of Dr. Birss' research group: Christina Bock, Dr. Gregory Borover, Kitty Dang, Huyen Dinh, Mohammed Kashanian, Peyman Khalafpour, Rudolf Potucek, Irina Serebrennikova, Dr. Sharon Thomas, Dr. Shen-Jiang Xia and Rong Yue, for their support in numerous ways;

All of the other participants in this IRAP project: John Lerbscher, Mark Stephenson, Jennifer Wong and Dr. Danya Yang;

All of the technical support staff; special thanks go to Keith Collins, Greta Prihodko, Mike Siewert, Mark Toonen and Kim Wagstaff.

The financial support from an NSERC Industrial Postgraduate Scholarships and funding from Travis Chemicals Inc and from the Department of Chemistry, at the University of Calgary, are also greatly appreciated.

DEDICATION

to

My Parents, Mr. Si Wong and Mrs. Ho Wong

TABLE OF CONTENTS

Approval Page	ii
Abstract	iii
Acknowledgements	iv
Dedication	v
Table of Contents	vi
List of Tables	ix
List of Figures	x
List of Symbols and Abbreviations	xiv
 I. INTRODUCTION	 1
1.1 Project Background	1
1.2 Project Organization	3
1.3 Thesis Organization	5
 II. BACKGROUND AND TECHNIQUES	 7
2.1 General Background to This Research	7
2.1.1 Basic principles of corrosion	7
2.1.2 Corrosion inhibitors	9
2.1.2.1 Inorganic corrosion inhibitors	11
2.1.2.2 Organic corrosion inhibitors	11
2.1.3 Quaternary pyridinium compounds (Quats)	13
2.1.4 Past relevant research	14
2.1.4.1 Studies of corrosion inhibition of steel by organic inhibitors ..	14
2.1.4.2 Adsorption and electrochemical studies of organic molecules on noble metal surfaces	17
2.2 Electrochemical Techniques Relevant to This Research	20
2.2.1 Cyclic Voltammetry (CV) and Linear Polarization (LP)	20
2.2.2 ac Impedance (acZ) Spectroscopy	21
2.2.2.1 Equivalent circuit elements	25
(a) Resistors	25
(b) Capacitors and Constant Phase Elements	26
(c) Inductors	27
2.2.2.2 Fitting data to an equivalent circuit	28
2.2.3 Quartz Crystal Microbalance (QCMB) technique	29
 III. GENERAL EXPERIMENTAL METHODS	 31
3.1 Electrochemical Cells and Electrodes	31
3.1.1 Cyclic Voltammetry (CV) experiments	31
3.1.2 Quartz Crystal Microbalance (QCMB) experiments	33
3.1.3 ac impedance (acZ) experiments	35

3.1.4	Cleaning of cells and electrodes	38
3.2	Solutions and General Experimental Conditions	39
3.2.1	Solutions	39
3.2.2	Structure of the quaternary pyridinium compounds (Quats)	40
3.3	Instrumentation	42
IV.	ADSORPTION STUDIES OF QUATS AT NOBLE METAL ELECTRODES IN VARIOUS SOLUTIONS	44
4.1	Noble Metal Electrodes	44
4.2	Interaction of Quats with Noble Metals in Perchlorate Containing Solutions	47
4.2.1	Quat adsorption at Au in 0.1 M KClO ₄ solution	47
4.2.2	Quat adsorption at Au in 0.1 M HClO ₄ solution	48
4.2.3	Quat adsorption at Pt in 0.1 M HClO ₄ solution	50
4.3	Interaction of Quats with Noble Metals in Neutral Phosphate Buffer Solution	52
4.3.1	CV studies of strongly adsorbing Quats 6 and 7 at Pt in neutral phosphate buffer solution	53
4.3.2	Suppression of hydrogen evolution reaction at Pt by Quat 6 and 7 adsorption	57
4.3.3	QCMB studies of Quat 7 adsorption at Pt in phosphate buffer solution	58
4.4	Possible Surface Structure of Adsorbed Quat 7 on Pt Based on QCMB Analysis	60
4.4.1	Monolayer coverage after exposure to 40 µM Quat 7 for ca. 30 minutes	60
4.4.2	Bilayer coverage after exposure to 40 µM Quat 7 for ca. 3 hours	62
4.5	Interaction of Quats with Noble Metals in Sodium Hydroxide Solution	64
4.5.1	Ranking of Quats based on Pt CV response in 0.1 M NaOH solution	65
4.5.2	QCMB studies of Quat adsorption at Pt in 0.1 M NaOH solution	67
4.6	Summary	69
V.	ELECTROCHEMICAL BEHAVIOUR OF QUATS AT GLASSY CARBON (GC) IN NEUTRAL PHOSPHATE BUFFER SOLUTION	70
5.1	Glassy Carbon Electrodes	70
5.1.1	Activation of GC surfaces	71
5.2	CV studies of Quat 6 at GC Electrode in Neutral Phosphate Buffer Solution	72
5.2.1	Reduction is required prior to oxidation	75

5.2.2	Diffusion controlled cathodic process (C_1)	75
5.2.3	Proposed reductive deposition / oxidative removal mechanism	78
5.3	Quat Multilayer Deposition at GC Electrode	81
5.4	Proposed Redox Mechanism of Quats at GC Electrodes	84
5.4.1	Reduction/oxidation of Quat as a monomer	84
5.4.2	Dimerization mechanism	85
5.4.3	Possible non-electrochemical Quat polymerization	86
5.5	Summary	88
VI.	CV AND acZ STUDIES OF CARBON STEEL IN CO₂ SATURATED NACE BRINE SOLUTION	89
6.1	Corrosion Involving Carbon Dioxide	89
6.1.1	Pitting corrosion in CO ₂ environment	89
6.1.2	General corrosion in CO ₂ environment	90
6.2	Study of Quats at Steel Electrodes in CO ₂ Saturated Brine Solution	91
6.3	CV Studies of Steel Specimen in NACE Brine Solution	92
6.3.1	Correlation of acZ results with CV data	94
6.4	acZ Studies of Steel Specimen in NACE Brine Solution Without Added Corrosion Inhibitor Formulation	95
6.4.1	Irreproducible results	95
6.4.2	Equivalent circuit approach analysis of acZ data	96
6.4.3	Change in impedance and open circuit potential with time	98
6.4.4	Corrosion mechanism of steel in NACE brine solution without added inhibitor formulation	101
6.5	acZ Studies of Steel Specimen in NACE Brine Solution With Added Corrosion Inhibitor Formulation	105
6.5.1	Development of two time constants	105
6.5.2	Change in resistance with time	106
6.5.3	Change in CPEs with time	108
6.5.4	Change of OCP with time	111
6.5.5	Corrosion mechanism of steel in NACE brine solution with added inhibitor formulation	112
6.6	Summary	113
VII.	CONCLUSIONS AND RECOMMENDATIONS FOR FUTURE WORK	115
7.1	Conclusions	115
7.2	Recommendations For Future Work	118
	REFERENCES	120

LIST OF TABLES

Table 3-1.	Chemical composition of 1018 carbon steel	36
Table 3-2.	Chemical composition of synthetic ocean brine solution	40
Table 3-3.	The number, code name, and structure of the organic compounds provided by Travis Chemicals Inc	41

LIST OF FIGURES

Figure 2-1.	The most probable Quat structure in commercial Quat-based inhibitor solutions	13
Figure 2-2.	Impedance as a planar vector in Cartesian coordinates	22
Figure 2-3.	Typical Bode plot used to represent impedance data	23
Figure 2-4.	Typical Nyquist plot used to represent impedance data	24
Figure 2-5.	Schematic of a sputter-coated quartz crystal and its response to a mass change on metal surface	30
Figure 3-1.	Typical electrochemical cell	31
Figure 3-2.	Electrodes and bubbler used in an electrochemical cell	34
Figure 3-3.	WE cell compartment of a QCMB cell	35
Figure 3-4.	Carbon steel WE	37
Figure 3-5.	A Mason jar for study of steel WEs in CO ₂ environment	38
Figure 4-1.	Cyclic Voltammogram and Massogram for Pt electrode in deaerated neutral phosphate buffer solution, $s = 100 \text{ mV/s}$	46
Figure 4-2.	Effect of addition of Quat 1 on Au CV in deaerated 0.1 M KClO ₄ solution, $s = 100 \text{ mV/s}$	48
Figure 4-3.	Comparison of the effect of addition of Quat 2 and 3,5-lutidine on Au CV in deaerated 0.1 M HClO ₄ solution, $s = 100 \text{ mV/s}$	49
Figure 4-4.	Effect of addition of Quat 2 on Pt CV in deaerated 0.1 M HClO ₄ solution, $s = 100 \text{ mV/s}$	51
Figure 4-5.	Suppression of Pt electrochemistry as a function of time of exposure to 40 μM Quat 7 in deaerated neutral phosphate buffer solution, $s = 100 \text{ mV/s}$	54

Figure 4-6.	Suppression of Pt oxide reduction peak current density as a function of the square root of time of exposure to 40 μ M Quat 7 in deaerated neutral phosphate buffer solution, $s = 100$ mV/s	56
Figure 4-7.	Steady-state CVs after the suppression of Pt CV response as a function of Quat 7 concentration in deaerated neutral phosphate buffer solution, $s = 100$ mV/s	56
Figure 4-8.	New redox peaks observed with extended lower potential limit after the suppression of Pt CV response by 300 μ M Quat 7 in deaerated neutral phosphate buffer solution, $s = 100$ mV/s	57
Figure 4-9.	Coverage of Pt, determined from QCMB vs. from CV experiments, after addition of 50 μ M Quat 7 to deaerated neutral phosphate buffer solution, $s = 100$ mV/s, in the first 30 minutes of experimentation	59
Figure 4-10a.	Maximum area occupied by one molecule of Quat 7 in a configuration parallel to the electrode surface (flat orientation)	61
Figure 4-10b.	Minimum area occupied by one molecule of Quat 7 with ring and side chain extended into solution (upright orientation)	62
Figure 4-11.	Possible Quat 7 bilayer on Pt electrode surface	64
Figure 4-12.	Percentage coverage of Pt, as gauged by the Pt oxide CV response, after addition of 70 μ M Quat to deaerated 0.1 M NaOH solution, $s = 100$ mV/s, time of exposure = ca. 30 minutes	66
Figure 4-13.	Coverage of Pt, determined from QCMB vs. from CV experiments, after addition of 50 μ M Quat 7 to deaerated 0.1 M NaOH, $s = 100$ mV/s	68
Figure 5-1.	CV of GC in deaerated neutral phosphate buffer solution, $s = 100$ mV/s curve a. no Quat; curve b. ca. 2 mM Quat 6 ($E_- = -1.0$ V); curve c. ca. 2 mM Quat 6 ($E_- = -1.5$ V).	73
Figure 5-2.	Anodic peak (A_1) current density as a function of Quat 6 concentration in deaerated neutral phosphate buffer solution, $s = 100$ mV/s	76

Figure 5-3.	Dependence of the C_1 peak current density on $s^{1/2}$ with ca. 2 mM Quat 6 in neutral phosphate buffer solution	78
Figure 5-4.	Large A_1 peak seen after Quat oxidation was prohibited, at GC, ca. 2 mM Quat 6 in deaerated neutral phosphate buffer solution, $s = 100$ mV/s curve a. steady-state CV with E_+ at 1.0 V; curve b. 5 th cycle with E_- at -0.2 V; curve c. 1 st cycle with E_+ set back to 1.0V.	80
Figure 5-5.	Charge density of A_1 peak at GC as a function of holding time at -1.5 V vs. SSCE with ca. 4 mM Quat 6 in deaerated neutral buffer solution	81
Figure 5-6.	Anodic vs. cathodic charge density with ca. 4 mM Quat 6 in deaerated neutral phosphate buffer solution at different scan rates	82
Figure 5-7.	Proposed redox mechanism of a typical Quat monomer	84
Figure 5-8a.	Dimerization of two radical intermediate species	86
Figure 5-8b.	Possible re-oxidation of the dimer	86
Figure 5-9.	Possible non-electrochemical polymerization route of a typical Quat	87
Figure 6-1.	Typical CV of steel specimen in CO_2 saturated NACE brine solution, $s = 50$ mV/s	93
Figure 6-2.	Illustration of the inductive behaviour of steel specimen in CO_2 saturated NACE brine solution at low frequencies, $ac V = \pm 10$ mV at +0.05 V vs. OCP	94
Figure 6-3.	Nyquist plots of steel specimen as a function of time in CO_2 saturated NACE brine solution with ammonium bisulfite added as oxygen scavenger, $ac V = \pm 5$ mV vs. OCP	96
Figure 6-4.	Overlay of acZ data of a blank in CO_2 saturated NACE brine solution to the R_s (R_1 CPE) circuit shown, $ac V = \pm 10$ mV vs. OCP	97
Figure 6-5.	Overlay of acZ data of a blank (same data as Figure 6-4) to the R_s (R_1 CPE L) circuit shown. Notice the great improvement of the fit at low frequencies	99

Figure 6-6.	Change in R_1 with electrode immersion time in CO_2 saturated NACE brine solution with no added inhibitor	100
Figure 6-7.	Change in the CPE and the inductance with immersion time in CO_2 saturated NACE brine solution with no added inhibitor	100
Figure 6-8.	Change in the OCP and system resistance of a blank as a function of time	102
Figure 6-9.	An illustration of an Evans diagram for a simple corrosion process	103
Figure 6-10.	An illustration of the changes in an Evans diagram to fit the experimental observations	103
Figure 6-11.	Typical set of impedance spectra observed for steel as a function of time in CO_2 saturated NACE brine solution containing formulated corrosion inhibitors electrode, ac $V = \pm 10$ mV vs. OCP	105
Figure 6-12.	Overlay of acZ data of a steel specimen in CO_2 saturated NACE brine solution containing formulated inhibitor to a modified Randles circuit shown, ac $V = \pm 10$ mV vs. OCP	107
Figure 6-13.	Change in the film and charge transfer resistance of a steel specimen in CO_2 saturated NACE brine solution containing formulated inhibitor as a function of time	108
Figure 6-14.	Change in CPE_{dl} and n value of a steel specimen in CO_2 saturated NACE brine solution containing formulated inhibitor as a function of time	109
Figure 6-15.	Change in CPE_f and its associated n value of a steel specimen in CO_2 saturated NACE brine solution containing formulated inhibitor as a function of time	110
Figure 6-16.	Change in the OCP of a steel specimen in CO_2 saturated NACE brine solution containing formulated inhibitor as a function of time	111

LIST OF SYMBOLS AND ABBREVIATIONS

A_1	anodic peak 1 at ca. -1.15 V vs. SSCE
ac	alternating current
acZ	ac impedance spectroscopy
b_a	Tafel slope of an anodic reaction
b_c	Tafel slope of a cathodic reaction
C	capacitance, $\mu\text{F cm}^{-2}$
C_1	cathodic peak 1 at ca. -0.25 V vs. SSCE
C_{dl}	double layer capacitance, $\mu\text{F cm}^{-2}$
C_f	film capacitance, $\mu\text{F cm}^{-2}$
CE	counter electrode
CPE	constant phase element, $\mu\text{F cm}^{-2}$
CV	cyclic voltammetry technique or cyclic voltammogram
dc	direct current
E	potential, V vs. a reference electrode
E_{-}	upper limit of potential, V vs. a reference electrode
E_{+}	lower limit of potential, V vs. a reference electrode
E_{corr}	corrosion potential; open circuit corrosion potential, V
EC	equivalent circuit
EQUVCRT	equivalent circuit software by Boukamp
f	frequency, Hz
GC	glassy carbon
HER	hydrogen evolution reaction

i	current density, $\mu\text{A}/\text{cm}^2$
I	current, A
j	complex number, $(-1)^{1/2}$
j_{corr}	corrosion current density, mA/cm^2 ; rate of corrosion
L	inductance, $\mu\text{H cm}^2$
LP	linear polarization technique
m	mass, g
n	exponent associated with a CPE
NACE	National Association of Corrosion Engineers
OCP	open circuit potential, V vs. a reference electrode
R	resistance, $\Omega \text{ cm}^2$
R_{ct}	charge transfer resistance, $\Omega \text{ cm}^2$
R_{f}	film resistance, $\Omega \text{ cm}^2$
R_{p}	polarization resistance, $\Omega \text{ cm}^2$
R_{s}	solution resistance, Ω
RE	reference electrode
RHE	reversible hydrogen electrode
QCMB	quartz crystal microbalance technique
Quats	quaternary pyridinium compounds
s	sweep rate or scan rate, mV/s
S.A.	surface area, cm^2
SCE	saturated calomel electrode
SSCE	saturated sodium calomel electrode

SHE	standard hydrogen electrode
SEM	scanning electron microscopy
t	time, s
V	voltage, V; potential vs. a reference electrode
XPS	X-ray photoelectron spectroscopy
WE	working electrode
Z	impedance
Z	modulus of impedance
Z'	real component of impedance
Z''	complex component of impedance
θ	phase angle, radians; phase shift between current and potential
ω	angular frequency, radian s ⁻¹ ; $2\pi f$

I. INTRODUCTION

1.1 Project Background

Carbon steel, which is a common metal used for the construction of pipelines and in down-hole drilling equipment in the oil and gas industry, is susceptible to various kinds of corrosion. In sweet systems (i.e., no H_2S), where high concentrations of CO_2 may be present, carbon steel often undergoes pitting corrosion [1, 2]. On the other hand, general corrosion is almost always associated with carbon steel in sour systems (i.e., H_2S), often resulting in the formation of an iron sulfide film on the surface of the metal [3, 4, 5]. Pitting corrosion is usually more dangerous than general corrosion in the sense that pitting can lead to the breakdown of the metal, and eventually the whole system, by totally damaging one small area of the system. The source of CO_2 can be from mineral dissolution or as a by-product of the petroleum forming process, while the presence of H_2S may be the result of bacterial action at any time in the history of the petroleum deposit [6]. Contact with brine solution (i.e., $NaCl$ solution), containing high concentrations of chloride ion, is another factor which can induce the corrosion of carbon steel. The brine solution is often fed into the system as a flooding agent or it can be a product of the refining process. The “6 o’clock” position inside a pipeline, where brine may accumulate, is often where pitting occurs.

Many different approaches have been taken to combat corrosion in the oil and gas industry. Some of the most practical and widely used methods [7] include the use of corrosion inhibitors [8, 9, 10, 11], plastic and cement liners, external pipe coatings,

cathodic protection, all plastic tubes and tanks, special alloys, special chemical treatments and solids removal, removal of corrosive gases, and reduction in temperature. A corrosion inhibitor, sometimes called the first line of defence against corrosion in the oil and gas industry, is defined by National Association of Corrosion Engineers (NACE) as “a substance which retards corrosion when added to an environment in small concentrations” [12]. Corrosion inhibitors are often by-products of other chemical processes and, therefore, relatively inexpensive for practical applications. Quaternary pyridinium compounds (Quats), one family of corrosion inhibitors, are by-products from the synthesis of nicotinamide adenine dinucleotide (NAD^+). Quats are positively charged and therefore reasonably soluble in aqueous media, and this allows their partitioning into the aqueous phase in the produced fluid.

Corrosion inhibitors can diminish the rate of corrosion in a few different ways [7]. They can increase either the cathodic or anodic polarization (or both) and hence, they may be cathodic or anodic inhibitors, respectively. They can also increase the electrical resistance at the metal-solution interface. Despite the fact that Quats are widely used in industry, little is known as to how they function as corrosion inhibitors. It is not clear if they inhibit corrosion by forming a protective film on a metal surface, thereby directly hindering the rate of metal dissolution, or if their role is more specifically to reduce the rate of the cathodic reaction of the corrosion process. The currently accepted mechanism of corrosion inhibition by Quats involves the co-ordination of the positively charged pyridinium nitrogen to a corroding iron surface [10, 13]. It is believed that this adsorption

process causes a reduction of the rate of the hydrogen evolution reaction (HER) and therefore Quats are labeled as cathodic inhibitors.

The primary research tool used in industry to establish the effectiveness of corrosion inhibitors is the wheel test technique, which is actually a gravimetric experiment. Although this technique can provide a general ranking of the performance of inhibitors, no other information is provided with regards to the behaviour of these inhibitors on the metal surfaces. This technique is also time-consuming and the results obtained from it are often irreproducible and scattered.

One of the main goals of this research has been to establish a quantitative test for the performance of novel corrosion inhibitors (Quats), synthesized by Travis Chemicals Inc (Calgary, Canada), and to identify the molecular properties which result in the best inhibitor adsorption and adhesion properties. It is well known that the degree of corrosion protection of the steel components used in practice, achievable with currently available Quat inhibitors, is strongly dependent on the local conditions. Hence, a better understanding of the factors which affect the corrosion inhibiting properties of these compounds, as well as the ability to predict their surface behaviour, is required.

1.2 Project Organization

This research project originated as a component of a National Research Council (NRC) / Industrial Research Assistance Program (IRAP), in collaboration with a local chemical company, Travis Chemicals Inc.

The team involved in this project consisted of several members. Dr. Neil Warrender, from Travis Chemicals Inc, has served as the overall project director. This project was originated in the hopes of correlating the molecular structure of various Quats with their effectiveness as corrosion inhibitors in order to synthesize and market better performing Quats in the future.

John Cossar at Travis' R&D Laboratory synthesized many different Quats, with systematically altered substituents. Testing of these compounds was carried out mainly by Mark Stephenson (Travis' Corrosion Division) and Jennifer Wong (Co-op student from the University of Calgary) using a gravimetric technique and ac impedance spectroscopy. A National Science and Engineering Research Council (NSERC) Industrial Postdoctoral Fellow, Dr. Danya Yang (now a permanent staff member at Travis Chemicals Inc), attempted to establish the orientation and bonding environment of the Quats at the metal and various oxide, sulfide and carbonate coated steel surfaces using computer modeling methods. Dr. Petr Vanýsek, from the Department of Chemistry at Northern Illinois University, served as an ac impedance advisor during the entire program.

The research at the University of Calgary was funded by a NSERC Industrial Postgraduate scholarship (to Rick Wong), supported by Travis Chemicals Inc. The goals of the work at the U of C were to examine the interaction of these Quats with different substrates using various techniques in order to gain insight into the adsorption and electrochemical behaviour of Quats. It was hoped that a rapid and reliable electrochemical method could be developed to evaluate the effectiveness of these compounds as corrosion

inhibitors. The degree of Quat coverage and adhesion were to be tracked by several different methodologies including cyclic voltammetry (CV), ac impedance (acZ), and the quartz crystal microbalance (QCMB) technique.

Since the use of a steel electrode would result in concurrent dissolution during the experiments, noble metal electrodes were utilized for fundamental studies concerning the interaction of Quats with metal substrates. Noble metal electrodes also have the advantage of easy control of their metallic vs. oxide-coated surface state by controlling the applied potential. This may help to understand if Quats prefer to adsorb on metallic corroding sites or on the surface of corrosion products (e.g., metal oxide or other surface films).

1.3 Thesis Organization

This thesis consists of seven chapters. Chapter one describes the organization of this project and its goals. The background regarding corrosion and the use of inhibitors, as well as details concerning the techniques used in this work, are given in Chapter two. The details of the experimental setup and the instrumentation used are summarized in Chapter three. A large body of the research, including establishing how the Quat inhibitors interact with electrode surfaces and determining the properties of the most strongly adsorbing Quats, was carried out with Pt, Au and glassy carbon (GC) electrodes; this is summarized in Chapters four and five. Chapter four provides the results of the study of Quat adsorption at Pt and Au electrodes using CV and QCMB methods. The

electrochemical behaviour of several of the better performing Quats was then studied in greater detail with the use of GC electrodes, as discussed in Chapter five. The behaviour of the formulated inhibitor mixture at carbon steel electrodes is discussed in Chapter six. This chapter contrasts the results obtained with steel samples with and without the addition of formulated inhibitors to synthetic ocean brine solution, using the ac impedance (acZ) technique. A summary of the results and recommendations for future work are given in Chapter seven.

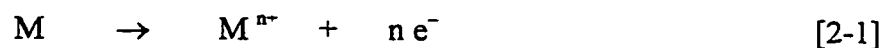
II. BACKGROUND AND TECHNIQUES

2.1 General Background to this Research

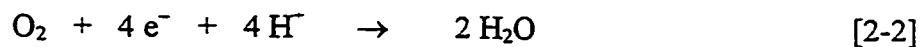
2.1.1 Basic principles of corrosion

Corrosion can be defined as “the deterioration of a material, usually a metal, by reaction with its environment” [7], or as the tendency of metals (usually refined from an ore) to return to their natural state via electrochemical processes.

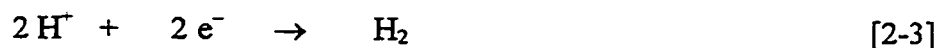
The oxidation of the metal, M, to its ionic form [eq. 2-1] or to a metal oxide, etc., is only one half of the electrochemical reaction in a corrosion process:



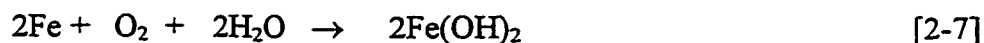
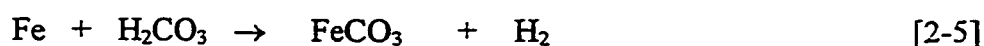
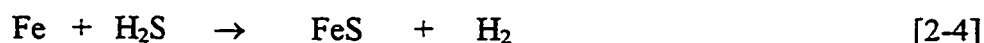
This half reaction is the anodic reaction of the overall corrosion process. The electrons produced in this half reaction must be consumed in order for corrosion to proceed. Therefore, an electron sink such as oxygen is required:



This reduction reaction is termed the cathodic half reaction of the overall corrosion process. When oxygen is not present, the reduction of protons [eq. 2-3] or water to form hydrogen gas can be the dominant cathodic half reaction.



The oxidized metal may also produce insoluble products such as Fe sulfide [eq. 2-4], Fe carbonate [eq. 2-5] or an oxide [eq. 2-6 and 2-7], commonly known as rust [7].



There are many different types of corrosion. Two of the more commonly encountered forms of corrosion in the oil and gas industry are general corrosion and pitting corrosion. General corrosion, also known as uniform attack, usually results in a layer of corrosion product accumulated on the metal surface. Pitting corrosion, also known as non-uniform attack or localized corrosion, results in the deterioration of a small area of the metal surface caused by the differentiation of regions on the metal surface. There are many other types of corrosion [14], including microbiologically induced corrosion (MIC) [15], crevice corrosion, galvanic corrosion, bimetallic corrosion, erosion corrosion, grain boundary corrosion, stress corrosion and hydrogen embrittlement.

One of the fundamental corrosion prevention methods is the use of surface barriers on the metal surfaces. These barriers can be protective coatings (i.e., paint), or adsorbed corrosion inhibitor films. Their presence can reduce the rate of one or both of the

corrosion half reactions. The surface barrier serves to separate the metal from the solution and reduce electrical current that flows through it. Other commonly employed corrosion prevention methods include the use of non-metallic materials, special alloys and cathodic protection [7]. The use of non-metallic materials such as plastics (polyethylene, polyvinyl chloride and acrylonitrile-butadiene-styrene), although they do not corrode like steel, has the problem of deterioration, especially at high temperature. Special alloys, such as those that result from the addition of chromium to steel to make stainless steel, generally do increase the corrosion resistance of the metal. However, these alloys are often quite expensive, and they often cannot be used in systems that have already been constructed. The use of a sacrificial anode, such as Mg or Zn, is one of the more common and efficient corrosion protection methods in use today. However, this method is usually used for external protection only.

2.1.2 Corrosion inhibitors

Corrosion inhibitors have been described as the first line of defense against corrosion in the oil and gas industry. It was estimated that the oil production/drilling/refinery business spent over 400 million dollars on corrosion inhibitors in the U.S. in 1986 [16]. By the year 2000, the market for corrosion inhibitors in the U.S. is expected to increase to 7.1 billion dollars per year [17, 18]. In fact, the cost from corrosion to U.S. industry exceeds 10 billion dollars per year, as in 1990 [19].

Corrosion inhibitors are often defined as “chemical compounds whose presence in small quantities can retard the corrosion of metal in an aggressive environment” [8]. Much research has been devoted to corrosion inhibitors. However, their development is still based primarily on trial and error experiments and there are no rules or theories to completely guide their development or use.

The mode of addition of corrosion inhibitors to an existing system can be characterized as either a continuous or a batch mode. A continuous mode of application occurs when inhibitors are constantly being injected into the produced fluids at levels anywhere between 10 to 10000 ppm, but usually between 50 and 500 ppm. This mode is often used when the film formed by the inhibitors on the metal surface has only a short lifetime once the chemical injection stops (i.e., adsorption relies on finite concentration of inhibitor molecules in the produced fluids). A batch mode of application involves the addition of a high concentration of inhibitor (i.e., 33 to 50%, or even “neat” chemical applied as a “slug”) added to the system periodically [7]. The film formed generally has a relatively long lifetime because the filming chemicals used are essentially insoluble in the produced fluids. In many cases, the batch mode is used to initiate inhibitor film formation, while the continuous mode would then be used to maintain the inhibitor film.

Corrosion inhibitors can be grouped into two main categories, inorganic and organic. The inorganic inhibitors had about a 39 % (311 million dollars) share of the overall corrosion inhibitor market in the US in 1986, while the rest were organic inhibitors (i.e., 61 %, 486 million dollars) [16]. Most inhibitors used for the control of corrosion caused by dissolved oxygen (i.e., rusting) are either inorganic or organic anions [7].

Cationic organic inhibitors are more effective for controlling corrosion caused by hydrogen sulfide or carbon dioxide. Depending on whether the inhibitor's primary function is to increase the anodic or the cathodic polarization, it can be further characterized as an anodic or cathodic inhibitor, respectively.

2.1.2.1 Inorganic corrosion inhibitors

Anions such as chromate, nitrite, molybdate, phosphate and silicate are often used as inorganic inhibitors, in the form of crystalline salts [7]. Salts of these anions can be effective in reducing the corrosion rate of Fe-based boilers and cooling water systems, which are exposed to air and are therefore susceptible to rusting. The exact mechanism of corrosion inhibition by these inorganic materials is not yet understood. Chromates, nitrites, molybdates and phosphates appear to promote the formation of stable iron oxide films on steel surfaces, thus protecting the underlying surface. Silicates do not lead to the formation of protective iron oxide films, but they evidently strengthen them in some way. Much recent research on inorganic corrosion inhibitors has been focused on chromates [20]. Despite the fact that chromates are one of the most effective inorganic corrosion inhibitors, their use has been declining due to government restrictions and pollution control regulations.

2.1.2.2 Organic corrosion inhibitors

Organic inhibitors can generally be divided into two main groups, anionic and cationic. Anionic organic inhibitors such as sulfonates, phosphonates and

mercaptobenzothiazoles (MBT) are used in cooling water and antifreeze solutions [7]. These compounds generally contain a large oily hydrophobic body and an ionic hydrophilic group, which allows their accumulation at oil/water and liquid/solid interfaces, such as at the surface of a metal immersed in water. In many cases, zinc is also used as an adjunctive inhibitor with phosphonates to form a protective inhibitor film [7].

The cationic organic inhibitors are typically oily liquids or wax-like solids. They often contain large hydrocarbon chains or rings with positively charged amine nitrogen groups on one end. The amine structure can be primary, secondary, tertiary, or quaternary. In water or acidic solutions, the primary, secondary, or tertiary amine groups take on an additional proton that gives them a net positive charge [7]. Common cationic organic inhibitors include imidazole and benzotriazole (BTA), which are tertiary amine compounds containing two and three amine groups, respectively. BTA has been the recent focus of research in the area of organic corrosion inhibitors [21] because it is an extremely effective inhibitor against both air and aqueous oxidation of Cu and Cu-containing alloys. The application of BTA as a corrosion inhibitor for Al alloys containing Cu has also gained much attention in the aircraft industry. Quaternary pyridinium compounds (Quats), which are quaternary amines, are also used in systems containing high concentrations of hydrogen sulfide or carbon dioxide. It should be noted that charged amines are often believed to be the active constituent in some of the oil field inhibitor compositions. The term “inhibitor”, in this case, refers to a multi-component mixture containing added surfactants, emulsifiers, filmers, etc.

2.1.3 Quaternary pyridinium compounds (Quats)

Quats are non-volatile water-soluble amines which are believed to be true film formers (by adsorption) [7]. However, due to their water solubility, the film formed by these chemicals usually has a short lifetime. Therefore, the mode of application of Quats is generally continuous, as opposed to imidazoline compounds, which are often added in a batch mode. Even though the exact mechanism of corrosion protection obtained from Quats is not well understood, it has been suggested that the adsorption of Quats reduces the rate of hydrogen formation (i.e., of the HER) and therefore, that they are cathodic inhibitors [22].

Quats used in the formulation of corrosion inhibitors are by-products from the synthesis of nicotinamide adenine dinucleotide (NAD^+). The exact composition of commercial Quats solutions is not known, but it is believed that it consists mainly of structures similar to that of the Quat shown below (Figure 2-1).

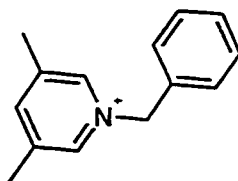
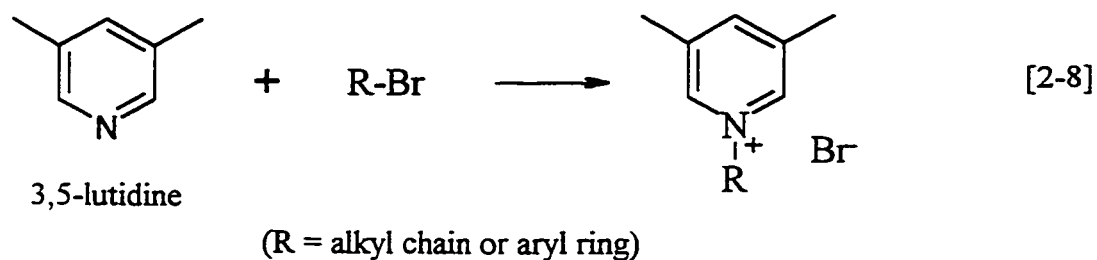


Figure 2-1. Most probable Quat structure in commercial Quat-based inhibitor solutions.

The Quats studied in the present work were synthesized by J. Cossar at Travis Chemicals Inc. They are formed by the alkylation or arylation of 3,5-dimethylpyridine

(3,5-lutidine, Aldrich) with a reagent which is usually in the bromide form [23], as shown in [eq. 2-8]. The reaction is generally carried out in ethyl acetate or dry DMF at room temperature. Crystallization may occur quite rapidly (in a few minutes), but the reaction is allowed to reach completion for longer than one week at 20 °C. The crystals are then vacuum filtered and rinsed with small portions of the organic solvent. The products are usually > 99 % pure, based on the assays using the HPLC technique.



2.1.4 Past relevant research

2.1.4.1 Studies of corrosion inhibition of steel by organic inhibitors

Elachouri et al [24] used linear polarization (LP) and gravimetric methods to study long chain alkanol bromides as inhibitors of iron corrosion in 1 M HCl solution. It should be noted that these are long chain quaternary ammonium bromide compounds. They showed that the addition of the alkanol bromides decreased the currents in the cathodic polarization curves, while the anodic polarization curves were not affected by their presence at potentials positive of -0.15 V vs. SCE. They concluded that these compounds were cathodic inhibitors, adsorbing on the iron surface. At more positive potentials, metal

dissolution destabilized the adsorbed inhibitor layer and therefore no suppression of oxidation currents was seen [25].

Malik [26] studied the influence of cetyltrimethyl ammonium bromide on iron carbonate surface films, using scanning electron microscopy (SEM) and LP techniques, on mild steel in CO₂ saturated 5 % NaCl solution (pH 6.5). He concluded that voids and grain boundaries were formed in the FeCO₃ structure in blank solutions, but that these defects were removed in the presence of the inhibitor in solution. He also found that the optimum concentration of the inhibitor depended on if the steel samples had been precorroded or not.

Li et al [10] investigated the inhibition of mild steel corrosion in 0.5 M H₂SO₄ by simple amines (including pyridine) using LP, ac impedance spectroscopy (acZ) and X-ray photoelectron spectroscopy (XPS) methods. They concluded that amine adsorption in the active region of mild steel corrosion occurred by the chemisorption of the amine on the exposed metal atoms. Therefore, amines with a high electron density at the N sites or π electron delocalization are better inhibitors. When the metal was extensively oxidized in the passive region, amines with a higher number of NH linkages, which can form hydrogen bonds through coordination with the oxidized surface, appeared to be the better inhibitors.

The influence of alkyimidazoles on the electrochemical behaviour of carbon steel in 3 % NaCl was studied by Srhiri et al [9] using the LP and acZ techniques. They noticed that the inhibition effect increased, not only with concentration of the inhibitor, but also with the number of carbon atoms in the hydrophobic chain. They hypothesized the formation of hemi-micelles (perpendicular adsorption) and a molecular bilayer of the

inhibitor on the electrode surface. They also observed an inductive loop at low frequencies when acZ was performed in solutions containing 10 mM n-alkylimidazoles at different anodic potentials.

Mild steel corrosion in 1 M HCl in the presence of benzimidazole derivatives was studied by Popova et al [27] using acZ spectroscopy. The equivalent circuit approach was used to analyze the impedance data and two time constants (i.e., reflecting the charge transfer reaction and the adsorption of the inhibitor) were often seen with inhibited samples. They also found that the double-layer capacity as well as the adsorption capacity had to be represented by a constant phase element, because the experimental data revealed frequency dispersion behaviour.

The adsorption kinetics of the adsorption of acetylenic alcohols (a type of organic corrosion inhibitor) on iron was investigated by Yang et al [28] in H₂SO₄ solutions using ellipsometry. With a few assumptions, they concluded that the changes in the ellipsometric parameters at low concentrations and/or at early times were caused by the reorientation of the adsorbed molecules from a flat to upright position. The growth of a multilayer film was then proposed to account for the further changes in the ellipsometric parameters. They found that long saturated hydrocarbon chains promoted the growth of the films. The same group also examined the competitive adsorption of chloride ion with 1-octyn-3-ol on Fe in HCl solution using XPS and ³⁶Cl-radiotracer measurements [29].

Altoé et al [2] evaluated commercial film-forming oilfield corrosion inhibitors (i.e., polyamines) in CO₂ saturated, 1 % NaCl solution (pH 3.9) with the aid of LP and

acZ techniques, on carbon steel rotating disc and cylinder electrodes. They found that the efficiency of the inhibitors depended upon their residual concentration and on the hydrodynamic flow conditions. They claimed that the LP technique provided some information about the degree of stability and deterioration of the inhibitor film. The acZ technique provided information about the corrosion mechanism and the effect of the type of solution flow, whether laminar or turbulent, on the growth of the inhibitor film. It should be noted that they also observed an inductive loop at low frequencies in their acZ data and a black film on the electrode surface when no inhibitor was added. Both the inductive loop and the black film disappeared when the inhibitor was added.

2.1.4.2 Adsorption and electrochemical studies of organic molecules on noble metal surfaces

Zilberman et al [30] conducted a study of the adsorption of pyridine and benzene on Au in LiClO_4 solution using the QCM technique. The important result observed was that the mass decreased when the organic molecule was adsorbed. They deduced that a mass decrease was possible if more than 4.4 water molecules desorbed due to the adsorption of one molecule of pyridine. In this work [30], they provided reasonable evidence to support the concept that electrosorption is a replacement reaction.

Czerwiński et al [31] studied the adsorption of 4,4'-bipyridyl (Bpy) at a gold electrode in 1 M HClO_4 solution and in 0.1 M NaClO_4 + 0.02 M phosphate buffer solution using the CV technique. Their results indicated that adsorbed Bpy molecules are perpendicularly oriented on the electrode surface. A few years later, Wilde et al [32]

utilized the QCMB technique to study the adsorption of Bpy at Au electrodes in 0.1 M KClO_4 + 0.02 M phosphate buffer solution (pH 7). They found that adsorption of Bpy at Au yielded a constant mass response over a 1.2 V potential range, even though the changes in the CV response were very minor. Also, the QCMB data showed clearly that the adsorbed Bpy was easily removed from the electrode by rinsing with fresh buffer solution. The same group also investigated the corrosion and complexation of Ag in the presence of Bpy in 0.1 M Na_2SO_4 solution [33]. They found that, without Bpy, the oxidation of Ag lead to a significant mass loss due to the formation of Ag^+ ions. In the presence of Bpy, the oxidation of Ag was associated with a significant mass gain because of the complexation reaction between Ag^+ and Bpy, leading to the deposition of AgBpy on the electrode surface. They concluded that the balance between these two processes (i.e., dissolution and complexation) depended on the scan rate, upper potential limit and the Bpy concentration.

The electrosorption of benzyldimethyldodecylammonium bromide (BDDB) on Au in 0.1 M Na_2SO_4 solution was investigated by Kouznetsov et al [34] using the QCMB technique. They deduced that the electrosorption of BDDB on Au at anodic potentials proceeded through the interaction of the amine with oxygen radicals (bromide ions were co-adsorbed). The overall process involved one electron per one adsorbed molecule and the reduction of Au oxide caused most of the adsorbed BDDB to desorb.

Wang et al [35] investigated the formation of inhibitory polyphenol layers on the surface of Au electrodes in pH 7.4 phosphate buffer solution using the QCMB method. They showed that the oxidation of phenol resulted in the loss of electrode activity

(i.e., the disappearance of the oxidation peak) in the following cycle. The corresponding QCMB profiles displayed only a single increase in mass (during the first cycle). Using Faraday's law, they calculated the coulometric inefficiency based on the charge passed in the anodic peak and the mass gain during the cycle of potential. They found a high coulometric inefficiency with a low concentration of phenol in solution, suggesting that this may be caused by the electrogeneration of dimers and oligomers, which then diffused away from the electrode surface.

In order to optimize the use of glassy carbon (GC) as the electrode for electrochemical detection in HPLC, Kusu et al [36] studied the adsorption of quaternary ammonium ions on the surface of a GC electrode in 0.1 M NaClO₄ solution using the specular reflection method. The decrease of reflectivity was used as an indication of adsorption because the quaternary ammonium ions have a higher refractive index than that of the bulk electrolyte solution. They found that, as hydrocarbon chains of quaternary ammonium ions become longer, the adsorptivity became stronger, especially at negative potentials.

The electrochemical reduction of 1,2,4,6-substituted pyridinium cations at Hg, Pt and GC electrodes in aprotic solvents such as dimethylformamide (DMF), acetonitrile and dimethylsulfoxide was studied by Volke et al [37] using dc polarography and CV. They found that substituting phenyl groups at the ring positions 2, 4 and 6 could increase the stability of the intermediate neutral radical species, produced during the reduction. They believed that dimers could not be formed in this case from the reaction of two radical species, due to the steric hindrance of the ring structures.

2.2 Electrochemical Techniques Relevant to This Research

2.2.1 Cyclic Voltammetry (CV) and Linear Polarization (LP)

The use of CV is not very common in corrosion studies with reactive metals such as Fe or Al because of the significant perturbation caused by this technique. Nevertheless, meaningful results can be obtained if a small potential window is utilized in each cycle. CV is a much more useful method when studying noble metal electrodes. LP is a more widely employed electrochemical technique for corrosion studies in the oil and gas industry. This technique is based on the theory of Stern and Geary [38, 39], showing that current is directly proportional to the applied potential at potentials near the OCP (E_{corr}). The polarization resistance (R_p) can be determined using Ohm's law, as follows:

$$R_p = \Delta V / \Delta I \quad [2-9]$$

where ΔV denotes a small applied potential and ΔI denotes the current which flows in response to the applied potential.

R_p is inversely proportional to the rate of corrosion, j_{corr} , as shown by the following expression [27]:

$$j_{\text{corr}} = b_a b_c [2.303 (b_a + b_c) R_p]^{-1} \quad [2-10]$$

where b_a and b_c represent the anodic and cathodic Tafel slopes of the two half reactions participating in the corrosion process, respectively. From [eq. 2-10], it can be seen that the magnitude of R_p is an indication of the rate of corrosion, with a lower R_p representing a more corrosive system.

2.2.2 ac Impedance (acZ) Spectroscopy

The use of acZ spectroscopy for corrosion studies of Al- and Fe- based materials, in particular, has gained much popularity over the last decades [40]. This electrochemical technique is relatively non-destructive (small ac voltage is applied) and can be used to study a wide variety of surfaces *in situ*.

There are many different ways to present impedance data. A Nyquist plot illustrates impedance results in Cartesian coordinates (Figure 2-2), where $|Z|$ is defined as $[(Z')^2 + (Z'')^2]^{1/2}$. Z' is the “real” component, while Z'' is the “imaginary” component of the “complex” impedance of the system. The term “imaginary” is somewhat misleading, as it merely represents the part of the total impedance for which current and potential are out-of-phase. Another common representation of impedance results is a Bode plot, in which the values of $|Z|$ (modulus of impedance) or θ (phase angle) are plotted as a function of the frequency of the applied ac perturbation (Figure 2-3). Note that the Bode plot of Figure 2-3 was simulated using seed values of a 100 Ω resistor (R_1) in series with a 1000 Ω resistor (R_2), which is in parallel to a 1 μF capacitor (C_1), commonly known as the $R_1(R_2C_1)$ circuit.

There are several approaches used to extract information from acZ data. First, it is possible to establish the values of the resistance and the capacitance directly from raw impedance data. R_1 and R_2 can be deduced from the modulus of the impedance in Figure 2-3 at low and high frequencies, respectively. The Nyquist plot in Figure 2-4 illustrates another representation of the same set of data.

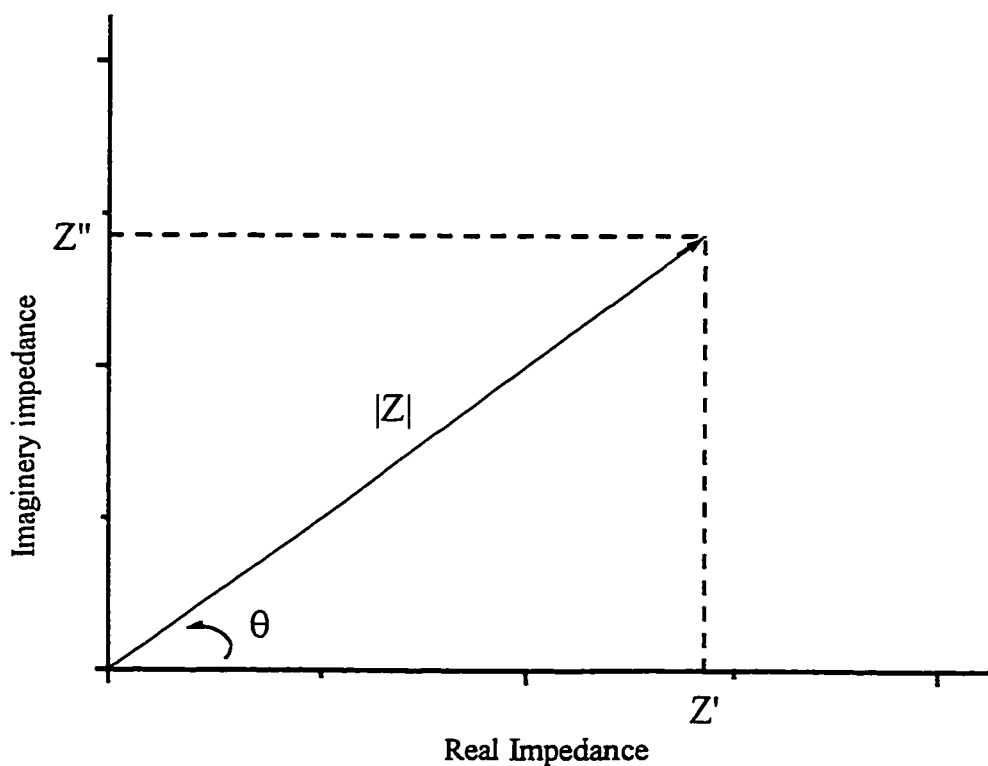


Figure 2-2. Impedance as a planar vector in Cartesian coordinates.

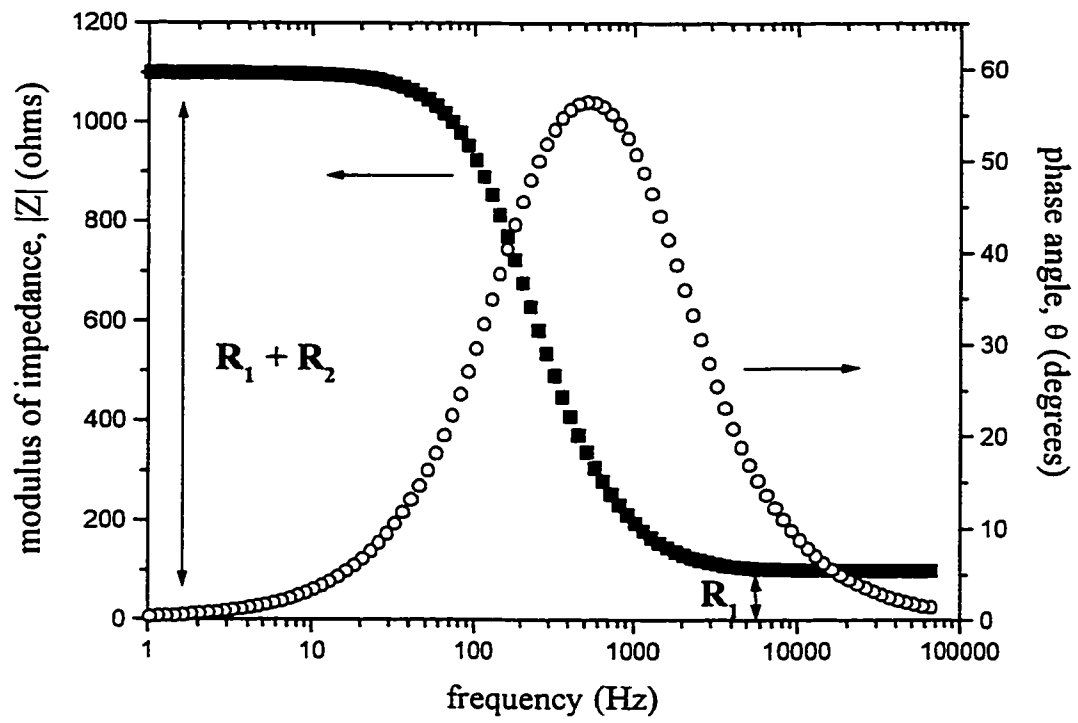


Figure 2-3. Typical Bode plot used to represent impedance data.

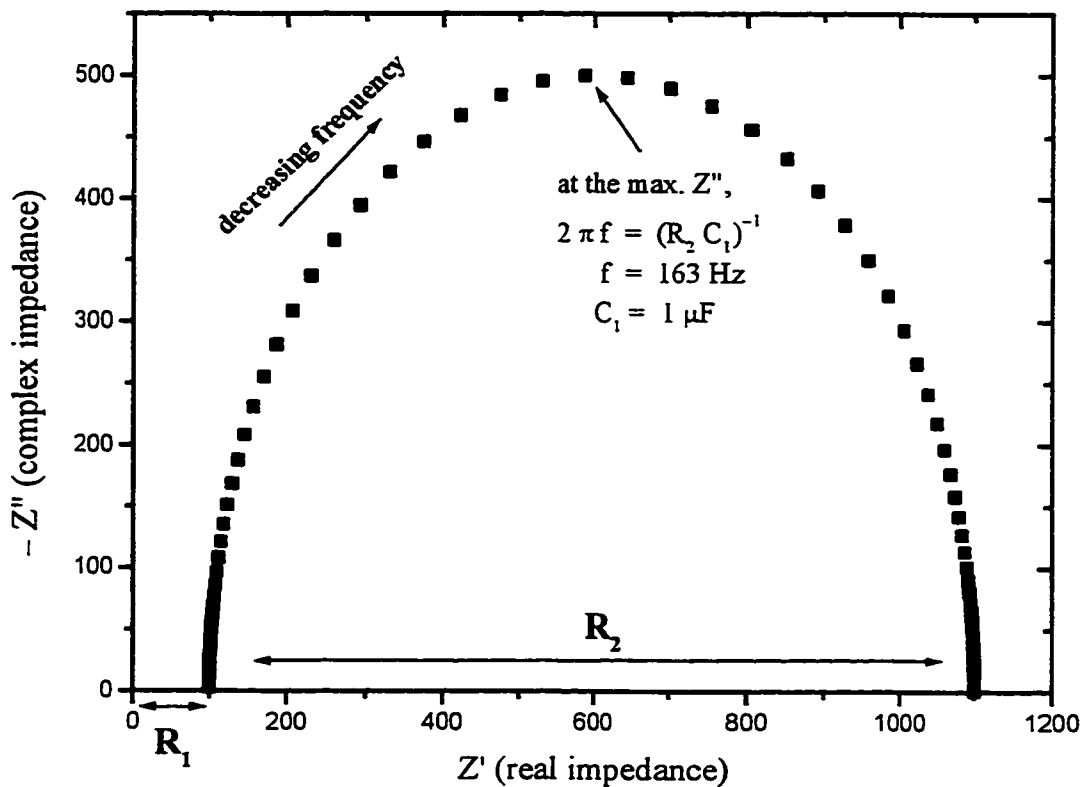


Figure 2-4. Typical Nyquist plot used to represent impedance data.

In Figure 2-4, the diameter of the semi-circle would be R_2 , while R_1 is equivalent to the x-axis intercept at high frequencies. The value of C_1 may be deduced from the frequency at the maximum of the complex impedance in this plot. In the present case, the frequency is 163 Hz at the maximum complex impedance, yielding a ca. 1 μF capacitor. Note that this method of determination of resistance and capacitance values from the raw impedance data may seem straightforward, but it gets more difficult when the set of impedance data is more complicated.

Fitting an experimentally obtained impedance data set to the response predicted by a proposed electrical circuit is another commonly used data analysis method. This method can reveal valuable information about the physical properties of the system under study. The software program used for this purpose in this thesis is ZView Equivalent Circuits, based on the LEVM 6.0 program written by Dr. J. Ross Macdonald [41]. A proposed electrical circuit can contain numerous elements (Section 2.2.2.1), and the complexity of the circuit depends on the system under study.

2.2.2.1 Equivalent circuit elements

(a) *Resistors*

A resistor is a device which can restrict the flow of current in a system. Its resistance (R) can be determined using either dc or ac current because the potential and the current flow are in-phase (i.e., the phase angle, θ , between the current and potential is zero) [42]. Because of this unique property, its resistance is the same as the modulus of impedance, $|Z|$, and its value is independent of frequency:

$$|Z|_R = R \quad [2-11]$$

Because $\theta = 0$ and the impedance of a resistor is independent of frequency, the Nyquist plot of an ideal resistor would be a single point on the Z' axis.

Resistors are found in all electrochemical systems. The solution resistance, R_s , reflects the resistance of current flow through the solution between the WE and the RE. The higher the concentration of the electrolyte solution and the larger the surface area of the WE, the lower R_s is. The inverse of the rate of reaction at the electrode/solution interface is termed the charge transfer resistance, R_{ct} . Also, most surface films provide some resistance to current flow in the system, R_f .

(b) *Capacitors and Constant Phase Elements*

A capacitor is a device which can store charge. It allows ac current to flow by becoming charged and discharged, and behaves such that current flow precedes the potential, so that its θ is exactly -90° . The impedance of a capacitor is expressed as follows:

$$|Z|_C = (j\omega C)^{-1} \quad [2-12]$$

where $\omega = 2\pi f$, $j = (-1)^{1/2}$, and C is the capacitance (in Farads). It should be noted that the impedance of a capacitor is inversely proportional to frequency (f), and hence its value is infinitely large when the frequency approaches zero, as in the case of a dc perturbation.

The most common capacitor encountered in electrochemical systems is at the electrode/solution interface, termed the double layer capacitance, C_{dl} . Often, films formed on the electrode surface also have capacitive behaviour. The capacitance of a dielectric

film material, C_f , decreases with increasing film thickness. On the other hand, films such as polyaniline [43] and Ir oxide [44], which yield an increasing capacitance with increasing film thickness, are called pseudocapacitors.

In reality, heterogeneities and nonuniformities resulting from surface roughness, impurities, dislocations, grain boundaries, fractality, distribution of the active centers, inhibitor adsorption and the formation of porous layers often cause capacitors to behave non-ideally [27]. The constant phase element (CPE) is therefore introduced in electrochemical systems to account for this frequency dispersion behaviour. The impedance of a CPE is described by the following expression:

$$|Z|_{\text{CPE}} = (j\omega)^{-n} \text{CPE}^{-1} \quad [2-13]$$

Note that when $n = 1$, CPE is equal to C and it will behave like an ideal capacitor. In many cases, the value of n can be used as an indication of how homogeneous the electrode surface is. An n value of less than ca. 0.95 indicates the presence of a non-ideal capacitor in the electrochemical system. When $n = 0.5$, the CPE denotes the special situation of a process governed by a diffusion controlled reaction. The impedance of this element is called the Warburg impedance, which is often found in the Randles circuit [45].

(c) *Inductors*

An inductor has the property that the current lags the potential, and the phase shift is exactly $+90^\circ$. The impedance of an inductor can be calculated as follows:

$$|Z|_L = j\omega L \quad [2-14]$$

where L is equal to the inductance. It should be noted that the impedance of an inductor decreases as the frequency decreases, which is opposite to the case of a capacitor.

Inductors are seldom found in electrochemical systems. The two most common electrochemical processes that may cause the system to behave like an inductor are nucleation phenomena and pitting [46].

2.2.2.2 Fitting data to an equivalent circuit

When a set of impedance measurements is obtained, the data can be fitted to the simulated results from a proposed equivalent circuit (EC) using the Zview for Windows software. Predicted seed values for each of the circuit elements in the EC are initially used. A good rule of thumb is to use $1000 \, \Omega$ for a resistor and $1 \, \mu\text{F}$ for a capacitor to initiate the best fit calculation. If the seed values are too far off from the best fit values, the program will provide a new set of seed values and another fitting is performed using these values. The fitting of the data is complete when the seed and displayed values are the same, the simulated results overlay well with the experimental data in the Bode or Nyquist depiction, and the chi-squared error value of the fit is less than 1×10^{-4} .

When the data weighting factor of the program is set to Data-Modulus, the chi-squared values for the fitting of the results are comparable to the chi-squared values obtained from the Boukamp EQUIVCRT software, which is a more commonly used

fitting program. It should be noted that the square root of the chi-squared value is equivalent to the average standard deviation of the fit to the original set of experimental data [47]. For example, if a chi-squared value of 1×10^{-4} is obtained for the fit, the standard deviation of the fit from the actual experimental data would be about 1 %.

The same set of impedance data often can be fitted to more than one proposed EC. Some of the values for the circuit elements, or the EC itself, may not be physically reasonable and therefore the results cannot always be interpreted. A trial and error approach is required for the fitting of impedance data of a new system to an EC. In general, a simple EC is preferred over a more complicated one if they both result in similar quality of fits.

2.2.3 Quartz Crystal Microbalance (QCMB) technique

The Quartz Crystal Microbalance (QCMB) method employs a piezoelectric quartz crystal, which oscillates in a shear mode at a particular resonant frequency when an ac field is applied across the crystal. A change in this frequency can be related to the mass change on the crystal surface using the simplified Sauerbrey equation [48, 49]:

$$\Delta f = -56.6 \text{ Hz cm}^2 \mu\text{g}^{-1} \Delta m \quad [2-15]$$

The crystal constant (56.6 in this case) depends on the type of crystal used and is often termed the crystal sensitivity factor.

The crystal is sputter-coated on both sides with the metal of interest, in a typical keyhole shape, for electrochemical studies (Figure 2-5). If a mass increase occurs on either side of the overlapping part of the keyhole-shaped metallic coatings, either from film formation or organic adsorption, the frequency of oscillation will decrease (and vice versa for mass loss). Therefore, tracking the change of the frequency of the crystal can reveal valuable information about film formation or adsorption processes. In electrochemical studies, only one side of the crystal, which serves as the WE, is immersed in solution, and the measured mass changes can be correlated with the current and charge passed.

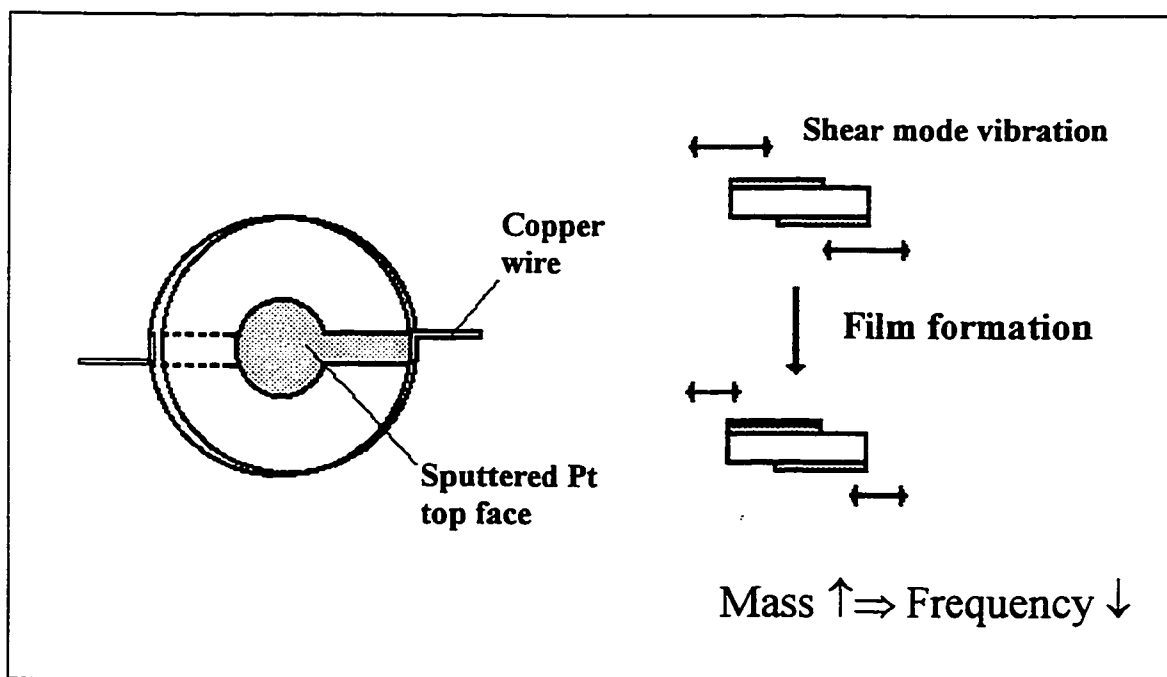


Figure 2-5. Schematic of a sputter-coated quartz crystal and its response to a mass change on metal surface.

III. GENERAL EXPERIMENTAL METHODS

3.1 Electrochemical Cells and Electrodes

3.1.1 Cyclic voltammetry (CV) experiments

The typical electrochemical cell used in the present work contained two compartments, joined by a Luggin capillary (Figure 3-1). A wet, closed stop-cock between the two compartments minimized solution mixing and, at the same time, allowed current flow. The volume of the WE cell compartment was 20 to 30 mL.

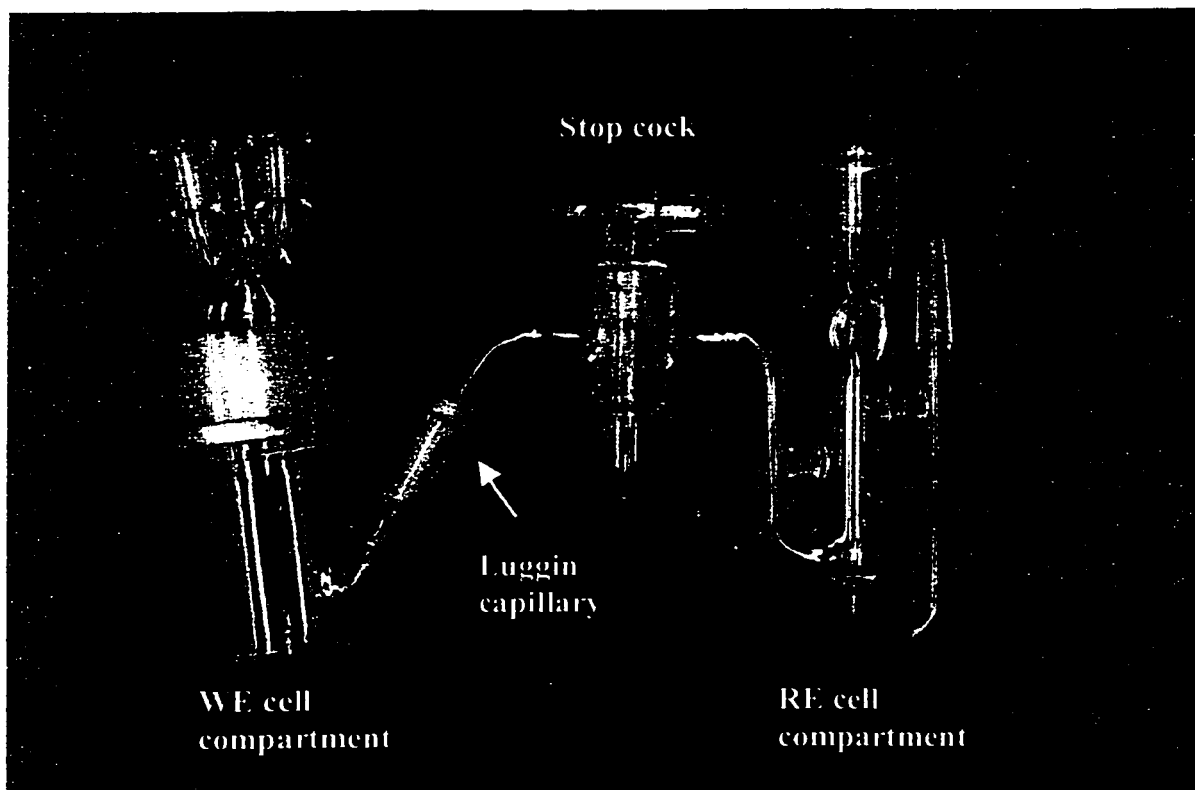


Figure 3-1. Typical electrochemical cell.

A gas bubbler (Legend 1, Figure 3-2) was placed in the WE cell compartment, allowing controlled passage of nitrogen gas through or above the electrolyte solution. The noble metal working electrodes (WEs) were polycrystalline gold or platinum wires, ca. 1.5 cm in length and 0.05 cm in diameter. The apparent surface area (S.A.) of this type of WE was ca. 0.25 cm². The wires were embedded in soft glass tubing and were electrically connected to a nickel wire; only the noble metal was exposed to solution (Legend 2, Figure 3-2).

Two GC electrodes were employed in this study. The first (BioAnalytical Systems) was a small carbon rod with an apparent exposed cross-sectional S.A. of ca. 0.08 cm², embedded in solvent resistant Kel-F plastic tubing. Electrical contact was made via a brass pin permanently mounted in the electrode. The electrode diameter was increased by embedding the plastic tubing in soft glass tubing in order to match the size of the cell top inlet, and the brass pin was electrically connected to a nickel wire.

The second GC working electrode was a rod which was electrically connected to a copper wire using 2400 Circuit Works Conductive Silver Epoxy (Allied Electronics). In order to ensure good connection and adhesion, normal epoxy was used on top of the silver epoxy. The electrode was then embedded in an inert resin supplied by Scandia (58 Hagen, Germany), exposing only the cross-sectional end (ca. 0.95 cm²) of the GC rod. The preparation of the resin involved the addition of 1 drop of 9102 hardener to 1 mL of Scandiplast 9101 resin.

Prior to use, the GC electrodes were hand-polished on a flat surface using 600 grit silicon carbide emery paper. This step should be kept to a minimum as this process can

readily damage the GC surface. The GC was then polished using a coarse suspension of alumina from Metaserv (7.0 micron) on a Rayfinal polishing cloth from Micro Metallurgical Ltd. Progressively finer alumina powder (1.0, 0.3 and 0.05 micron) from E.T. Enterprises was then used until a mirror-like surface was obtained [50, 51].

The polished electrode was then cleaned with triply distilled water in a FS3 Fisher Scientific ultrasonic bath for at least 10 minutes prior to its exposure to the electrolyte solution. The purpose of this ultrasonic procedure was to remove any alumina powder left on the GC surface from the polishing step.

The counter electrode (CE) was always a large surface area Pt gauze electrode (Legend 3, Figure 3-2). The Saturated Sodium Calomel Electrode (SSCE) was used as the reference electrode (RE) in all experiments (Legend 4, Figure 3-2). Its potential was ca. 0.235 V vs. SHE and was checked periodically vs. a large scale standard SCE. The SSCE was located in a separate compartment (see Figure 3-1) and connected to the WE cell compartment via the Luggin capillary.

3.1.2 Quartz Crystal Microbalance (QCMB) experiments

The AT - cut, 5 MHz crystals used in this work were sputter-coated in a low pressure Ar environment (high vacuum conditions) with Ti at 250 mA for 30 seconds (ca. 10 nm), followed by Pt or Au at the same current for 3 minutes (ca. 150 nm). The apparent S.A. of the metal, deposited in the keyhole shape (shown in Figure 2-5), was ca. 0.5 cm². Copper wires were used for electrical connection to the sputtered metal, and were attached to each side of the crystal with conducting silver epoxy. During the

electrochemical experiments, the crystal was sandwiched between two O-rings, with one side exposed to the electrolyte solution, serving as the WE (Figure 3-3). The CE and RE were the same as those described in Section 3.1.1. The volume of the solution in this WE cell compartment was 40 to 50 mL.

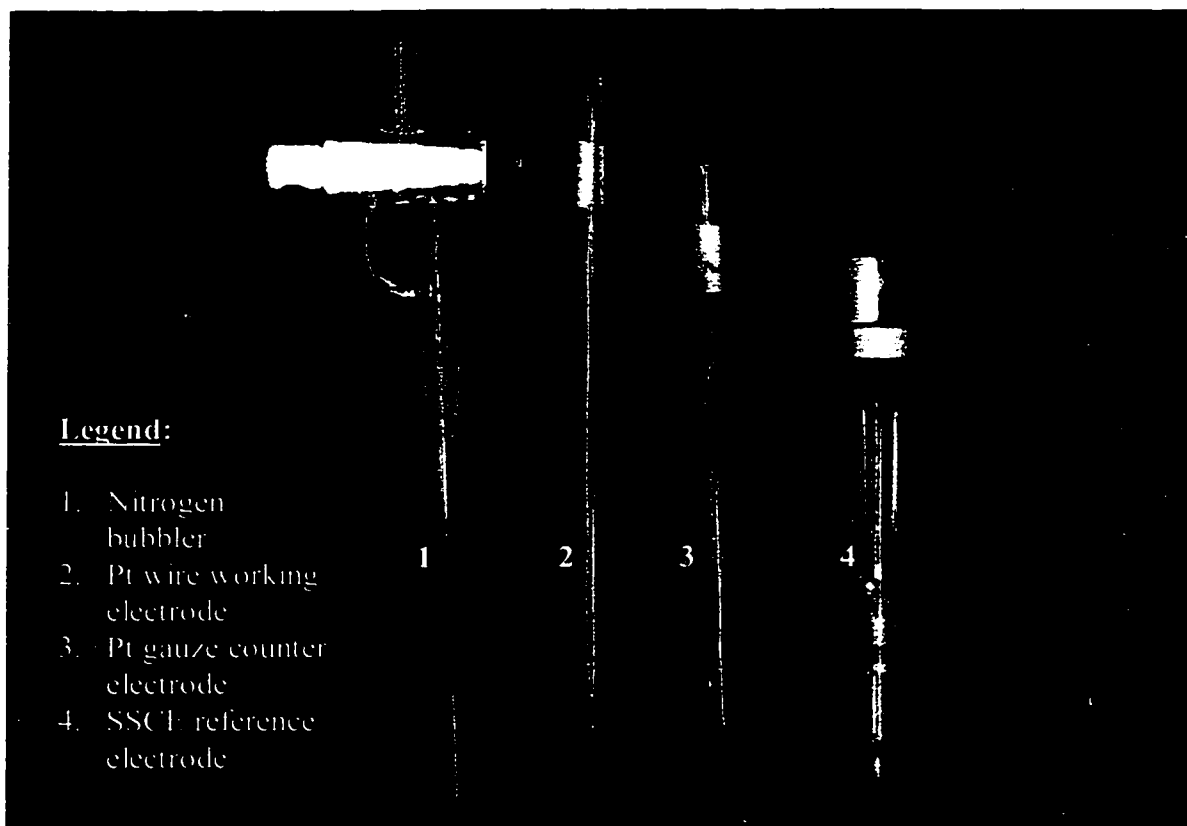


Figure 3-2. Electrodes and bubbler used in an electrochemical cell.

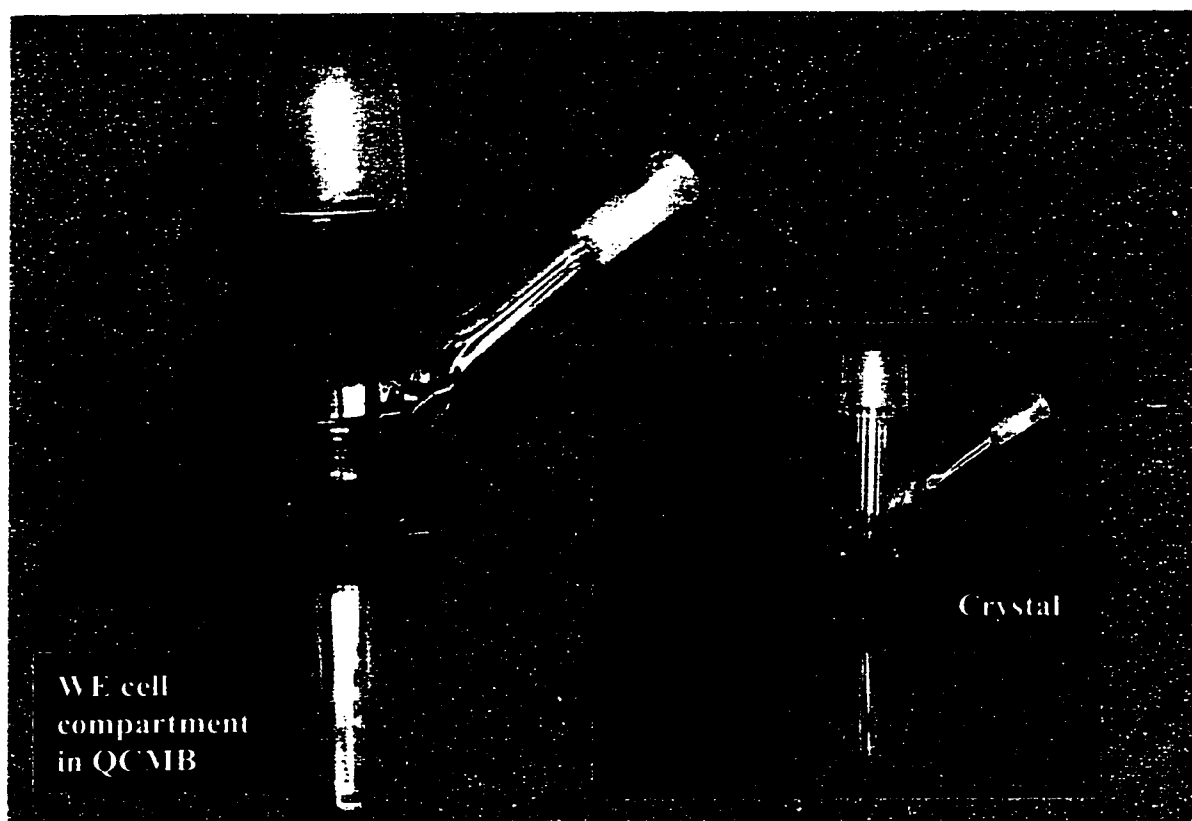


Figure 3-3. WE cell compartment of a QCMB cell.

3.1.3 ac impedance (acZ) experiments

The working electrodes (WEs) in these experiments were 1018 Carbon Steel rods, supplied by CAPROCO, with an apparent S.A. of 9.1 cm^2 . The composition of 1018 carbon steel is shown in Table 3-1. New electrodes were used for each set of experiments. The electrodes were degreased in an ultrasonic bath containing acetone for ca. 10 minutes prior to use. The electrodes were lengthened to fit into the cell by screwing them onto the end of steel rods, which were wrapped with Teflon tape

(Figure 3-4). In order to prevent leakage at the junction, an O-ring was always used to seal the connection.

Table 3-1. Chemical composition of 1018 carbon steel

Element	% composition
Carbon	0.15 – 0.20
Manganese	0.6 – 0.9
Phosphorus	0.04
Sulfur	0.05

The counter electrode (CE) in the acZ experiments was usually a large surface area Pt gauze electrode (see Section 3.1.1). Carbon steel electrodes, the same as the WEs, were also used as the CEs in many cases. A SSCE was used as the reference electrode (RE) for the experiments carried out at the University of Calgary, while Hastalloy electrodes were used as the REs at Travis Chemicals Inc in their acZ work with steel WEs. Even though the WE potentials were then difficult to compare, the use of the Hastalloy REs allowed the utilization of a high pressure and high temperature cell. A fourth electrode (a Pt auxiliary electrode) was connected to the RE via a 6.8 μF capacitor for ac impedance measurements in order to compensate for the phase shift due to the time delay of the SSCE at high frequencies. Electrodes were placed in solution in a Mason jar (Figure 3-5), containing ca. 300 mL of synthetic brine solution, in the acZ experiments.

The solution was saturated by continuous bubbling with CO₂ gas prior to and throughout each experiment.

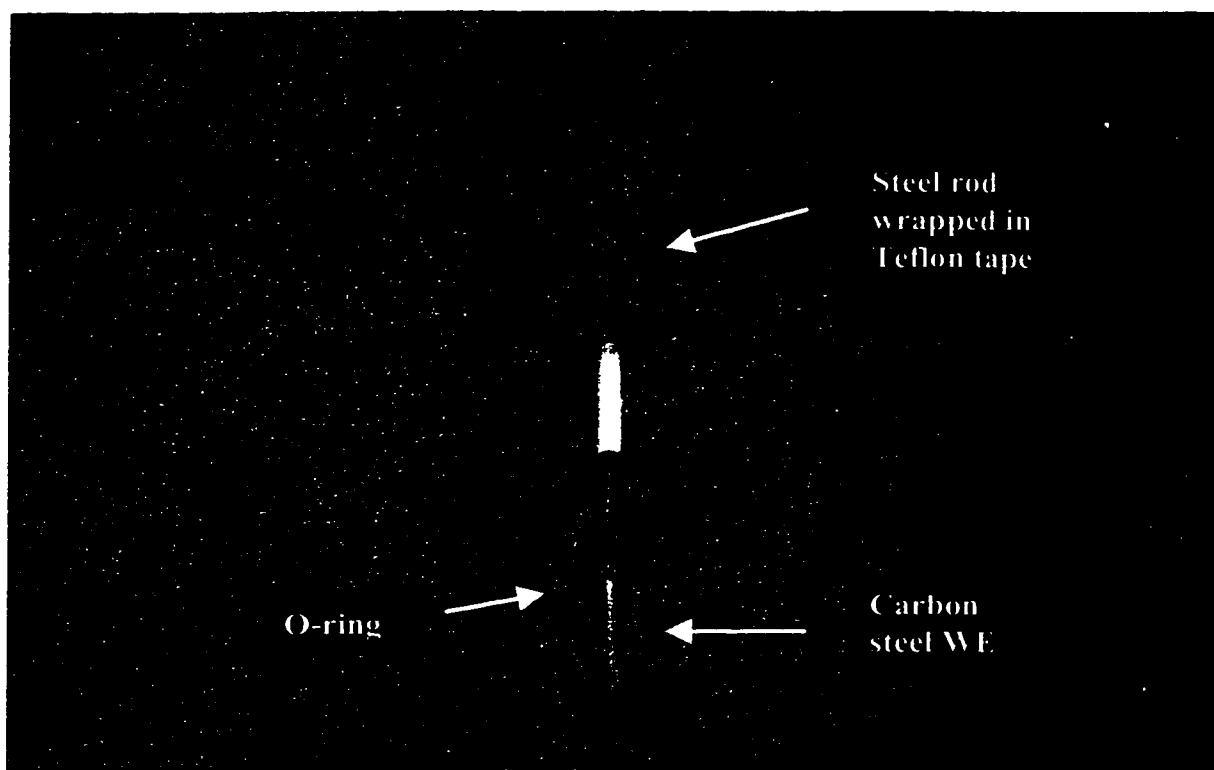


Figure 3-4. Carbon steel WE.

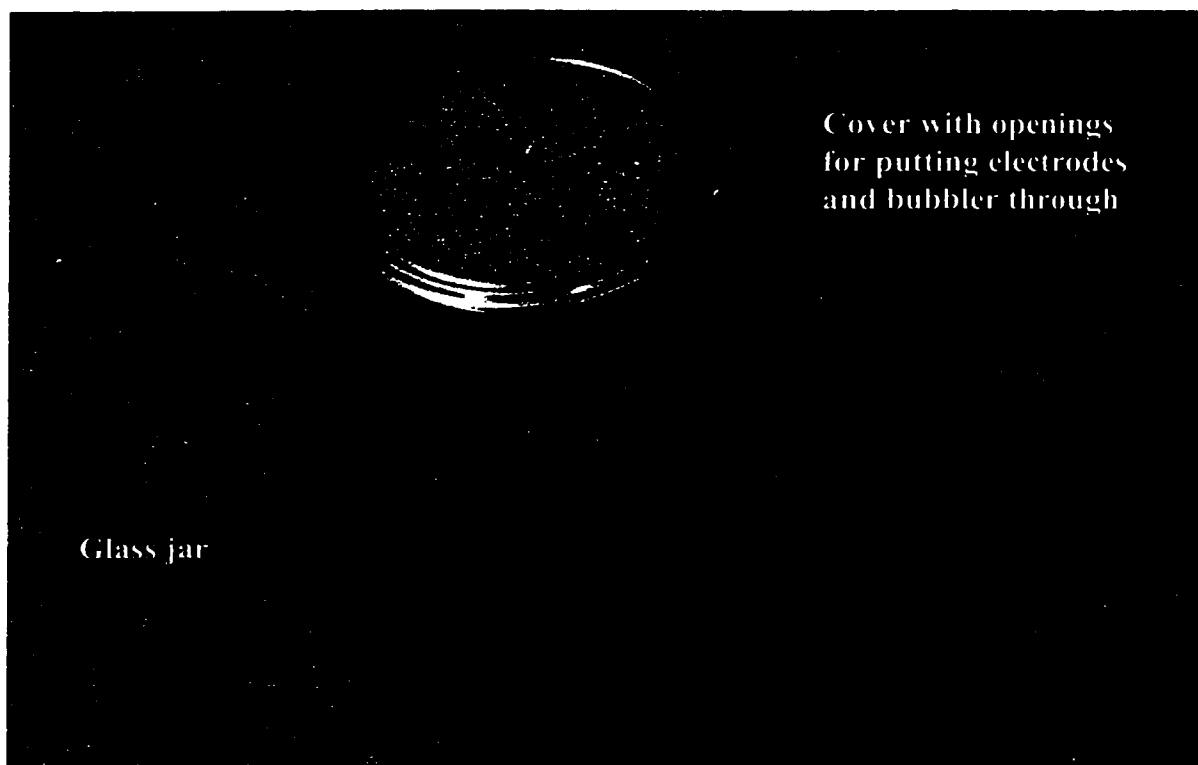


Figure 3-5. A Mason jar for study of steel WEs in CO₂ environment.

3.1.4 Cleaning of cells and electrodes

All cells were cleaned periodically by soaking in a concentrated sulfuric acid solution containing ammonium peroxydisulfate (18 g/L) at least overnight. The cells were then rinsed thoroughly with triply distilled water prior to their use. Au and Pt electrodes, including the Pt gauze counter electrodes, were cleaned both chemically and electrochemically. Chemical cleaning involved the dipping of the electrodes into a solution with half volume of concentrated sulfuric acid and half volume of hydrogen peroxide (29 to 32 %) for approximately 15 minutes. The electrodes were then

transferred into a 1 M perchloric acid solution for electrochemical cleaning. This involved the alternating formation of hydrogen and oxygen gas on the electrode surface by applying a relatively high potential both positively (ca. 1.5 V vs. SSCE) and negatively (ca. – 0.4 V vs. SSCE) at a sweep rate of 1 V/s.

3.2 Solutions and General Experimental Conditions

3.2.1 Solutions

Water was triply distilled using a Corning Mega-Pure-6A System. A 0.05 M KH_2PO_4 / 0.03 M NaOH pH 7.2 phosphate buffer solution was prepared according to the CRC Handbook [52]. A 0.1 M perchloric acid solution was prepared using 70 % perchloric acid, while the 0.1 M sodium hydroxide solution was made using solid sodium hydroxide. The 0.1 M neutral perchlorate solution was prepared using potassium perchlorate. The electrolyte solutions were degassed throughout the experiments by purging with nitrogen gas. The slow rate of nitrogen bubbling also promoted solution mixing when aliquots of the Quats were added to the electrolyte solutions in the cell. The temperature of the solutions was ca. 20 to 22 °C.

Synthetic ocean brine was prepared according to the procedure described in ASTM D-1141-90 [53]. The composition of this NACE brine solution is shown in Table 3-2. During the experiments, the electrolyte solution was purged continuously with carbon dioxide, both to displace oxygen and to provide a realistic carbon dioxide environment. The temperature and pH of the solution was ca. 21 °C and 6, respectively.

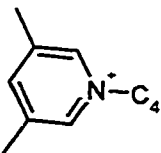
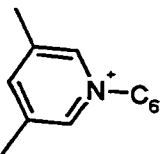
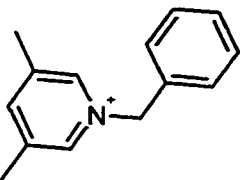
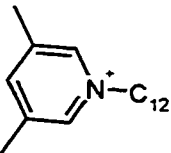
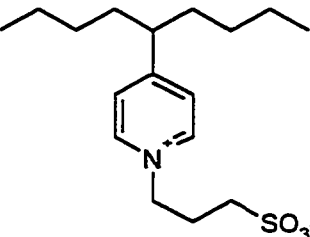
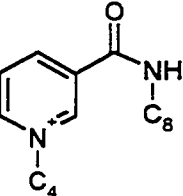
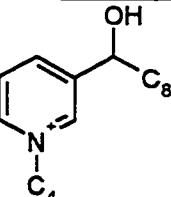
Table 3-2. Chemical composition of synthetic ocean brine solution.

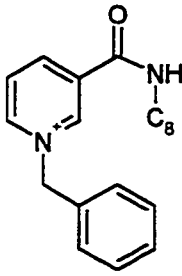
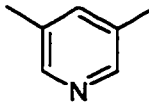
Compound	Concentration, g/L
NaCl	24.53
MgCl ₂	5.20
Na ₂ SO ₄	4.09
CaCl ₂	1.16
KCl	0.695
NaHCO ₃	0.201
KBr	0.101
H ₃ BO ₃	0.027
SrCl ₂	0.025
NaF	0.003

3.2.2 Structure of the quaternary pyridinium compounds (Quats)

Eight of the many different novel Quats synthesized and provided by Travis Chemicals Inc were tested in this research work. They were at least 98 % pure, with impurities including the starting materials and/or alcohol used to dissolve the Quats. The structures of the eight Quats, as well as of the starting material (3,5-lutidine), are illustrated in Table 3-3. It should be noted that all Quats, except Quat 5, were provided in solution in the bromide form. The concentration of Quats in the electrochemical cell solutions ranged from ca. 40 μ M to 4 mM.

Table 3-3. The number, code name, and structure of the organic compounds provided by Travis Chemicals Inc.

Compound	Code at Travis Chemicals Ltd.	Structure	Additional Notes
Quat 1	4b-2		
Quat 2	6b-2		
Quat 3	30b-2		- believed to be the most representative of the commercial Quat mixture
Quat 4	12b-2		
Quat 5	26-9x		- zwitterionic (no counter anion) - did not perform well in wheel testing
Quat 6	4b-12.8		- most promising in sweet conditions by wheel testing
Quat 7	4b-35		- similar to Quat 6, but thermodynamically more stable

Quat 8	30b-12.8		
3,5-lutidine	Starting material		- does not contain positive charge, hence, does not dissolve readily
Commercial Quat mixture	Quat Mixture A	The structure of the component is not known. However, it is believed that the major component has similar structure to Quat 3	- Travis Chemicals Inc purchased this mixture and added their own formulation before selling to other companies

3.3 Instrumentation

All CV measurements were performed using an EG&G 273 potentiostat and were recorded on a Hewlett Packard 7045B X-Y recorder. For QCMB measurements, a home-made 9 V oscillator was used to power the shear mode oscillation of the crystal. The crystal frequency was then monitored using a Philips PM 6654C programmable high-resolution timer/counter, and a BBC SE780 X-Y recorder was used to record the data. acZ measurements were performed using a Solartron SI 1287 electrochemical interface and a Solartron SI 1255 HF frequency response analyzer. An ac voltage of 10 mV was applied at the open circuit potential, OCP (also known as E_{corr}), of the WE at frequencies ranging from 100 kHz to 0.1 Hz. The current range was set in the auto mode to avoid the current overload during the experiments.

acZ data acquisition was achieved using Zplot for Windows software (version 2.b), written by Derek Johnson at Scribner Associates, Inc. The data was then analyzed using ZView Equivalent Circuit software, which was based on the LEVM 6.0 program written by Dr. J. Ross Macdonald [41].

IV. ADSORPTION STUDIES OF QUATS AT NOBLE METAL ELECTRODES IN VARIOUS SOLUTIONS

4.1 Noble Metal Electrodes

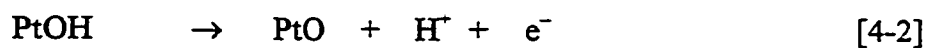
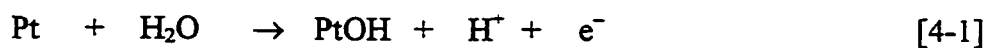
The study of the adsorption of the various novel quaternary pyridinium compounds (Quats) on electrode surfaces was initiated using noble metal electrodes. The use of noble metal electrodes has several advantages over steel electrodes, the material most commonly encountered in practice. First, noble metals do not dissolve readily in most electrolyte solutions, so that the complications arising from concurrent dissolution during electrochemical experimentation can be avoided. Secondly, a noble metal surface can be controlled easily between its metallic and oxide-coated state by changing the applied potential of the electrode.

Gold and platinum electrodes are two widely used noble metal electrodes. The cyclic voltammogram (CV) of Au in most solutions reveals a wide double layer region (ca. 0 to 1.2 V vs. RHE), over which adsorption can be studied without any interference from Au oxidation/reduction reactions. On the other hand, the double layer region for Pt is relatively narrow, from ca. 0.3 to 0.7 V vs. RHE. However, the CV of Pt shows a pair of redox peaks (ca. 0 to 0.3 V vs. RHE) due to atomic hydrogen adsorption/desorption, which can also reveal competitive adsorption processes by their magnitude. Adsorption can also be detected by the delays or the complete suppression of Au oxide (> 1.3 V vs. RHE) or Pt oxide (> 0.9 V vs. RHE) formation.

There have been many studies of the adsorption of organic molecules on Au and Pt electrode surfaces [31, 54, 55, 56, 57, 58, 59, 60, 61, 62, 63, 64]. Many factors must be carefully controlled in order to obtain meaningful results, as adsorption processes are very sensitive to the electrode surface preparation, solution pH, the presence of trace contaminants, the degree of crystallinity of the surface [65], competitively adsorbing species, etc.

Many different electrochemical techniques have been employed to study the absorption of organic species on electrode surfaces (Section 2.1.4.2). The comparison of Au or Pt CVs, with and without added organic to solution, has been used as a detection method for organic adsorption on electrode surfaces. Another commonly employed electrochemical technique is the quartz crystal microbalance (QCMB) method, which can measure *in situ* mass changes of the electrode at the nanogram scale [30, 32, 34, 61, 62, 66, 67, 68, 69]. Other widely used techniques used for the studies of organic adsorption on electrode surfaces include *in situ* infrared spectroscopy [61, 66, 70], differential capacity/ac impedance measurements [54, 56, 57, 62] and ellipsometry [28, 29].

The upper part of Figure 4-1 shows a typical CV of Pt in neutral phosphate buffer solution. When the potential is scanned positively of ca. 0.2 V vs. SSCE, Pt is oxidized to form a Pt oxide film [71]:



A place-exchange mechanism is widely accepted for Pt oxide formation [72, 73]. In the reverse cycle, the Pt oxide film is reduced back to metallic Pt. The redox peaks between -0.3 and -0.7 V are due to the adsorption/desorption of atomic hydrogen during the negative and positive scans, respectively:



It should be noted that all currents in a CV are proportional to the exposed surface area of the WE. The lower part of Figure 4-1 illustrates the mass gain (i.e., frequency decrease) of the crystal associated with the formation of Pt oxide, and the mass loss during oxide reduction.

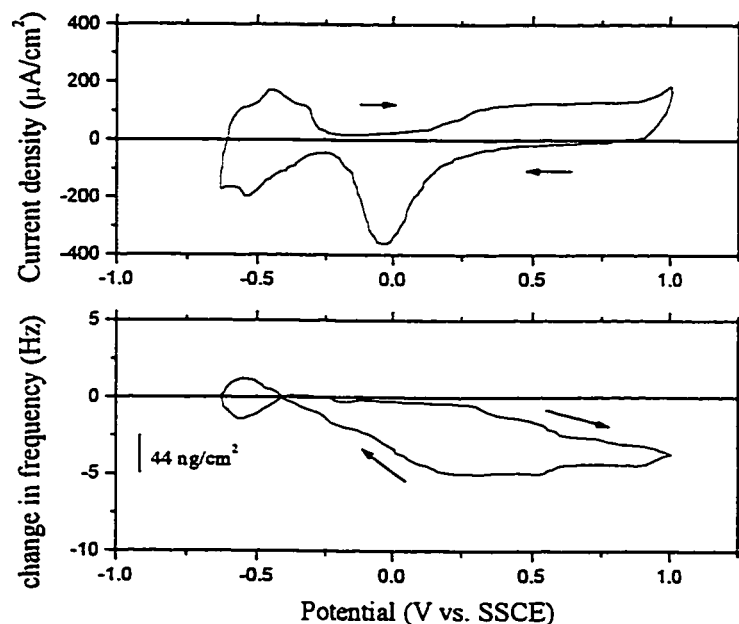


Figure 4-1. Cyclic Voltammogram and Massogram for Pt electrode in deaerated neutral phosphate buffer solution, $s = 100$ mV/s.

4.2 Interaction of Quats with Noble Metals in Perchlorate Containing Solutions

4.2.1 Quat adsorption at Au in 0.1 M KClO₄ solution

Preliminary adsorption studies were conducted using Au wire electrodes in unbuffered 0.1 M KClO₄ solution, as it is widely believed that perchlorate ions do not competitively adsorb on Au [32, 64, 71]. Also, many papers, that display CVs of Au in 0.1 M KClO₄ solution, have been published [32, 54, 57, 64] and thus a valid comparison of the CV response for Au could be made in this solution. Aliquots of Quats 1-3 and 5 (see Table 3-3) were added, in separate experiments, to 0.1 M KClO₄ solution, but only a minor effect on the Au CV was observed in all cases. Figure 4-2 shows that the main oxide reduction peak at 0.25 V decreased in size, while the reduction peak at 0.7 V became larger after the addition of Quat 1. However, the total oxide reduction charge remained approximately constant. This indicates that, while the formation/reduction of Au oxide was somewhat affected by the presence of the Quat in this solution, little evidence for its adsorption could be gathered from this work. Similar results were also obtained for Quats 2, 3 and 5.

In these experiments, the bromide counter anion was removed prior to the addition of Quats 1-3 to the perchlorate solution, using an anion-exchange column. This was done in order to avoid bromide ion adsorption and its oxidation in the potential window of the CV study. The high basicity of the resin used in the anion-exchange column prevented the study of Quats 6 to 8, which contain one or more functional groups that might react with

the column. Overall, it was not possible to discriminate between the behaviour of the various Quats at Au in 0.1 M KClO_4 , due to their weak interaction with the metal.

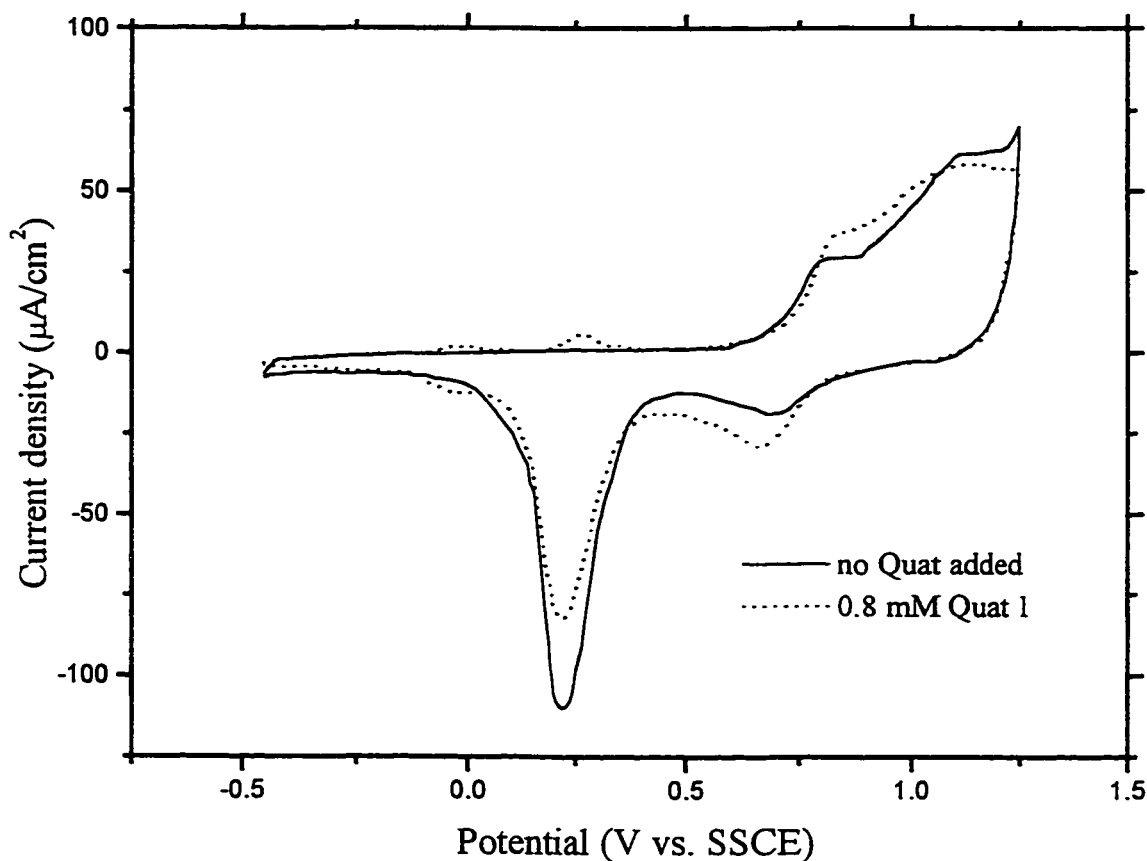


Figure 4-2. Effect of addition of Quat 1 on Au CV in deaerated 0.1 M KClO_4 solution, $s = 100 \text{ mV/s}$.

4.2.2 Quat adsorption at Au in 0.1 M HClO_4 solution

The addition of Quats 1-3 and 5 (see Table 3-3), without Br^- , in separate experiments, also yielded only a minor (and similar) effect on the Au CV in 0.1 M HClO_4 solution, as shown in Figure 4-3. Quats 6 to 8 were not studied because of the difficulty

of replacing the bromide counter anions (see Section 4.2.1). Interestingly, similar results were obtained by the addition of 3,5-lutidine (see Table 3-3), the starting material in the synthesis of Quats, to this solution. This suggests that the interaction of the positively charged Quats with Au is similar to that of the protonated 3,5-lutidine in this acidic solution. It should be noted that the addition of ca. 0.3 mM pyridine in 0.1 M HClO₄ has also been reported to give very similar results using a Au electrode [57]. Figure 4-3 shows a similar degree of blockage of Au oxide formation by the adsorption of Quat 2 and 3,5-lutidine, as seen by the reduced oxide reduction charge, in 0.1 M HClO₄.

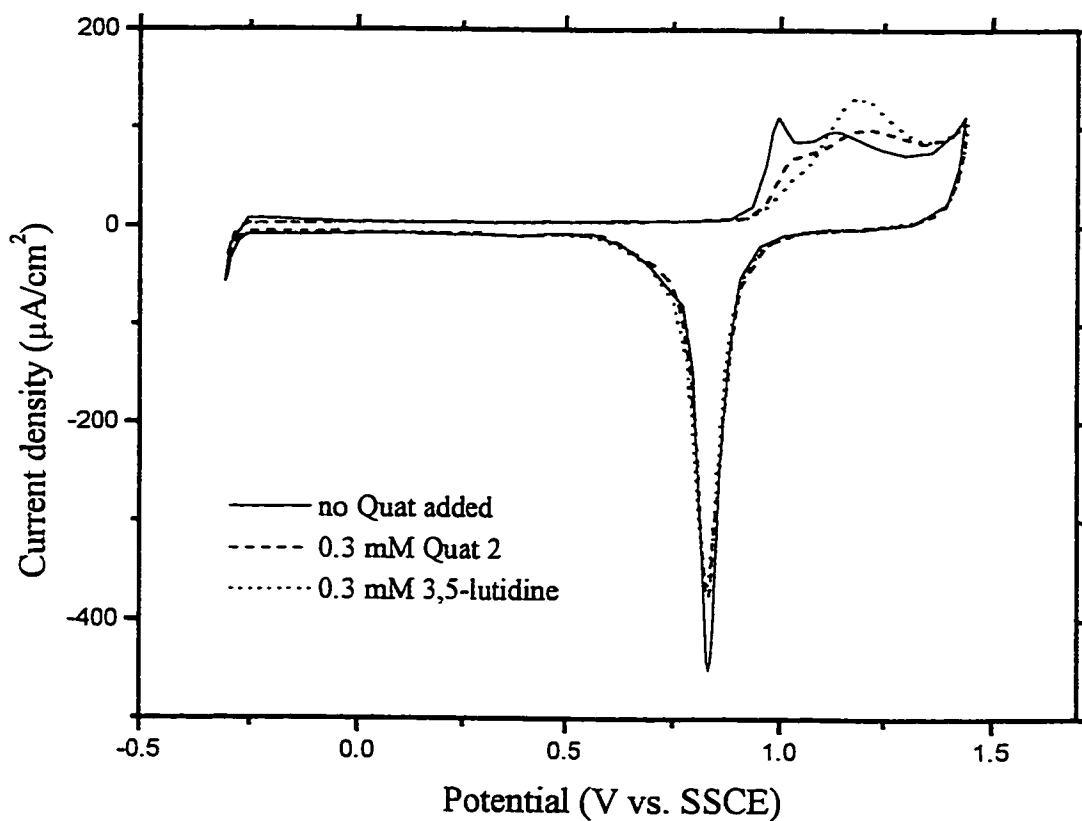


Figure 4-3. Comparison of the effect of addition of Quat 2 and 3,5-lutidine on Au CV in deaerated 0.1 M HClO₄ solution, $s = 100$ mV/s.

4.2.3 Quat adsorption at Pt in 0.1 M HClO₄ solution

Quats 1, 2 and 5 (see Table 3-3) were added, without Br⁻, in separate experiments, to a 0.1 M HClO₄ solution in order to examine each of their effects on the Pt CV. An enhancement of the anodic charge in the oxide formation region was observed in all cases, while the charge of the oxide reduction peak was more notably suppressed than in the case of Au (Figure 4-4). Quat 7 (see Table 3-3) was also anion-exchanged to remove Br⁻, but the addition of this Quat, without Br⁻, to 0.1 M HClO₄ solution resulted in a similar impact on the Pt CV, as shown in Figure 4-4. It should be noted that these CVs are almost the same as those seen after the adsorption of benzoic acid [60, 64], acetic acid [63] and various protein/amino acids [58, 59] at Pt in perchloric acid solutions. The enhanced anodic charge in Figure 4-4 may be caused by the oxidation of some adsorbed Quats, perhaps causing them to be desorbed and then rapidly replaced during the same scan cycle, along with some Pt oxide formation. The suppression of the oxide reduction charge suggests that the adsorbed Quats blocked some sites on the Pt surface. However, this type of oxidative desorption process might be expected to be diffusion controlled, and yet solution agitation had no impact on the CV in this work. Others have used this enhanced anodic charge to calculate the surface coverage of adsorbed species [58, 59]. Figure 4-4 also shows the suppression of the hydrogen peaks at ca. 0.0 to -0.3 V. This suggests that Quats are adsorbed at all potentials. In fact, a similar coverage is obtained from the hydrogen peaks and the Pt oxide reduction peak in this case (i.e., ca. 30 %).

As a measurable suppression of oxide formation was seen in the Pt CV in these solutions, the QCMB technique was utilized in order to examine the mass change resulting from the adsorption of these Quats on Pt in 0.1 M HClO_4 solution. However, no significant mass gain or loss was observed in these experiments, indicating that either only small amounts of the Quats were adsorbed on the electrode, or that a replacement process has occurred at the electrode surface, so that the net mass change is very small. The replacement of water molecules by adsorbed organic molecules has been proposed by Zilberman et al [30] from their QCMB work (see Section 2.1.4.2).

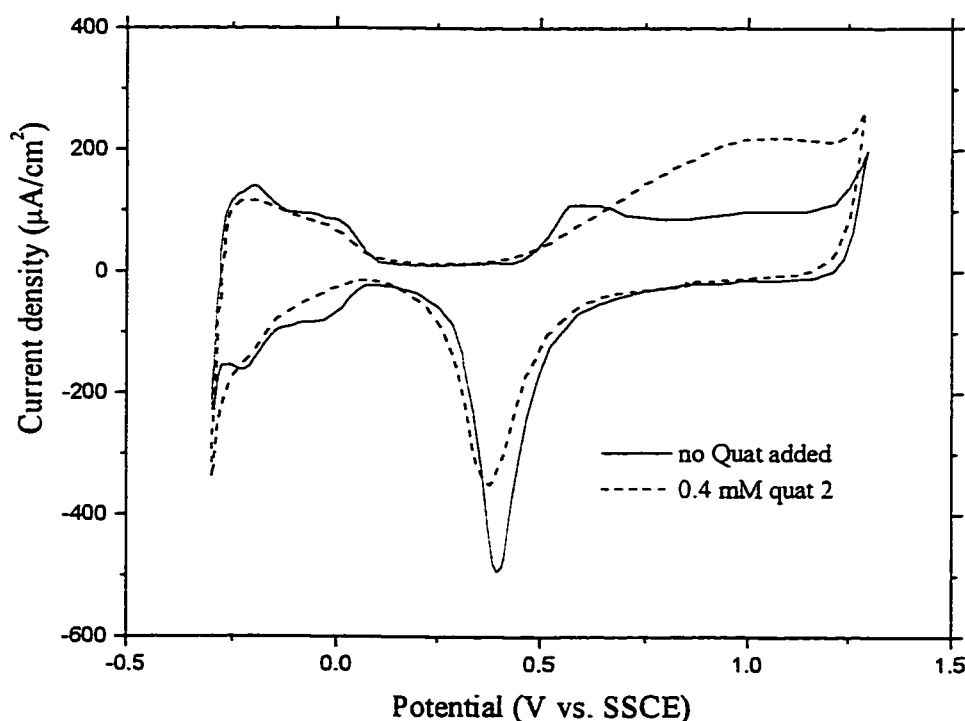


Figure 4-4. Effect of addition of Quat 2 on Pt CV in deaerated 0.1 M HClO_4 solution, $s = 100 \text{ mV/s}$.

4.3 Interaction of Quats with Noble Metals in Neutral Phosphate Buffer Solution

The use of a phosphate buffer solution eliminates the possibility of local pH effects which can arise in unbuffered solutions (i.e., KClO_4) when electrochemical reactions are made to occur. Also, neutral solutions are a more realistic medium than acids and bases for this project. However, a complication with the use of this buffer solution is that phosphate ions are known to adsorb strongly on Pt and Au surfaces [32, 74, 75]. Au electrodes were used in the early experiments, but several irreproducible adsorption/desorption peaks were sometimes observed in the double layer region at ca. -0.2 to 0.3 V vs. SSCE (not shown), complicating these studies. Therefore, the adsorption of Quats on Pt in phosphate buffer became the main focus of this part of the research. When Quats 1 and 2 (representative of Quats 1 to 5, as all five Quats were found to have a similar electrochemical response at Pt) were added, separately in different experiments, to a neutral phosphate buffer solution, only a minor impact on the Pt CV was seen (not shown). The result was very similar to the case in acid (see Figure 4-5). However, when Quats 6 to 8 were added to this phosphate buffer solution, the Pt CV response was suppressed almost completely (see Sections that follow). These results are similar to the studies of Kusu et al [36], who found that quaternary ammonium bromide containing long hydrocarbon chains are more strongly adsorbed than the ones with short hydrocarbon chains (see Section 2.1.4.2). However, the long hydrocarbon chain appears to be more effective, from the present results, when it is a side-chain, rather than the pyridinium chain (compare the structures of Quats 1 to 4 with 6 to 8 in Table 3-3). This

may argue that the pyridinium nitrogen is involved in the Quat adsorption process, as proposed by Kouznetsov et al [34], and that long pyridinium chains will sterically hinder the interaction of the pyridinium nitrogen with the metal surface.

4.3.1 CV studies of strongly adsorbing Quats 6 and 7 at Pt in neutral phosphate buffer solution

The addition of Quat 7, in its bromide form, to a 0.05 M KH_2PO_4 /0.03 M NaOH pH 7.2 phosphate buffer solution caused a pronounced decrease of the Pt CV signal with time of exposure to solution. The Pt electrochemical response was almost completely suppressed at long times, suggesting full surface coverage by the Quat (Figure 4-5). This shows that Quat 7 is strongly adsorbed on Pt in these experiments. Usually, organic compounds tend to adsorb/desorb with changing potential [30, 54]. In the present case, Quat 7, once adsorbed, appears to remain on the surface, independent of potential in this Quat containing neutral phosphate buffer solution.

The addition of Quat 6, in its bromide form, to the phosphate buffer solution resulted in a similar complete suppression of the normal Pt CV response, as shown in Figure 4-5 for Quat 7. Since the addition of the same concentration of potassium bromide has only a minor impact on the Pt CV in phosphate buffer solution (not shown), these results cannot imply blockage by bromide adsorption. The addition of Quat 7, which had been ion-exchanged to remove the bromide ion, resulted in a Pt CV response in phosphate buffer similar to that of Figure 4-5. Hence, the suppression of the Pt electrochemical response must be the result of the adsorption of Quats 6 and 7 and the removal of Br^- is

not necessary for the study of these strongly adsorbed Quats in the phosphate buffer solution.

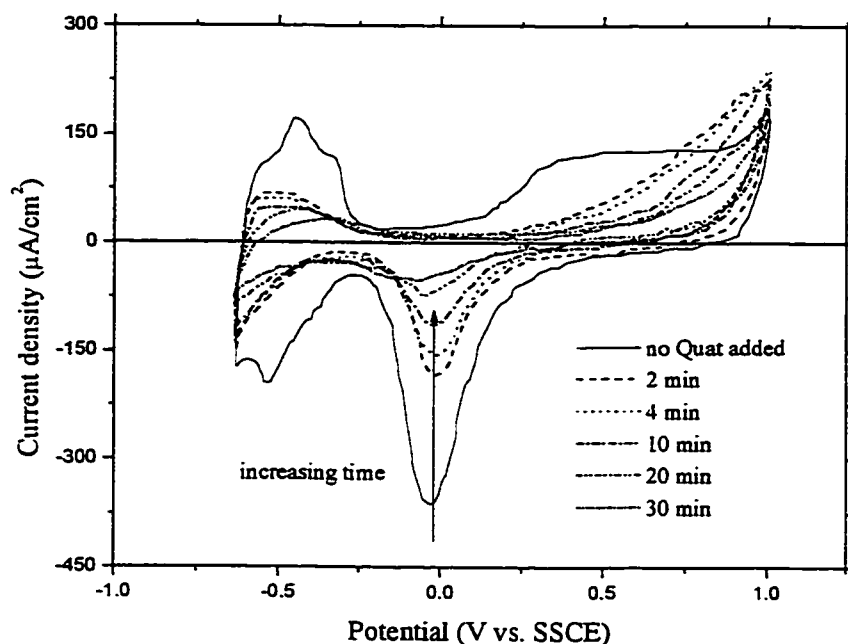


Figure 4-5. Suppression of Pt electrochemistry as a function of time of exposure to 40 μM Quat 7 in deaerated neutral phosphate buffer solution, $s = 100 \text{ mV/s}$.

It should be noted that the suppression of the Pt CV signal in phosphate buffer solution after the addition of Quat 6 was slightly greater than after adding the same amount of Quat 7. This may be caused by the presence of the amide side chain, an electron-withdrawing group, on Quat 6, thus enhancing its adsorption due to delocalization of the electron density of the pyridinium nitrogen. It was proposed elsewhere that the adsorption of quaternary ammonium compounds occurs through the interaction of the N atom with O atoms of metal oxide surface films (see the work of

Kouznnetsov et al [34] in Section 2.1.4.2). In the present work, there is no evidence that the adsorption of Quats occurs through the interaction of pyridinium nitrogen with Pt oxide sites, as adsorption appears to be independent of potential. Even though it is not clear from this work if the Quats prefer to adsorb on metallic or oxide-coated surfaces, stronger adsorption is still expected for a Quat with an electron-deficient pyridinium nitrogen than a Quat with an electron-rich pyridinium nitrogen if adsorption is indeed via this positively charged N atom.

The degree of suppression of the Pt oxide reduction peak (Figure 4-5) was found to be linearly proportional to the square root of time of exposure to the Quat containing phosphate buffer solution, as shown in Figure 4-6. This dependency of current with the square root of time often reflects a mass transport process governed by diffusion. However, at longer times ($> ca. 300$ seconds), the buildup of density gradients and the presence of stray vibrations should interfere with the diffusion layer through the process of convection, causing the currents to be larger than predicted by a diffusion process alone [76]. Since the present experiment lasted over 30 minutes, the square root dependency observed in Figure 4-6 is not likely to be caused by a diffusion process, but rather a result of a kinetic limitation associated with the adsorption of Quat 7 at the metal surface.

The effect of Quat 7 concentration on the degree of suppression of the Pt CV response in the phosphate buffer solution was also examined. It can be seen clearly that the rate of Quat 7 adsorption is directly related to its concentration in solution (Figure 4-7). In practice, the concentration of Quats employed is usually between 50 and 500 μM , but it can be anywhere from 10 μM to 10 mM.

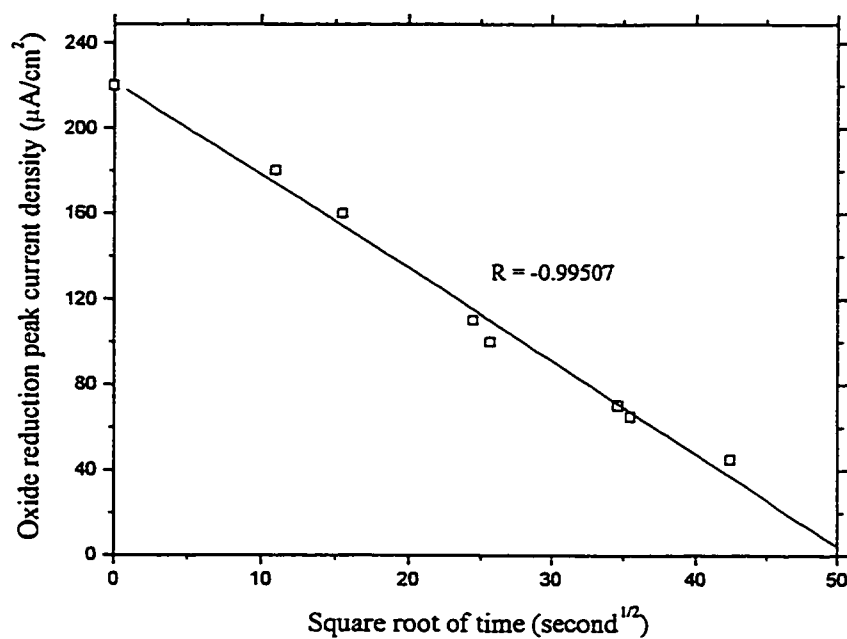


Figure 4-6. Suppression of Pt oxide reduction peak current density as a function of the square root of time of exposure to 40 μM Quat 7 in deaerated neutral phosphate buffer solution, $s = 100 \text{ mV/s}$.

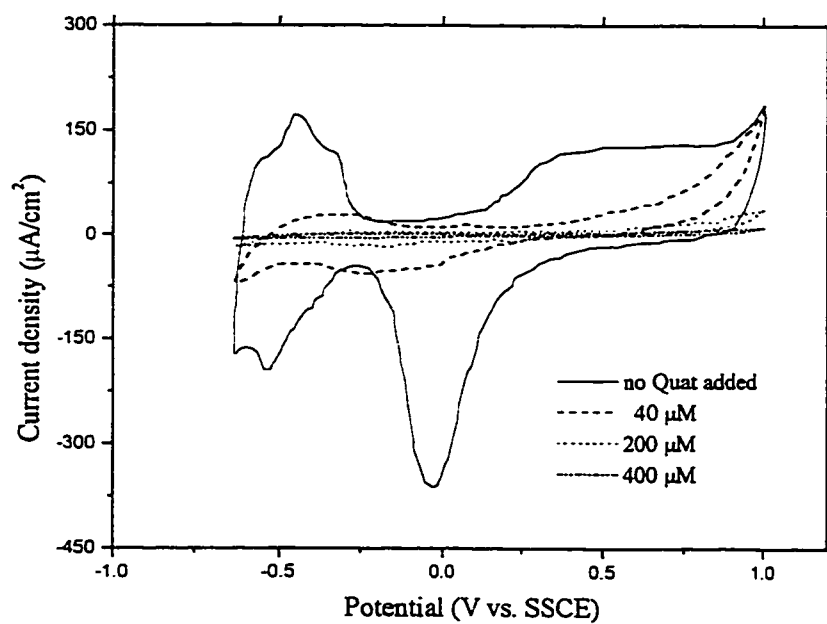


Figure 4-7. Steady-state CVs after the suppression of Pt CV response as a function of Quat 7 concentration in deaerated neutral phosphate buffer solution, $s = 100 \text{ mV/s}$.

4.3.2 Suppression of hydrogen evolution reaction at Pt by Quat 6 and 7 adsorption

The addition of Quat 7 to the phosphate buffer solution, not only suppressed Pt oxide formation and atomic hydrogen adsorption, but also the rate of the hydrogen evolution reaction (HER). This result supports the belief that Quats are cathodic inhibitors [22]. An interesting consequence of the suppression of the HER is that the lower potential limit could be extended more negatively than normal, revealing a new pair of redox peaks, A_1/C_1 , even with some concurrent hydrogen evolution (Figure 4-8). The origin and behaviour of these redox peaks will be examined in greater detail in the next chapter using a glassy carbon (GC) substrate. The use of GC reduces the interference from the HER current because it has a high overpotential for this reaction.

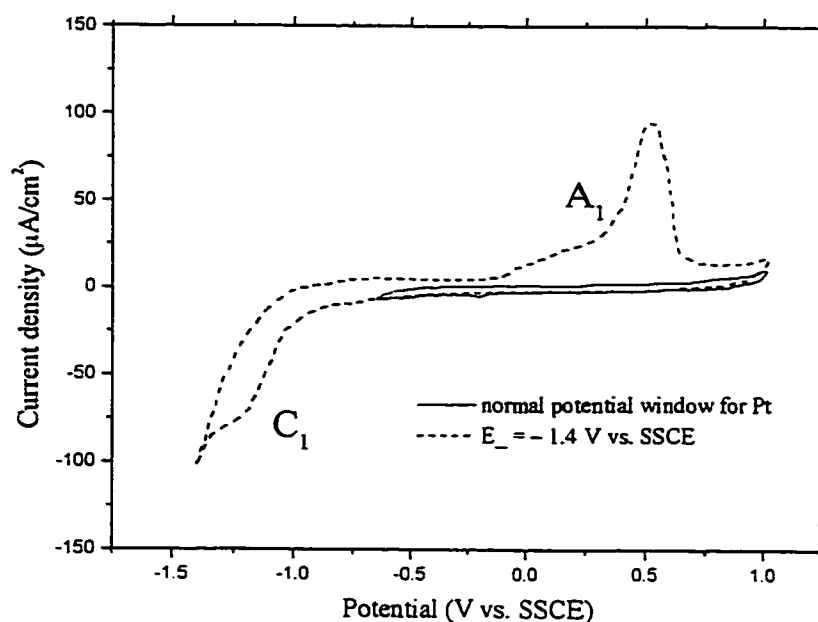


Figure 4-8. New redox peaks observed with extended lower potential limit after the suppression of Pt CV response by 300 μM Quat 7 in deaerated neutral phosphate buffer solution, $s = 100 \text{ mV/s}$.

4.3.3 QCMB studies of Quat 7 adsorption at Pt in phosphate buffer solution

The crystal frequency was tracked at -0.65 V vs. SSCE to eliminate the complication of any frequency changes due to oxide formation/reduction at potentials positive of ca. -0.45 V vs. SSCE (see lower part of Figure 4-1). Experiments began by cycling the potential between -0.65 to 1.0 V in phosphate buffer solution without any added Quat, similar to Figure 4-1, until a steady-state frequency response was obtained. The addition of Quat 7 to the phosphate buffer solution caused an initial frequency increase of ca. 5 Hz and then the frequency began to decrease as the CV signal became suppressed with time. The initial frequency increase may be the result of the replacement of adsorbed phosphate ions and/or water by the Quat on the Pt surface. Since phosphate ions are heavier per unit area than are the Quats, a mass decrease could result. A similar decrease in mass during the adsorption of organic molecules has been reported by Zilberman et al [30] (see Section 2.1.4.2). Further adsorption of Quat 7 then caused a continuous mass gain, along with a further suppression of the Pt CV signal. Figure 4-9 shows the coverage of Pt by Quat 7, calculated from both the CV and QCMB results, in the first 30 minutes of potential cycling. The coverage is calculated based on the degree of suppression of the Pt oxide reduction peak and from the absolute crystal mass gain at -0.65 V vs. SSCE. This figure shows clearly that the suppression of current is linearly related to the mass gain. This conclusively indicates that the suppression of Pt oxide formation (reduction) in the CV response is caused by Quat 7 adsorption.

The suppression of current in the Pt CV was almost complete after ca. 30 minutes of exposure time to Quat 7 in the phosphate buffer solution. However, the crystal mass continued to increase even after this. This result indicates that only the initially adsorbed Quat 7 affects the Pt CV response in this phosphate buffer solution, and that further Quat adsorption also occurs, not evident electrochemically. This supports the notion of Quats as film-forming corrosion inhibitors.

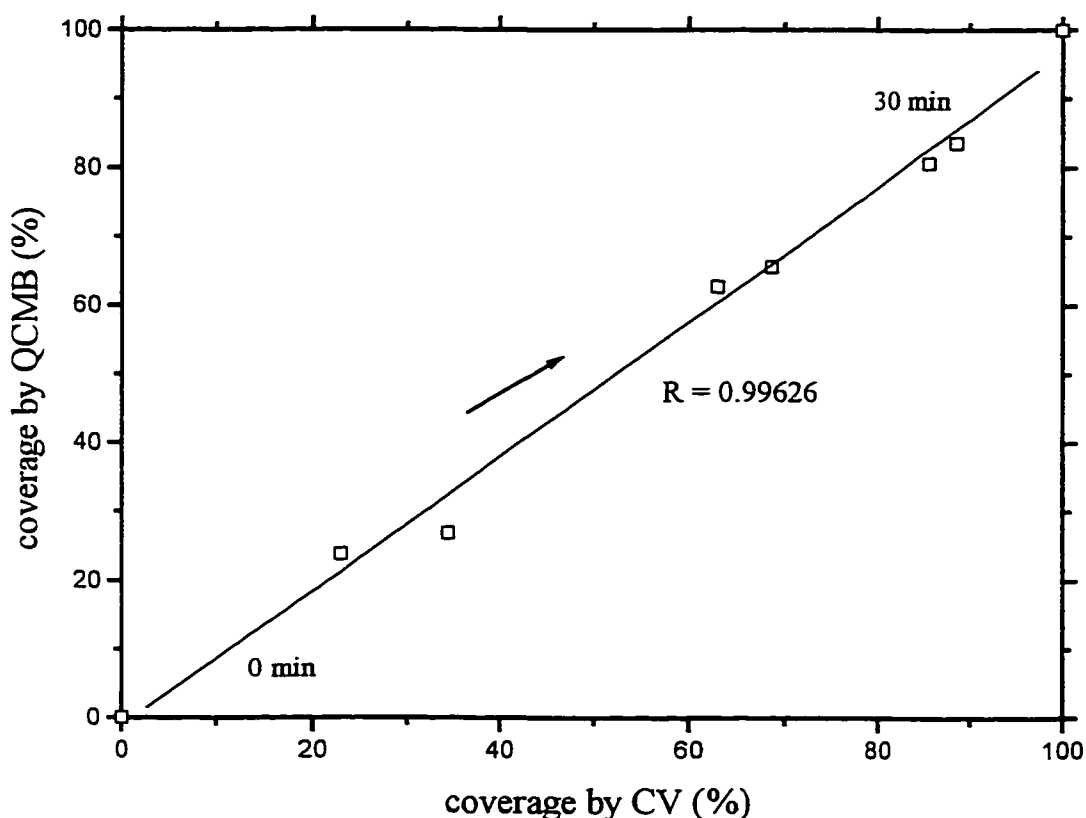


Figure 4-9. Coverage of Pt, determined from QCMB vs. CV experiments, after addition of 50 μM Quat 7 to deaerated neutral phosphate buffer solution, $s = 100 \text{ mV/s}$, in the first 30 minutes of experimentation.

4.4 Possible Surface Structure of Adsorbed Quat 7 on Pt Based on QCM Analysis

4.4.1 Monolayer coverage after exposure to 40 μM Quat 7 in phosphate buffer solution for ca. 30 minutes

When a steady-state Pt CV response was reached, in which the current was essentially fully suppressed, after ca. 30 minutes of exposure to Quat 7 in the neutral phosphate solution, the frequency had decreased by ca. 10 Hz. Using the Sauerbrey equation [eq. 2-15] and the molecular weight (with and without bromide as the counter anion) of Quat 7, this corresponds to 3.0 to 3.8×10^{14} molecules cm^{-2} , respectively. The co-adsorption of the counter anion along with a positively charged organic compound as an ion pair has been suggested elsewhere [34, 77].

Using an approximate estimation of bond lengths (C-C ca. 1.54 Å, ring diameter ca. 2.8 Å [78]), the maximum and minimum area occupied by each molecule would be ca. 50 Å² and 20 Å², respectively (Figure 4-10). It was assumed that the maximum area would be obtained with the ring parallel to the Pt surface and the chains extended along the electrode surface. The minimum area was calculated based on the assumed direct adsorption of the pyridinium nitrogen atom on the Pt surface [10, 34], with the ring and chains extended into solution. Many prior researchers [9, 28, 29, 54] have proposed similar surface behaviour of adsorbed organic molecules on electrode surfaces (see Section 2.1.4), with the two orientations commonly referred to as flat and upright. The reciprocal of these numbers yields the minimum and maximum number of molecules which would occupy the crystal surface, i.e., 2.0×10^{14} molecules cm^{-2} and 5.0×10^{14}

molecules cm^{-2} , respectively. Stolberg et al [54] reported in their study of pyridine at a Au electrode in 0.1 M KClO_4 solution that the minimum and maximum number of pyridine molecules in a monolayer were 1.8×10^{14} molecules cm^{-2} and 4.2×10^{14} molecules cm^{-2} , respectively, based on the calculation of relative Gibbs surface excess. Therefore, the estimation in the present study is reasonable. The fact that the experimentally determined coverage (3.0 to 3.8×10^{14} molecules cm^{-2}) is within this range (2.0 to 5.0×10^{14} molecules cm^{-2}) indicates that approximately one monolayer of Quat 7 adsorbs from the phosphate buffer solution onto the Pt surface after ca. 30 minutes of exposure time. However, the exact orientation of the Quat on the Pt surface remains uncertain from this study. A similar result could be obtained for Quats 6 and 8, while all of the other Quats tested exhibited a much lower coverage, too small to be detected via the QCMB method.

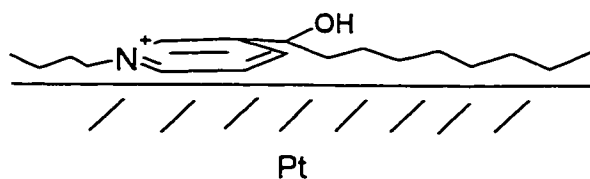


Figure 4-10a. One molecule of Quat 7 with ring and side chain parallel to the electrode surface (flat orientation) – possible maximum area configuration.

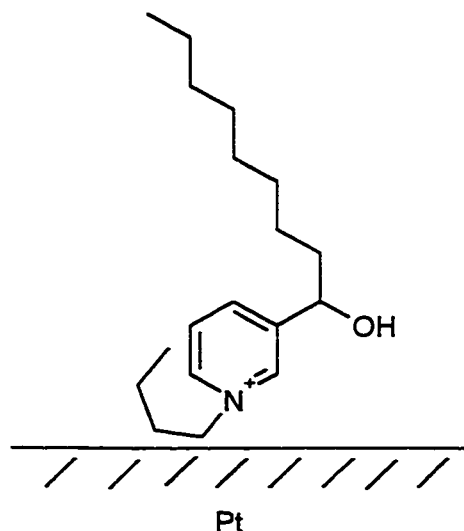


Figure 4-10b. One molecule of Quat 7 with ring and side chain extended into solution (upright orientation) – possible minimum area configuration.

4.4.2 Bilayer coverage after exposure to 40 μ M Quat 7 in phosphate buffer solution for ca. 3 hours

After the Pt electrode was exposed to the phosphate buffer solution containing 40 μ M Quat 7 for ca. 30 minutes, the suppression of the Pt CV signal had ceased, but a continuous mass gain (a total of ca. 21 Hz) was still observed in the QCMB experiment. Based on Section 4.4.1, a monolayer of Quat 7 may have already adsorbed on the Pt surface during the first 30 minutes of the experiment. Further Quat adsorption would only be possible if re-orientation of the monolayer occurs in order to allow more Quat to adsorb, or if a Quat multilayer is formed.

Often, organic adsorption is assumed to commence in the flat orientation, either at low concentrations of the organic in solution and/or at short times [28, 29].

Re-orientation may then occur, first to a partially upright position, and then to totally upright, as more organic is adsorbed on the electrode surface with time. In some cases, adsorbed molecules change their orientation on the electrode surface from flat to upright, and vice versa, as a result of changing potential [54]. However, in the present work, no effect of changing potential was observed on the adsorption of Quat.

It should be noted that a molecular bilayer may form if the adsorbed molecule contains a polar head and a hydrophobic tail [9], as in the present case. Multilayers [28, 29] or micelle [9] formation is also possible at high surface concentrations. Based on the calculation in Section 4.4.1, the 21 Hz total frequency change corresponds to ca. 6.2 to 8.0×10^{14} molecules cm^{-2} , depending if the bromide ion is co-adsorbed or not. The calculation of the maximum and minimum area of each molecule suggests that 2.0×10^{14} molecules cm^{-2} and 5.0×10^{14} molecules cm^{-2} of Quat could occupy the crystal surface (Figure 4-10). The experimental results indicate that approximately two layers of adsorbed Quat 7 are present on the electrode surface after long times of potential cycling in this solution. Figure 4-11 illustrates a bilayer structure that is consistent with this result. The formation of this bilayer would help to minimize the contact of the non-polar hydrophobic chains with the polar solvent.

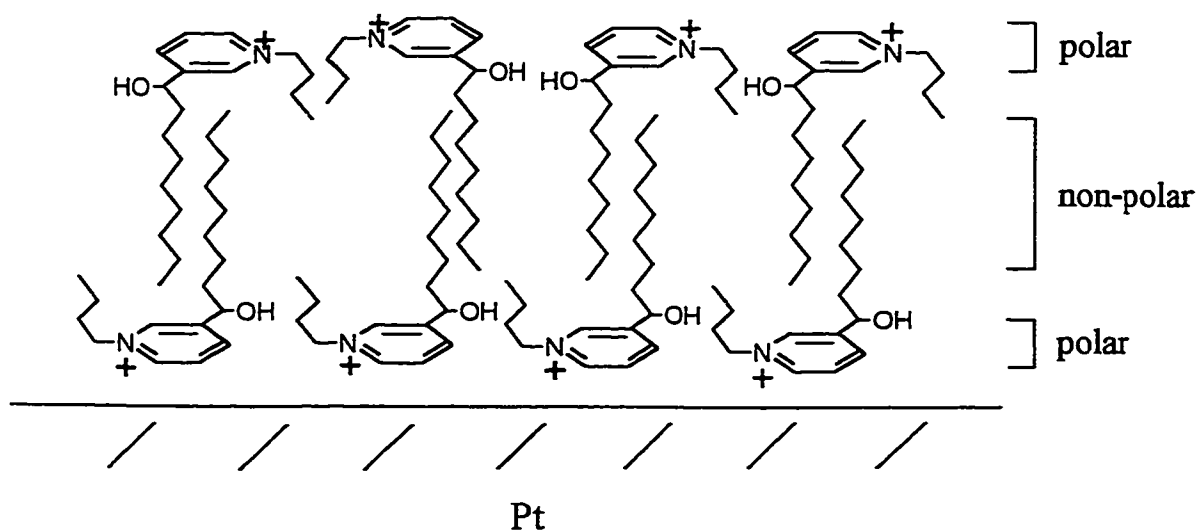


Figure 4-11. Possible Quat 7 bilayer on Pt electrode surface (based on [9]).

4.5 Interaction of Quats with Noble Metals in Sodium Hydroxide Solution

Despite the fact that basic solutions are probably the least realistic medium for the study of the Quats, the use of 0.1 M NaOH completely eliminated any possible complication due to bromide ion adsorption and oxidation, as the entire potential window is moved negatively vs. the SSCE. Therefore, the ranking of the various Quats could be achieved at Pt in 0.1 M NaOH solution without the need for anion exchange to remove the bromide ion.

4.5.1 Ranking of Quats based on Pt CV response in 0.1 M NaOH solution

The extent of suppression of the Pt oxide reduction peak (i.e., coverage), at a constant upper potential limit of 0.6 V vs. SSCE, has been used to rank the Quats, provided by Travis Chemicals Inc, in 0.1 M NaOH solution. However, this ranking can only be viewed as semi-quantitative, partly because of the difficulties encountered in estimating the zero current baselines in the CVs. Nevertheless, the relative impact on the Pt CV response after the addition of 70 μ M of each of the Quats (see Table 3-3) to a 0.1 M NaOH solution is contrasted in Figure 4-12. It can be seen that Quats with long hydrocarbon chains generally result in higher coverage (compare Quats 1 to 4), similar to the previous studies in the literature [9, 36]. Also, Quats containing a long hydrocarbon side chain (Quats 6 to 8) appear to be more strongly adsorbed than the Quats with a long pyridinium chain. In theory, a long pyridinium chain may interfere in the interaction of the pyridinium nitrogen of a Quat with the metal surface (see Section 4.3). Although it was difficult to distinguish the performance of Quats 6 and 7 in this basic solution, Quat 6 was found to be more strongly adsorbed than Quat 7 in the neutral phosphate buffer solution (Section 4.3.1). The reasons for enhanced Quat adsorption in basic > neutral > acidic solutions remain unknown.

The results of Figure 4-12 were found to be comparable to those obtained for carbon steel electrodes using the standard corrosion wheel test (a gravimetric experiment) at Travis Chemicals Inc, thus confirming the validity of the present electrochemical and QCMB results. The fact that 3,5-lutidine (the starting material) suppressed Pt oxide

formation to an even greater extent than did some of the Quats may be related to its charge neutrality. A neutral organic compound might have a greater tendency to deposit on the electrode than would a charged one. However, in practice, the limited solubility of this neutral compound would prevent it from reaching the target areas in pipelines and other corrosion susceptible areas. Quat Mixture A in Figure 4-12 is the commercial Quat solution (containing a mixture of Quats, possibly having the structure of Quat 3) used by Travis Chemical Inc to formulate commercial corrosion inhibitors.

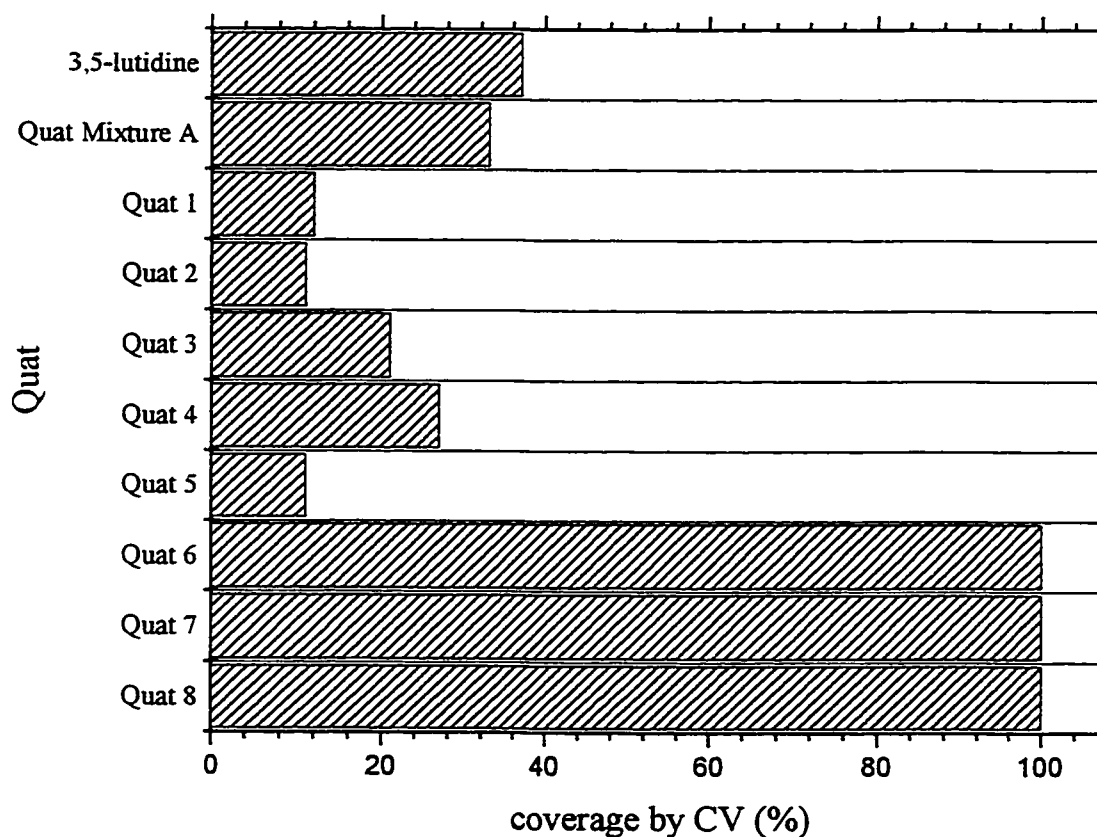


Figure 4-12. Percentage coverage of Pt, as gauged by the Pt oxide CV response, after addition of 70 μM Quat to deaerated 0.1 M NaOH solution, $s = 100 \text{ mV/s}$, time of exposure = ca. 30 minutes.

4.5.2 QCMB studies of Quat adsorption at Pt in 0.1 M NaOH solution

QCMB experiments were attempted using a Pt WE in 0.1 M NaOH, similar to the studies in neutral solution (Section 4.3.3). However, concurrent dissolution of Pt made this study difficult. Nevertheless, the addition of either Quat 6 or 7 to the solution created a non-reproducible initial change of frequency. This may have been caused by an irreproducible change in the solution viscosity or of the double layer properties as a result of the addition of Quat to the solution. It is not known why this was seen only in basic solutions. After these initial changes, the frequency remained relatively constant, while the CV response associated with oxide formation and reduction decreased with time of cycling. The mass then began to increase again after the CV currents were almost completely suppressed, as shown in Figure 4-13. These results are very different from those obtained in the neutral phosphate buffer solution (see Figure 4-9). Figure 4-13 seems to indicate that Quat adsorption was completed in a very short period of time in this 0.1 M NaOH solution. Potential cycling may then cause some structural change in the adsorbed layer, yielding a protective coating. However, the validity of these experiments is still questionable because of the unstable mass of the electrode prior to inhibitor addition, and the irreproducible initial frequency change seen immediately after its addition.

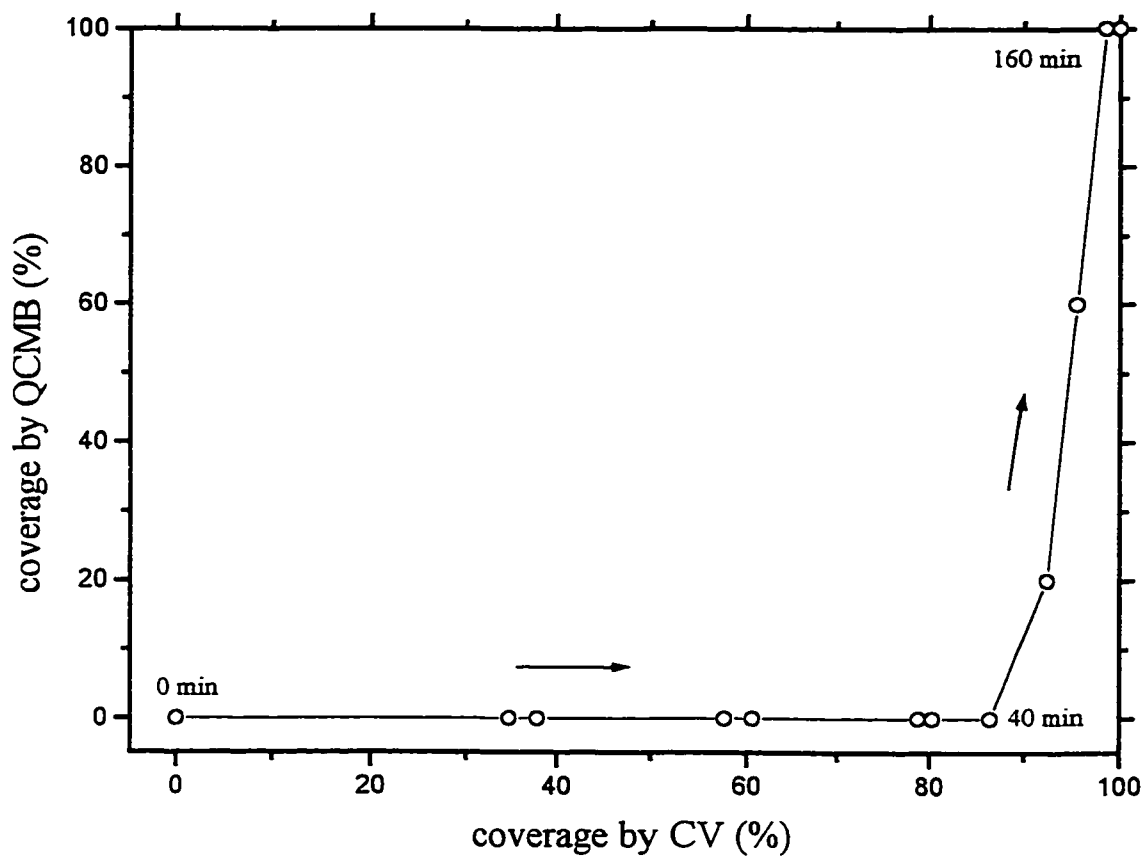


Figure 4-13. Coverage of Pt, determined from QCMB vs. from CV experiments, after addition of 50 μM Quat 7 to deaerated 0.1 M NaOH, $s = 100 \text{ mV/s}$.

4.6 Summary

Ranking of the Quats for their tendency to adsorb on Pt was achieved by comparing the amount of suppression of the Pt oxide reduction peak in 0.1 M NaOH. In general, higher coverage resulted from the addition of Quats with a longer hydrocarbon chain. Also, Quats containing a long side chain (Quats 6 to 8) were more strongly adsorbed than Quats with a long pyridinium chain. These results were comparable to those obtained on carbon steel using the standard corrosion wheel test at Travis Chemicals Inc. It is not clear if Quats prefer to adsorb on metallic or oxide coated surfaces, as adsorption appears to be independent of potential. The reasons for the preference of Quat adsorption in basic > neutral > acidic solutions also remain unknown from this work.

The CV data showed that the most strongly adsorbing Quats (Quats 6 to 8), not only suppressed the normal Pt electrochemical response, but also the rate of the HER. The coverage of Quat 7, calculated based on the degree of suppression of the Pt oxide reduction peak, was found to be linearly related to the absolute mass gain of the crystal in the first 30 minutes of exposure to a 40 μ M Quat containing neutral phosphate buffer solution. This coverage was at the monolayer level, based on the analysis of the mass change after this time. The orientation of adsorbed Quat 7 on the Pt surface could not be established unambiguously from this data. A further mass gain was seen with longer times of potential cycling. However, this did not lead to any further suppression of the Pt CV signal. Based on the mass gain, a bilayer structure is proposed after 3 hours of exposure to this solution.

V. ELECTROCHEMICAL BEHAVIOUR OF QUATS AT GLASSY CARBON (GC) IN NEUTRAL PHOSPHATE BUFFER SOLUTION

5.1 Glassy Carbon Electrodes

Carbon electrodes have been widely used in the past for fundamental electrochemical studies. They provide a wide potential window for cyclic voltammetry as they have a high overpotential for the hydrogen evolution reaction (HER) and do not dissolve or become oxidized readily at positive potentials [79]. Glassy carbon (GC) electrodes, one of the most common types of carbon electrodes, are impermeable to gases or liquids. They are hard and have a slightly lower electrical and thermal conductivity than do graphite electrodes [80, 81]. Because GC is hard, it cannot be utilized for QCMB measurements, since it would not oscillate with the quartz crystal if attached to the crystal surface [79]. Nevertheless, GC has been used extensively as a substrate for studies involving cyclic voltammetry, ac impedance spectroscopy, differential-pulse voltammetry, *in situ* electrochemical reflectance spectroscopy, scanning electron microscopy, X-ray photoelectron spectroscopy, scanning probe microscopy and other studies [82].

GC is prepared from polymeric resins, such as polyacrylonitrile or phenol/formaldehyde polymers, using a high temperature treatment which releases H, N, and O atoms from the resin and leaves an extensively conjugated sp^2 carbon structure [80]. The lattice structure and surface morphology of GC is a result of many factors [83], but it is beyond the scope of this thesis to examine these parameters in more detail.

5.1.1 Activation of GC surfaces

GC electrodes must be pretreated (also known as activated) in most cases in order to obtain a suitable electrochemical response for analytical applications. The most common type of pretreatment is the electrochemical activation process, which is used to obtain a reproducible electrode surface. Electrochemical activation involves anodizing the GC at a high oxidizing potential to allow the formation of a surface film. The graphite oxide film generated by this process is often porous, hydrated and nonconductive in nature, and it is believed to contain quinone-like groups and carboxylic functionalities [82]. Quinones, which are non-aromatic conjugated cyclohexadienones, can be synthesized by the oxidation of phenols or aniline [78]. However, since one of the main purposes of using the GC electrode in the present work was to eliminate the presence of surface oxide films encountered with Pt / Au electrodes, this electrochemical activation process was avoided here.

In order to obtain a fresh and reproducible GC surface for each experiment, mechanical polishing was used as the surface activation method in the present study. The mechanism of activation by polishing is not clear, since so many surface variables change during polishing [80]. Therefore, most laboratories have developed their own polishing procedure to produce a GC surface with unknown structure, but reproducible electrochemical properties. It should be noted that, in addition to the charging current, some faradaic current is often seen in the double layer region as a result of surface redox processes of the functional groups exposed by polishing [80]. Nevertheless, using a

carefully polished GC electrode, it was hoped that the adsorption of Quats on a GC electrode surface free of any other surface films could be detected.

5.2 CV Studies of Quat 6 at GC Electrode in Neutral Phosphate Buffer Solution

In Chapter 4 (Section 4.3.2), it was shown that, once sufficient Quats 6 and 7 had adsorbed on the Pt electrode surface in neutral phosphate buffer solution, the rate of the HER was sufficiently suppressed such that the lower potential limit could be extended to ca. -1.4 V vs. SSCE. This revealed a new set of redox peaks, clearly related to the presence of the Quats in solution. However, it was not possible to carry out a rigorous study of these redox peaks, due to some concurrent hydrogen evolution. Hence, this study of the redox chemistry of Quats 6 and 7 was initiated at GC electrodes.

Potential cycling of polished GC in the range of -1.5 to 1.0 V vs. SSCE in a 0.05 M KH_2PO_4 / 0.03 M NaOH pH 7.2 phosphate buffer solution (no Quat added) initially revealed a clean CV response, showing primarily only double layer charging current. There was no interference from the formation/reduction of an oxide film at positive potentials and only little current due to the HER was seen at negative potentials [79, 80, 81]. The CV response reached a steady-state after about 30 minutes of potential cycling (Figure 5-1, curve a).

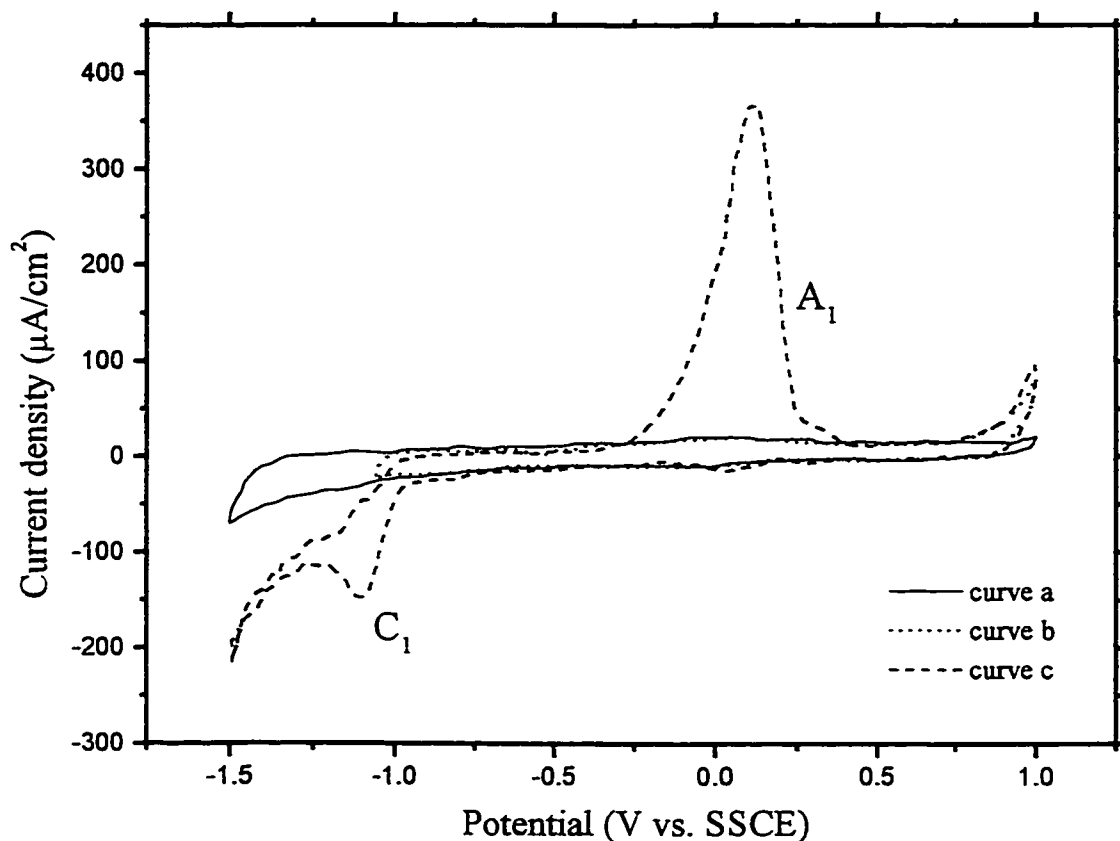


Figure 5-1. CV of GC in deaerated neutral phosphate buffer solution, $s = 100$ mV/s.
 curve a. no Quat;
 curve b. ca. 2 mM Quat 6 ($E_- = -1.0$ V);
 curve c. ca. 2 mM Quat 6 ($E_- = -1.5$ V).

Upon addition of 2 mM Quat 6 to solution, little evidence of its adsorption on the GC electrode between -0.65 and 1.0 V vs. SSCE (Figure 5-1, curve b) was seen, even though Quat 6 was found to be strongly adsorbed on Pt in the same potential range (Section 4.3.1). Adsorption would normally have been seen by a substantial suppression of the double layer charging current [84]. The absence of this could suggest that Quat 6 does not adsorb on a GC surface. Alternatively, the effect of the adsorbed Quat on the

interfacial capacitance may simply be too minor to detect. As stated above (Section 5.1), it is not possible to carry out the *in situ* mass measurement to seek the presence of adsorbed Quat 6 on the GC surface. It should be noted that the anodic current observed at potentials greater than ca. 0.85 V vs. SSCE is due to the oxidation of bromide ions [eq. 5-1][85], as confirmed by the addition of 2 mM KBr alone to the electrolyte solution (not shown in Figure 5-1).



Interestingly, a new pair of redox peaks, A_1 and C_1 , which are very similar to those observed at Au and Pt electrodes after the adsorption of Quats 6 and 7 (Figure 4-8), are revealed in Figure 5-1 (curve c) when E_- was extended to -1.5 V vs. SSCE. It should be noted that the anodic peak, A_1 , was resolved into two peaks at the early stages of the experiment (not shown), but the steady-state CVs showed only a single A_1 peak. Peaks A_1 and C_1 were not only observed at GC for Quats 6 and 7, but also for Quats 1 and 2 (the only other Quats examined at the GC electrode), which do not contain any functional group (see Table 3-3). This suggests that the redox chemistry in Figure 5-1 is associated with the pyridinium structure itself, rather than any of the attached functional groups. Because peaks A_1 and C_1 were not as well formed and not as stable for Quat 7, as for Quat 6, the following discussion will focus on the electrochemical behaviour of Quat 6 at GC in neutral phosphate buffer solution.

5.2.1 Reduction is required prior to oxidation

The fact that the anodic peak (A_1), centered at 0.0 V, is not observed when E_- is -1.0 V (Figure 5-1, curve b) proves that the two peaks (A_1 and C_1) are coupled and that Quat reduction is required prior to its oxidation. These two redox peaks decrease slightly in size and the A_1 peak appears to shift positively with long times of cycling. These results suggest that the reduced products are not fully re-oxidizable, and that some unreacted products may build up on the GC surface with time. The peak potentials and the rate of decrease of the two redox peaks varied somewhat for the different Quats. In general, when the pyridinium charge is expected to be more positive (i.e., in the presence of a substituted electron-withdrawing group on the ring, as in Quat 6), the C_1 peak potential is somewhat less negative. This result shows that the C_1 peak is associated with the reduction of the pyridinium nitrogen of the Quats. However, it should be noted that the potentials of peaks A_1 and C_1 may also move due to other factors (i.e., film resistance, reaction kinetics, etc.), so that shifts of these peak potentials cannot be reliably interpreted.

5.2.2 Diffusion controlled cathodic process (C_1)

It was found that the A_1 and C_1 peak currents increased linearly with increasing Quat concentration. However, the shape of the C_1 peak and its slight overlap with the HER complicated the determination of its peak current. Therefore, Figure 5-2 only shows

the A_1 peak current density as a function of Quat concentration in the phosphate buffer solution.

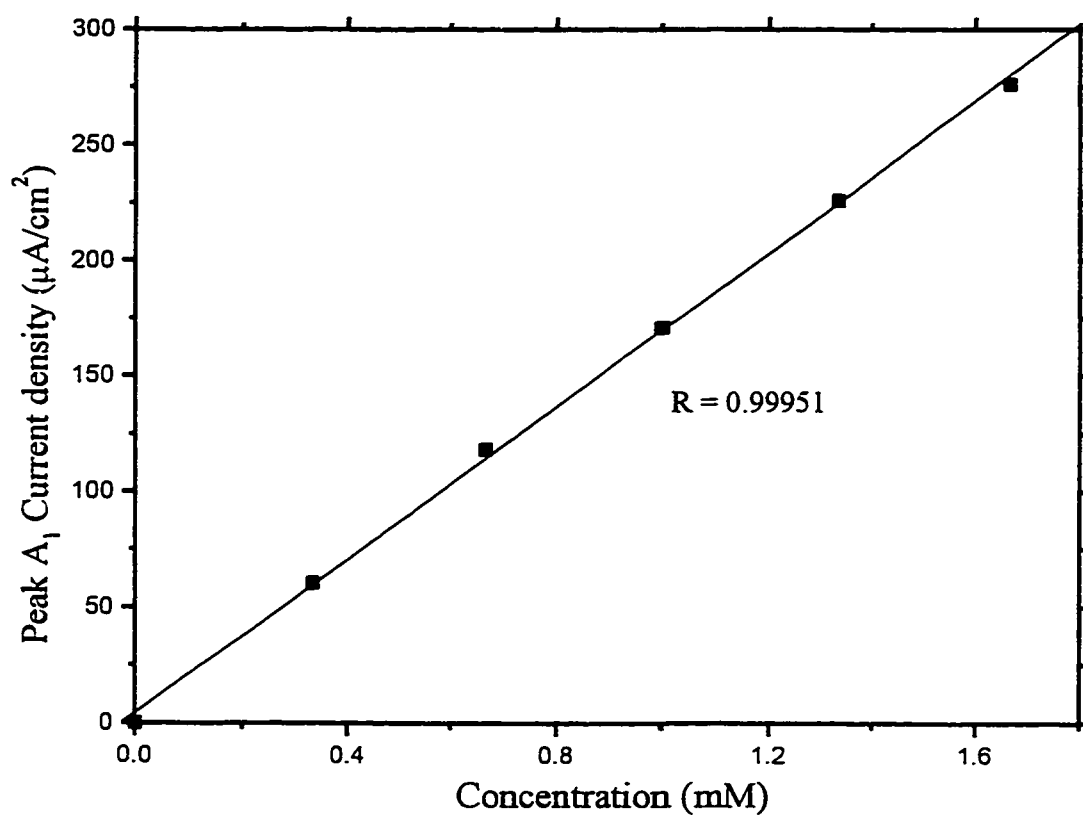


Figure 5-2. Anodic peak (A_1) current density as a function of Quat 6 concentration in deaerated neutral phosphate buffer solution, $s = 100 \text{ mV/s}$.

It should be noted that the A_1 and C_1 peak currents (and hence charge) also increased significantly with solution stirring. The fact that the peak currents increased with both increasing concentration and solution agitation strongly suggests that a solution

diffusion controlled process is involved in this study. Since the C_1 peak current became much noisier when the solution was stirred vigorously by N_2 bubbling, the cathodic reaction was most likely solution diffusion controlled. However, this stirring effect seemed to diminish with time of cycling, and the CV obtained in a stirred solution was eventually very similar to that in an unstirred solution. It is possible that a buildup of unoxidized film material on the GC surface with time could cause the rate of the reaction to become controlled by factors other than solution diffusion.

In order to examine the diffusion controlled characteristics of this reduction process (C_1) further, the effect of scan rate on the cathodic peak current was tested in the early stages of the experiments. The zero current baseline was estimated in the same way in each of the scan rate experiments for consistency, assuming that the small current due to the HER was the same in each experiment. The C_1 peak current density was found to have a square root scan rate dependency, as shown in Figure 5-3. This demonstrates again that the cathodic process (C_1) is indeed governed by a solution diffusion process, likely the transport of the Quat from the solution to the electrode surface, at this early stage of experimentation.

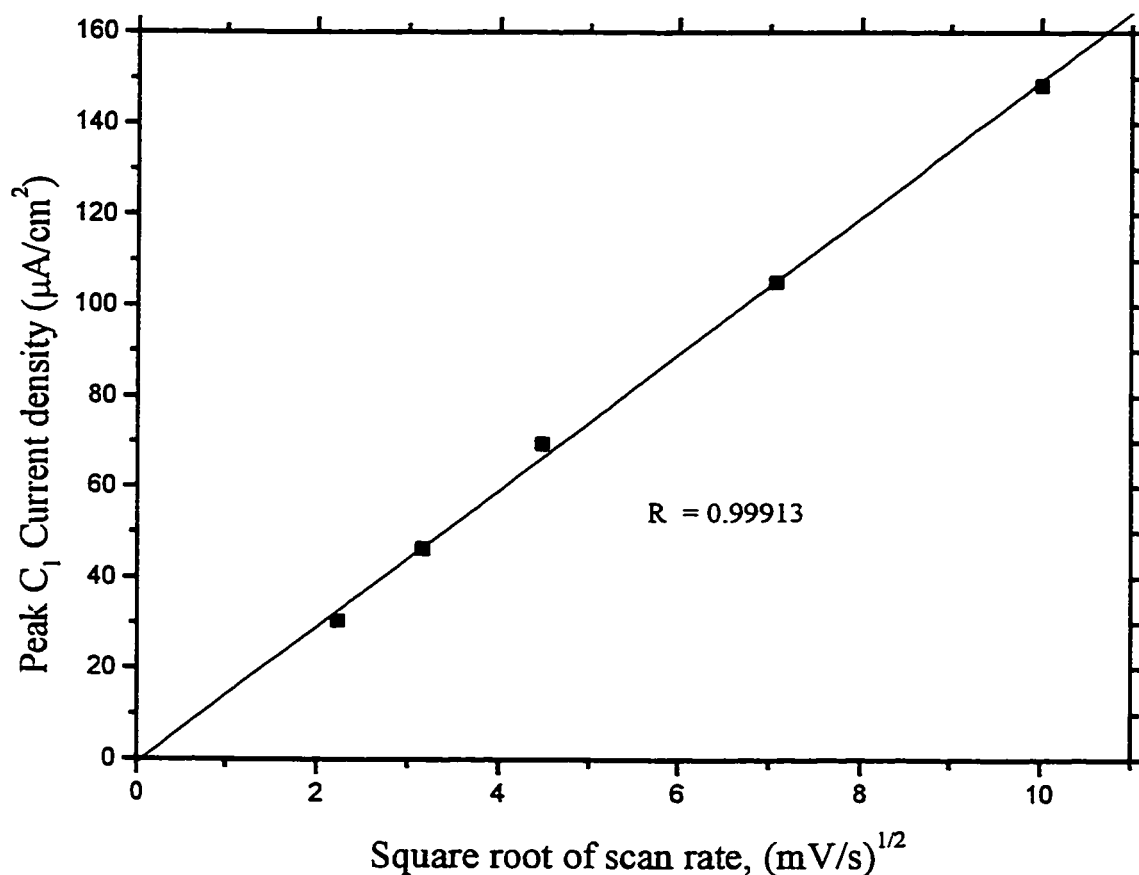


Figure 5-3. Dependence of the C₁ peak current density on $s^{1/2}$ with ca. 2 mM Quat 6 in neutral phosphate buffer solution.

5.2.3 Proposed reductive deposition / oxidative removal mechanism

When E_{+} was lowered to prevent the oxidation process at -0.2 V, but retaining an E_{-} of -1.5 V, the C₁ peak was still present, but its size decreased with each cycle of potential (Figure 5-4, curve b). The capacitance of the double layer also seemed to be decreasing with time in these experiments, suggesting that the cathodic process (C₁)

resulted in the deposition of some reduced product on the electrode surface with each cycle of potential. Therefore, when the anodic process (A_1) was not permitted to occur, more Quat was reduced and deposited on the GC surface in each cycle. The deposition of this reduced species blocked the electrode surface, reducing the activity of the surface towards further Quat reduction and decreasing the capacitance of the double layer.

When E_{r} was then extended back to its original value (from -0.2 V to 1.0 V), a very large anodic peak appeared in the next positive scan (Figure 5-4, curve c). It can be seen that the potential at which this oxidation process occurs has shifted positively, suggesting that it now required a larger driving force. This may indicate that the deposited products are not very conductive and therefore a higher surface resistance is present, or that the redox reaction has itself become more irreversible. The reappearance of both redox peaks (A_1 and C_1) implies that the A_1 peak is related to the corresponding oxidative removal of the deposited products formed in the cathodic peak (C_1). Hence, when the oxidation was allowed to re-occur, the deposited products were removed from the electrode, allowing more Quat to be reduced in the following cycles.

In order to further examine the behaviour of this system, the GC electrode was removed from the solution at $E_{\text{r}} = -1.5$ V. It was then rinsed, and blotted carefully with a tissue to remove any adhering solution and then placed in fresh phosphate buffer solution (without any added Quat). When the potential of the working electrode was scanned positively from -1.5 V, the anodic peak (A_1) was observed again. The cathodic peak (C_1) at -1.0 V was not seen in the following cathodic scan, and the A_1 peak decreased in size very quickly with each cycle. The A_1 peak disappeared fully after ca. 5 full cycles. These

results clearly show that the deposition of a reduced surface film occurs at negative potentials in the Quat containing solution, that it re-oxidizes in the A_1 peak, and that the product then re-dissolves in solution.

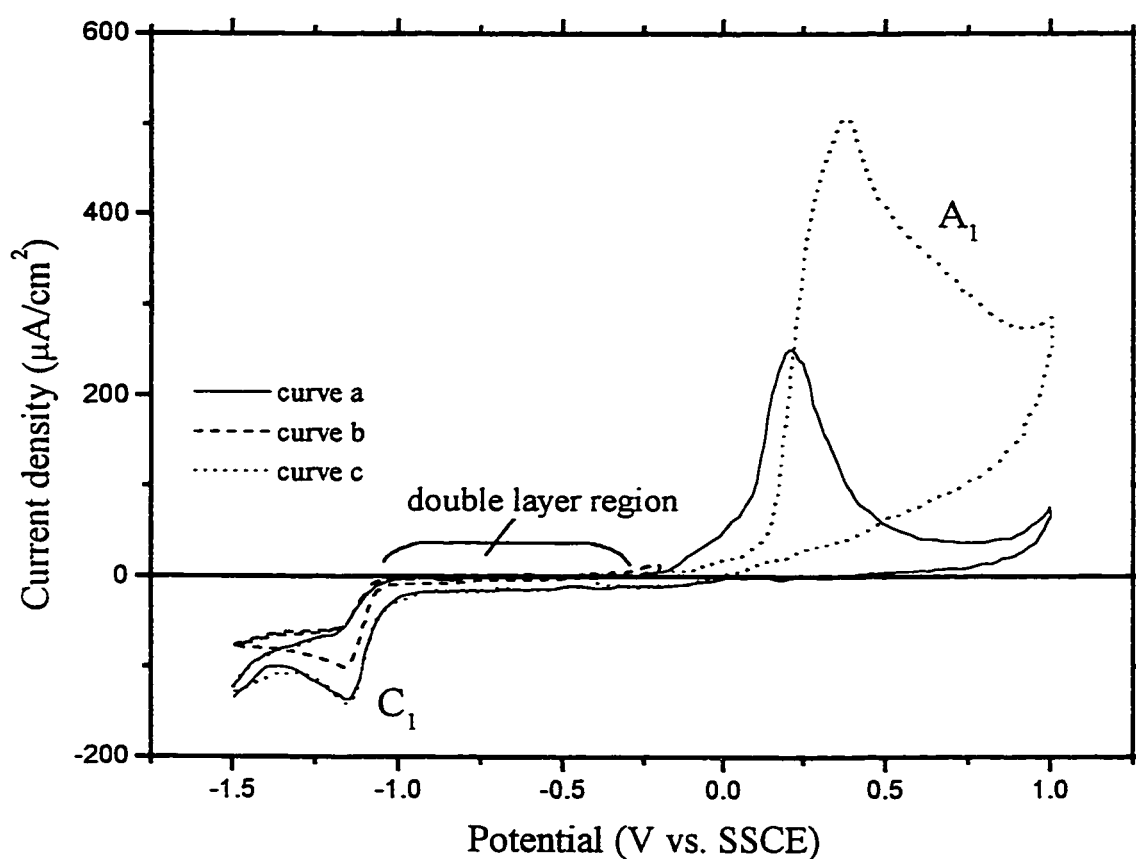


Figure 5-4. Large A_1 peak seen after Quat oxidation was prohibited, at GC, ca. 2 mM Quat 6 in deaerated neutral buffer solution, $s = 100$ mV/s.
 curve a. steady-state CV with $E_{\text{+}}$ at 1.0 V;
 curve b. 5th cycle with $E_{\text{+}}$ at -0.2 V;
 curve c. 1st cycle with $E_{\text{+}}$ set back to 1.0 V.

5.3 Quat Multilayer Deposition at GC Electrode

Experiments were then designed to examine the effect of time of holding at E_- (-1.5 V) in the presence of ca. 4 mM Quat 6 in the pH 7.2 phosphate buffer solution. The A_1 peak at 0 V in the following anodic scan was expected to increase in size with holding time at E_- . This result was indeed observed in these experiments. A plot of the A_1 charge density as a function of holding time at E_- is illustrated in Figure 5-5. The charge density appeared to reach a threshold value of ca. $4000 \mu\text{C}/\text{cm}^2$ after holding at E_- for ca. 20 minutes. A similar charge density was also obtained when a very slow cathodic scan rate (i.e., 5 mV/s) was employed, as shown in Figure 5-6.

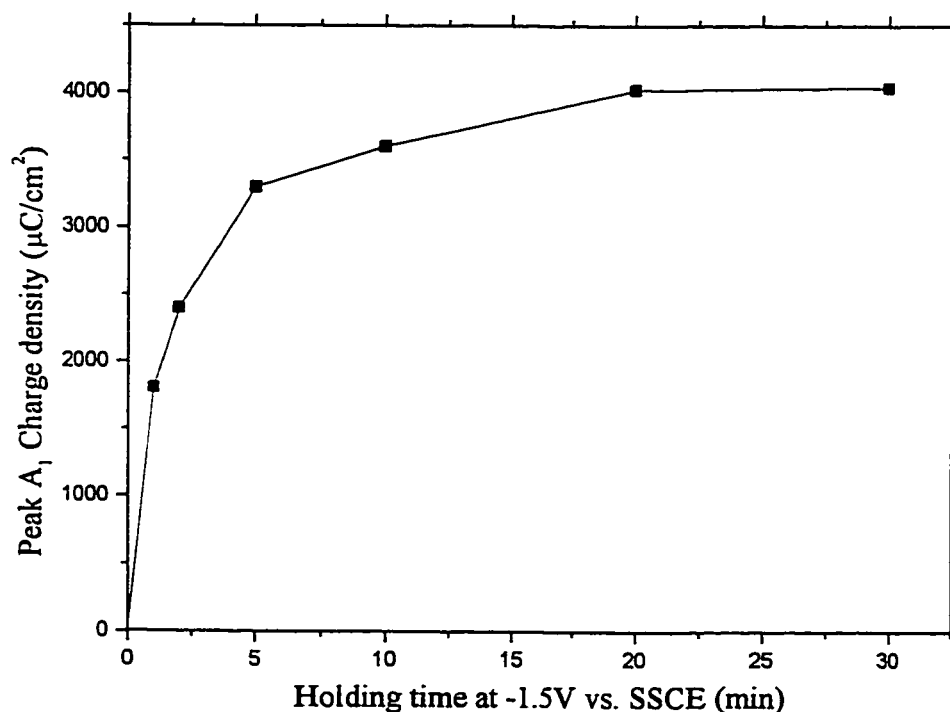


Figure 5-5. Charge density of A_1 peak at GC as a function of holding time at -1.5 V vs. SSCE with ca. 4 mM Quat 6 in deaerated neutral phosphate buffer solution.

Figure 5-6 also shows that the anodic and cathodic charges are very similar, especially at high scan rates, confirming that most of the reduced products are being reoxidized in this particular set of experiments and also that the baseline beneath peak C_1 is being appropriately selected, in general.

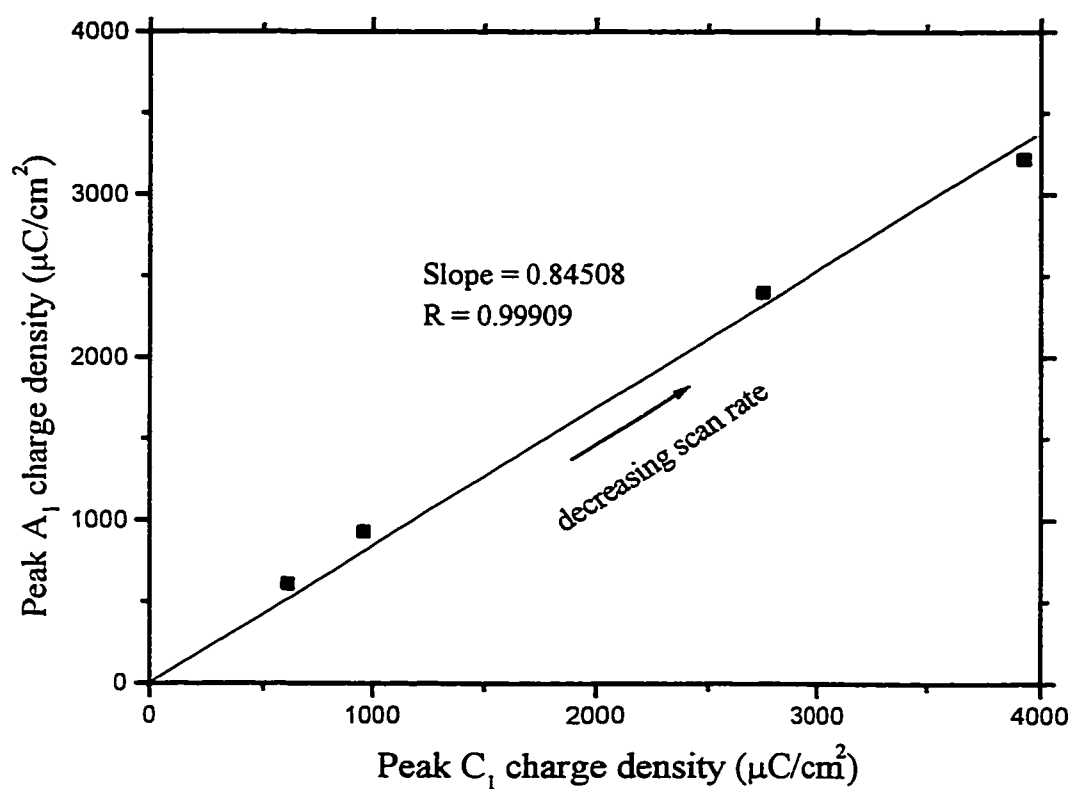


Figure 5-6. Anodic vs. cathodic charge density with ca. 4 mM Quat 6 in deaerated neutral phosphate buffer solution at different scan rates.

The charge density observed is much greater than that expected from monolayer coverage. It was estimated in Section 4.5 that the minimum surface area of Quat 7 (very similar to Quat 6 in structure) on the electrode surface is ca. 20 \AA^2 . This number is a reasonable estimation, as shown by Rahman et al [86]. In their work, each pyridine molecule occupies ca. 24 \AA^2 on various oxide surfaces, based on the analysis of adsorption data using the Langmuir equation. Assuming that the reduction reaction involves a two electron process (Section 5.4.1), if each molecule of Quat occupies 20 \AA^2 , this yields $5 \times 10^{14} \text{ molecules/cm}^2$ for one monolayer of Quat (i.e., 160 \mu C/cm^2). Therefore, 4000 \mu C/cm^2 would be equal to ca. 25 monolayers. It is not clear at this time what the structural and electrical properties of this relatively thick film are. Clearly, there is sufficient conductivity for film oxidation to occur at all, although the large separation of peaks A_1 and C_1 is a likely indication of the presence of some film resistance. Also, efforts to form more than ca. 4000 \mu C/cm^2 of reduced product were not successful. Future work should include efforts to analyze the film product using NMR and MS techniques.

The ratio of the peak A_1 to peak C_1 charge density is significantly less than 1 at low scan rates (Figure 5-6). This deviation may be a result of the fact that not all of the reduced species can be re-oxidized in the next anodic cycle, as discussed in Section 5.2.1. Another factor may be that some charge due to the HER is included in the total measured cathodic charge. Since the HER rate is independent of scan rate, a relatively higher charge would be passed at slower scan rates, consistent with Figure 5-6.

5.4 Proposed Redox Mechanism of Quats at GC Electrodes

5.4.1 Reduction/oxidation of Quat as a monomer

Figure 5-7 shows a possible mechanism for Quat monomer reduction (this does not include multilayer formation). Previous workers [87, 88] have suggested a similar redox mechanism for the reduction of dihydronicotinamide adenine dinucleotide (NADH), which has a very similar structure to that of the Quats studied here. Interestingly, some of the by-products formed in the production of NADH are often used in the commercial Quat mixtures in industry. Volke et al [37, 89] has also proposed a similar reduction mechanism for analogous substituted pyridinium compounds, but in aprotic solvents.

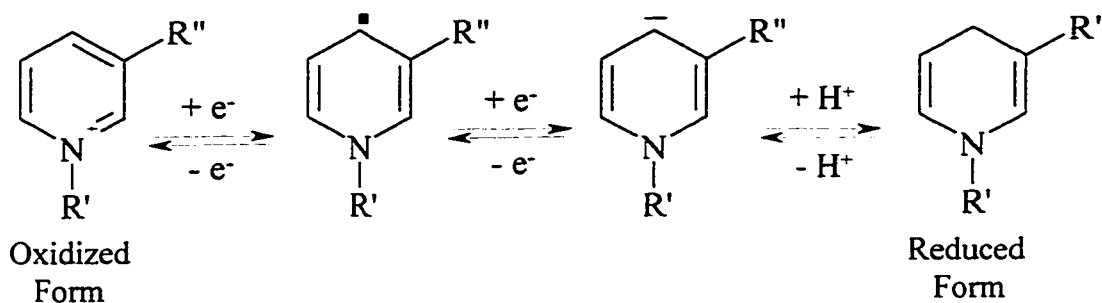


Figure 5-7. Proposed redox mechanism of a typical Quat monomer.

This proposed mechanism shows that the reduced product can be re-oxidized, forming the original structure and hence, that the reaction can be reversed. When the Quat is reduced, it loses its positive charge and becomes a neutral species (i.e., a tertiary

amine). This neutral organic molecule would tend to come out of the polar aqueous solution and deposit on the GC electrode surface. When it is re-oxidized, it would regain its positive charge and likely re-dissolve. Two electrons and one proton are required in order to reduce the positively charged pyridinium compound to a neutral species in this mechanism. This would be consistent with a shift of the reaction redox potential negatively by -29.5 mV per pH unit. However, it was very difficult in this study to track the dependence of this reaction with pH due to its irreversibility and the notable effect of the amount of reduced material deposited on peak C₁, and therefore, this predicted pH dependency could not be tested.

5.4.2 Dimerization mechanism

The radical intermediate suggested to form in the proposed mechanism in Figure 5-7 can also initiate the formation of other products. For example, when two of these species react together, a dimer (Figure 5-8a) could be formed if steric hindrance is not a factor (see the study by Volke et al [37] in Section 2.1.4.2). Each dimer would require two electrons to produce the initial two radicals. However, the cleavage of any bonds in the re-oxidation step is not likely and therefore, the reaction in Figure 5-8a would probably be irreversible. Instead, a dimeric oxidation product has been suggested in Figure 5-8b. It should be noted that this redox mechanism would result in an anodic to cathodic charge ratio of 2. One electron would be required to form each radical (two electrons per dimer), while four are required in the oxidation step. As was shown in

Figure 5-6, in the early stages of experimentation, the charge density in peaks A₁ and C₁ are essentially the same, thus ruling this process out under those conditions. However, after long times of exposure of the GC electrodes to the Quat solutions, the residue which appears to build up on the surface may, in fact, be related to the formation of this type of dimer.

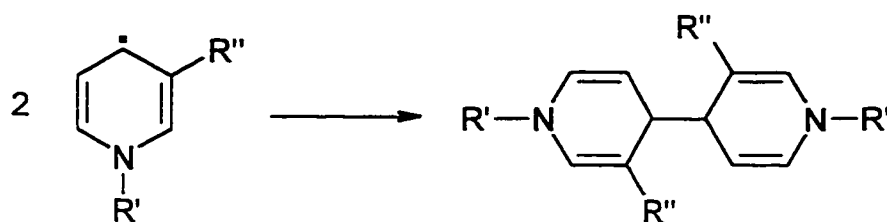


Figure 5-8a. Dimerization of two radical intermediate species.

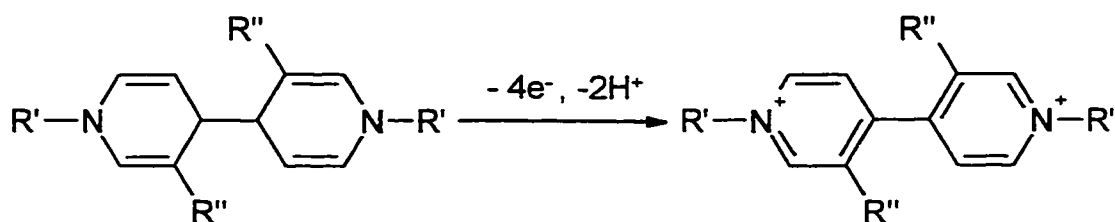


Figure 5-8b. Possible re-oxidation of the dimer.

5.4.3 Possible non-electrochemical Quat polymerization route

It should be noted that the radical intermediate may also initiate a non-electrochemical polymerization process, as shown in Figure 5-9. This polymerization

reaction would require the loss of one proton per Quat for its propagation, and may be more significant in basic solutions. Indeed, in exploratory experiments carried out in 0.1 M NaOH solutions, a yellow product was often seen to deposit on the electrode surface [90]. This may indeed reflect the formation of some polymeric product under these conditions. It is notable that a polymeric product is not likely to be electrochemically oxidizable. However, the formation of this type of polymeric product, along with the products from dimerization, could be consistent with the non-reactive residue which builds up on the electrode surface with time.

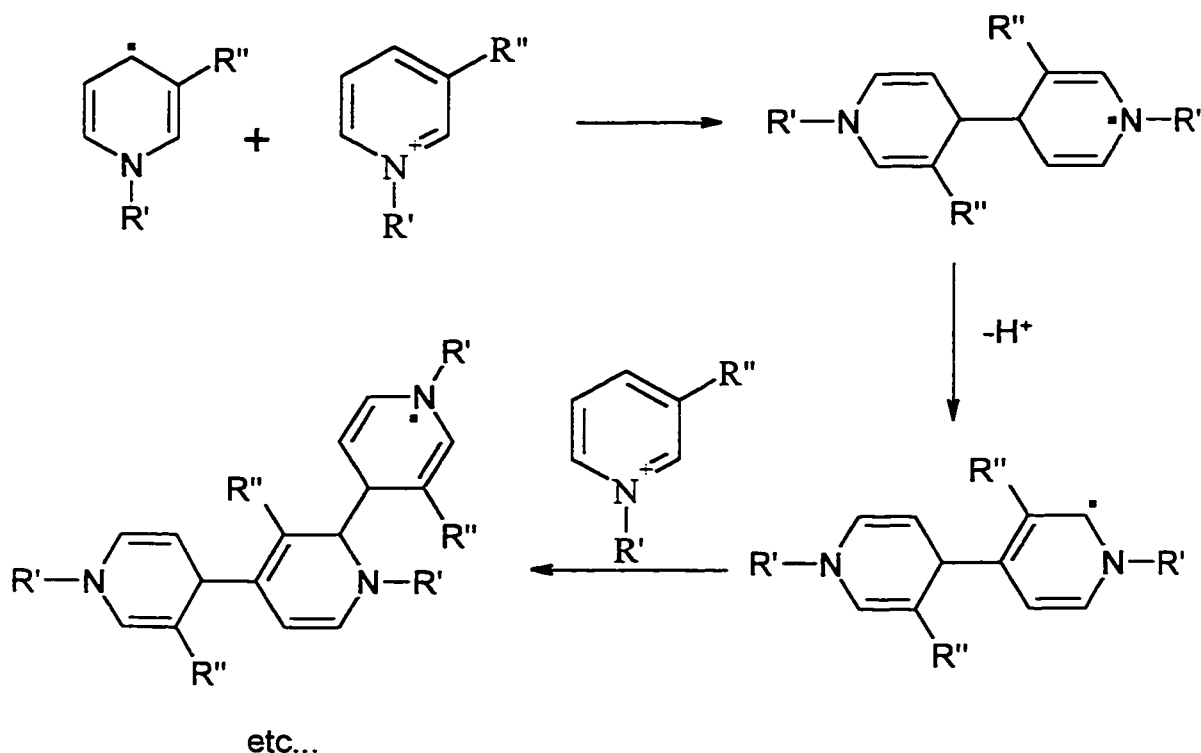


Figure 5-9. Possible non-electrochemical polymerization route of a typical Quat.

5.5 Summary

Little evidence for Quat adsorption on GC electrodes was seen in the normal Pt potential range (i.e., -0.65 to 1.0 V vs. SSCE), even when Quats 6 and 7 (which were strongly adsorbed on Pt and Au electrodes in Chapter 4) were added to neutral phosphate buffer solutions. This indicates that either the Quats prefer metal or oxide coated surfaces for adsorption, or that the interfacial capacitance change at GC electrodes is too small to be measured.

However, all Quats have been found to be reducible at more negative potentials (ca. -1.15 V vs. SSCE) at GC electrodes in neutral phosphate buffer solutions. The rate of reduction is controlled by the rate of diffusion of the Quats to the GC surface, and the reduced products form a surface film up to ca. 25 monolayers in thickness. The structure and electrical properties of this film remain unknown from this study. However, in the early stages of experimentation, essentially all of this film product can be re-oxidized and redissolved at ca. -0.25 V vs. SSCE, in two overlapping anodic peaks. It is most likely that the reduced product is the neutral monomer, and the two peaks may reflect deposit of different morphology or crystallinity. The slow buildup of some non-oxidizable residues on the electrode surfaces may indicate that some dimerization and/or polymerization products are formed with time of cycling.

VI. CV AND acZ STUDIES OF CARBON STEEL IN CO₂ SATURATED NACE BRINE SOLUTION

6.1 Corrosion Involving Carbon Dioxide

The oil and gas industry often faces corrosion problems that arise from the presence of large quantities of salt water containing CO₂ and/or H₂S in pipelines and down-hole drilling equipment. These gases usually are by-products from the production of natural gas and oil [2]. Corrosion involving CO₂ is a complex process. Its rate is affected by a combination of environmental conditions [26, 91, 92, 93, 94] such as pH, temperature, pressure, solution chemistry, flow and metallurgy.

6.1.1 Pitting corrosion in CO₂ environment

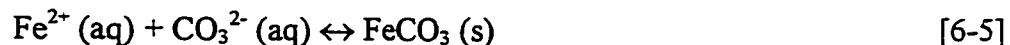
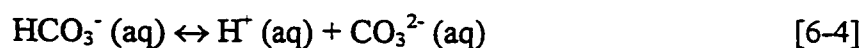
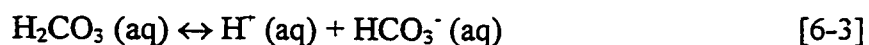
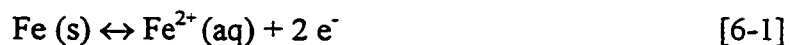
A pit is defined as “a hole that develops in a metal surface such that its width is comparable with, or less than, its depth” [14]. It is an example of non-uniform corrosion, also known as localized corrosion, caused by the variations in reactivity of a surface. Pits are often seen at the “6 o’clock” position on the inside walls of failing pipes where salt water containing high concentrations of CO₂ may accumulate.

The study of pitting is a difficult task and the use of electrochemical techniques for its study is still at an early stage. Attempts have been made to correlate the pitting process with impedance measurements [95]; however, there is no simple correlation between the development of pits on electrodes and these results.

6.1.2 General corrosion in CO₂ environment

Another common corrosion process involving CO₂ is called general corrosion, also known as uniform corrosion. In this process, a film of corrosion product usually accumulates on the metal surface. This corrosion product is often a surface film of iron carbonate in the form of siderite (FeCO₃) [1, 26, 96, 97]. It has also been suggested that products such as Fe(HCO₃)₂, Fe(OH)₂, γ-Fe₂O₃, Fe₃O₄, and Fe₃C [96, 98, 99] form, depending on the conditions.

FeCO₃ surface film formation occurs when the turbulence of flow is not high enough to prevent its formation and in the presence of water chemistry which makes the solid FeCO₃ corrosion product stable [99]. Some of the processes involved are:



The concentration of each of these solution species can have a major impact on the stability of the FeCO₃ product formed on the metal surface.

6.2 Study of Quats at Steel Electrodes in CO₂ Saturated Brine Solution

As this research project was intended to establish an electrochemical test method which could rank the efficacy of corrosion inhibitors, it was necessary to test the best performing Quats (as determined at Pt electrodes in Chapter 4) at carbon steel substrates, the material encountered in practice. This study was carried out in CO₂ saturated synthetic ocean brine solution instead of H₂S saturated solution because of the safety concerns regarding the handling of H₂S.

When only Quat 6 or 7 (which were the strongly adsorbing Quats at noble metal electrodes, see Chapter 4) were added to the brine solution, somewhat surprisingly, their presence had little or no effect on the impedance and CV results for steel electrodes in CO₂ saturated brine solution (not shown). Even the addition of the commercial Quat solution (Quat Mixture A, see Table 3-3) or Quat 3 (which had a similar adsorption behaviour to Quats 1, 2 and 4) did not have any significant effect on the impedance and CV results. This suggests that the additives in the formulation (mainly surfactants and so-called “filmers”, which include high molecular weight amines, imidazolines and fatty acids, etc.) are required in order for the Quats to function at steel in a CO₂ environment. This result is in contradiction with the very significant coverage of Quats 6 and 7 on Pt, as discussed in Chapter 4. Indeed, there was no significant difference observed between the electrochemical response of steel after the addition of additives alone vs. the addition of additives plus the Quats (i.e., corrosion inhibitor formulation). Even though Quats were considered to be the active ingredient of the inhibitor mixture in sour systems (this was not

tested in this thesis work), their function in sweet systems is not known with certainty. It may be that the main function of the Quats is to increase the solubility of the inhibitor mixture so that it can reach distant areas (e.g., the end of a pipeline or deep into a drilling hole) in sweet systems.

These results were further verified by experiments conducted at Travis Chemicals Inc using their high temperature (60 °C) impedance system and autoclaves. It should be noted that ammonium bisulfite was added to the brine solutions as an oxygen scavenger in these experiments, therefore these data might not be reliable (see Section 6.4.1). Nevertheless, the results clearly showed that the impact of the addition of the additives on the acZ of steel was much greater than that from the addition of the Quats.

For this reason, this chapter summarizes the results obtained, using CV and acZ techniques, for steel electrodes, with and without the addition of the corrosion inhibitor formulation (Quat 7 with additives such as surfactants, emulsifiers and the so-called “filmers”, which include high M.W. amines, imidazolines and fatty acids). The study was performed in CO₂ saturated synthetic ocean brine solutions in order to gain more insights on the impact of the addition of inhibitors in CO₂ corrosion.

6.3 CV Studies of Steel Specimen in NACE Brine Solution

The setup of the cell used for the acZ measurements is described in Section 3.1.3. Cycling in the range of the OCP \pm 75 mV revealed an anodic “hysteresis response” of the carbon steel electrode in the NACE brine solution with no added inhibitor, as shown in

Figure 6-1. This behaviour may be interpreted as active pitting of the system under study during which the surface area of the WE increases within each cycle of potential [46].

Electrode surface preparation was found to be extremely important in this study. The degree of polishing used was reflected in the magnitude of the currents at the start of the experiment. It was found later that electrodes which were not hand-polished (i.e., as in the received condition), but were degreased in an ultrasonic bath, gave very reproducible pitting currents in the brine solution.

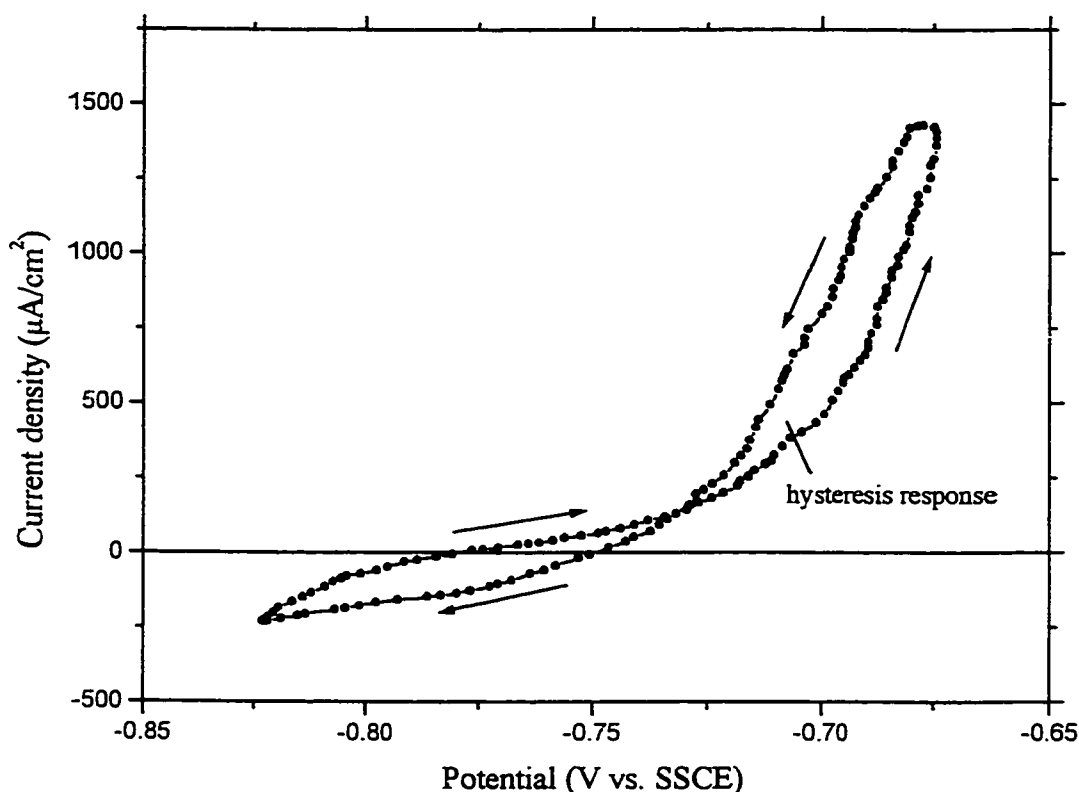


Figure 6-1. Typical CV of steel specimen in CO_2 saturated NACE brine solution, $s = 50 \text{ mV/s}$.

6.3.1 Correlation of acZ results with CV data

The acZ system allows CVs to be collected prior and after the acquisition of each set of ac impedance measurements. It was found that the CV results correlated well with the ac impedance measurements, with the suppression of the pitting current reflected by an increase in the measured resistance. An inductive loop was observed in the Nyquist plot at frequencies down to 0.01 Hz at the OCP, or when measurements were made at ca. 50 mV positive of the OCP (similar to the work by Shiri et al [9], see Section 2.1.4.1), as shown in Figure 6-2. This inductive behaviour at low frequencies was found to correlate well with the hysteresis response in the CVs. The acZ measurements were usually made at the OCP in this study and, under these conditions, the inductive behaviour was seldom seen.

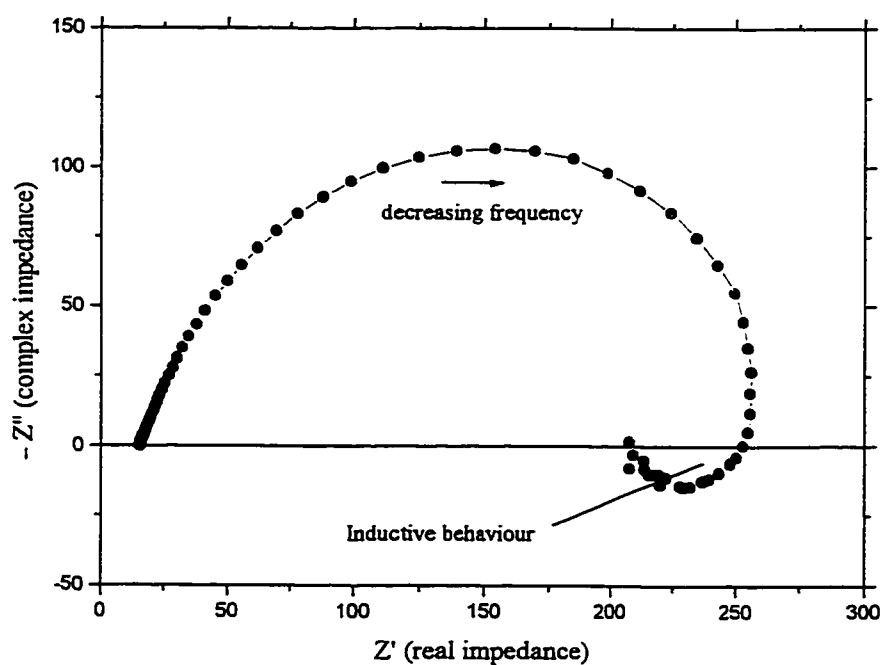


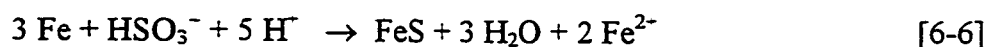
Figure 6-2. Illustration of the inductive behaviour of steel specimen in CO_2 saturated NACE brine solution at low frequencies, ac $V = \pm 10$ mV at +0.05 V vs. OCP.

6.4 acZ Studies of Steel Specimen in NACE Brine Solution Without Added Corrosion Inhibitor Formulation

6.4.1 Irreproducible results

In many cases, the acZ data for steel specimens in the NACE brine solution containing no added corrosion inhibitors, also referred to as the “blanks”, were scattered and unreliable. It was found that many experimental factors had to be carefully controlled in order to obtain meaningful results. Cleaning of the cells and of the counter and fourth electrode surfaces were all extremely important for these measurements, as transfer of inhibitor from previous experiments can increase the resistance of the “blank” under study significantly.

The addition of ammonium bisulfite, normally used as an oxygen scavenger, was found to be problematic, as the blank sample resistance (diameter of semi-circle) was seen to increase with time, as shown in Figure 6-3. It is now believed that excess bisulfite will react with iron to form an iron sulfide surface film [eq. 6-6], perhaps the blackish film often seen on working electrode surfaces at the end of these experiments [23].



The presence of this film would increase the resistance of the system, in agreement with the ac impedance measurements. Partly based on our results, ammonium bisulfite has now been replaced by ferrous sulfate (FeSO_4) as the oxygen scavenger in experiments carried out at the Travis Chemicals Inc laboratory.

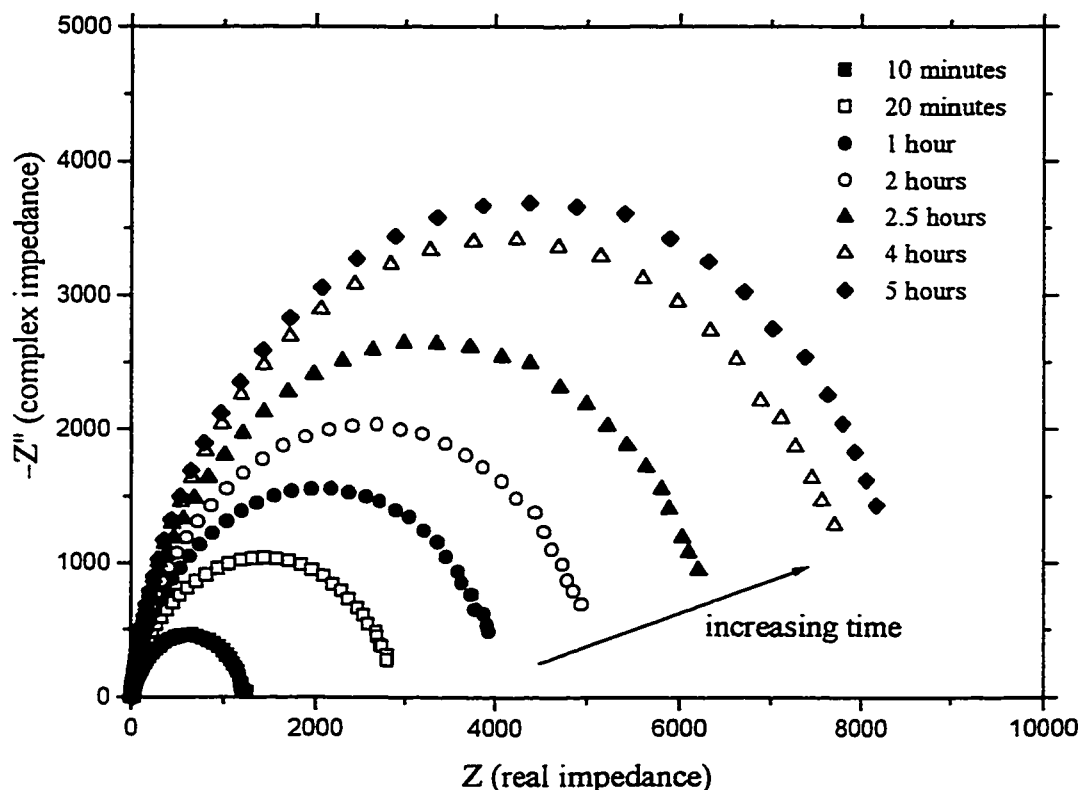


Figure 6-3. Nyquist plots of steel specimen as a function of time in CO_2 saturated NACE brine solution with ammonium bisulfite added as oxygen scavenger, $\text{ac V} = \pm 5 \text{ mV vs. OCP}$.

6.4.2 Equivalent circuit approach analysis of acZ data

Numerous attempts were made to fit the impedance results of the blanks to different variations of the Randles circuit [27, 100] and other circuits [40, 101]. It was found that a $R_s (R_1 \text{ CPE})$ circuit, as shown in Figure 6-4, seemed to be a good representative circuit for these blanks (circuit elements are discussed in Section 2.2.2.1).

It should be noted that R_s denotes the solution resistance between the WE and RE and that this value is inversely proportional to the conductivity of the electrolyte solution. The value of $R_1 + R_s$ obtained should be comparable to the R_p value obtained from the LP technique.

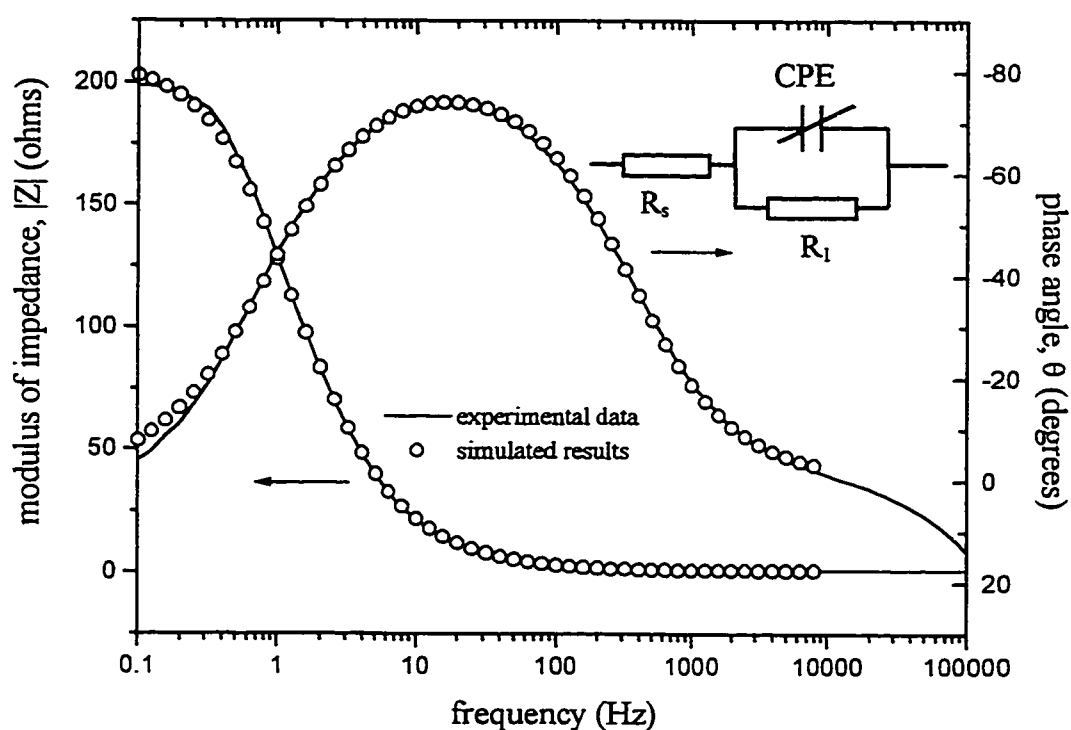


Figure 6-4. Overlay of acZ data of a blank in CO_2 saturated NACE brine solution to the R_s (R_1 CPE) circuit shown, ac $V = \pm 10$ mV vs. OCP.

From the overlay shown in Figure 6-4, the values of the circuit elements for this particular set of data were $R_s = 0.95 \, \Omega$, $R_1 = 1894 \, \Omega \, \text{cm}^2$, $\text{CPE} = 115 \, \mu\text{F}/\text{cm}^2$ and $n = 0.908$. Note that the impedance of a CPE is described by [eq. 2-13] in Section 2.2.2.1b. The chi squared value was 2.61×10^{-4} when some of the high frequency points were removed from the data set, hence the standard deviation of the fit was ca. 1.6 %. The high frequency data were not included because an inductance from an artifact was present [43], as seen from the positive phase angles of the data points above 10 kHz.

It should be noted that the fit of the overlay is not very good at low frequencies. Since an inductor would be expected to be present (due to pitting) if the impedance were measured at even lower frequencies, it would be logical to incorporate an inductor into the equivalent circuit to compensate for this deviation at low frequencies. Interestingly, when an inductor was added to the circuit (i.e., $R_s (R_1 \text{ CPE } L)$), the fit of the data points at low frequencies was greatly improved (i.e., a decrease in standard deviation from 1.6 % to 0.93 % was seen) with no significant change in the values of the other circuit elements (Figure 6-5). The value of L obtained from this fitting was $2021 \, \mu\text{H} \, \text{cm}^2$.

6.4.3 Change in impedance and open circuit potential with time

The impedance of each blank was measured as a function of electrode immersion time in the brine solution. Figure 6-6 shows that the total resistance of the system (i.e., R_1) increased in the first few hours, and then decreased again with time. On the other hand, the values of the constant phase element and the inductance decreased slightly

at the beginning of the experiment and then increased with time, as shown in Figure 6-7. The standard deviation of the fit to the circuit of Figure 6-5 ranged from 0.63 to 1.9 % in a random fashion. It should be noted that the solution resistance (R_s) remained at ca. $1\ \Omega$ throughout the experiment.

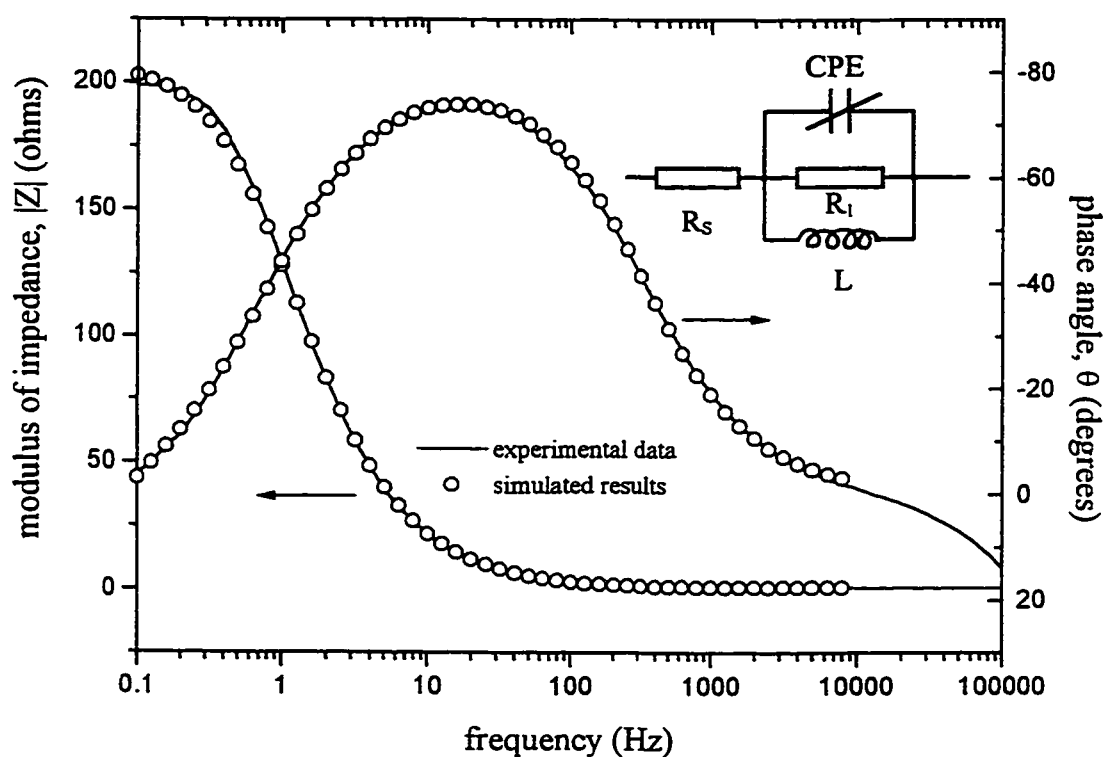


Figure 6-5. Overlay of acZ data of blank (same data as Figure 6-4) to the R_s (R_1 CPE L) circuit shown. Notice the great improvement of the fit at low frequencies.

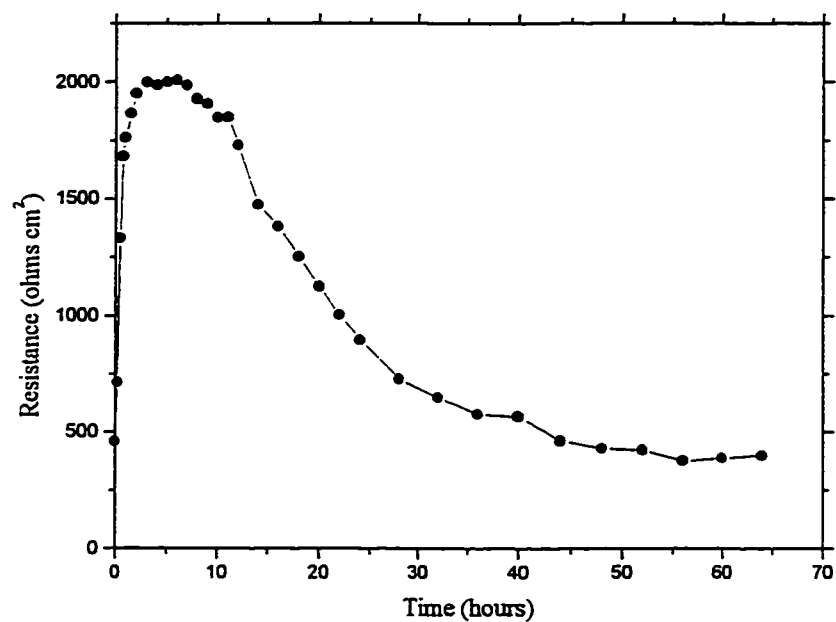


Figure 6-6. Change in R_1 with electrode immersion time in CO_2 saturated NACE brine solution with no added inhibitor.

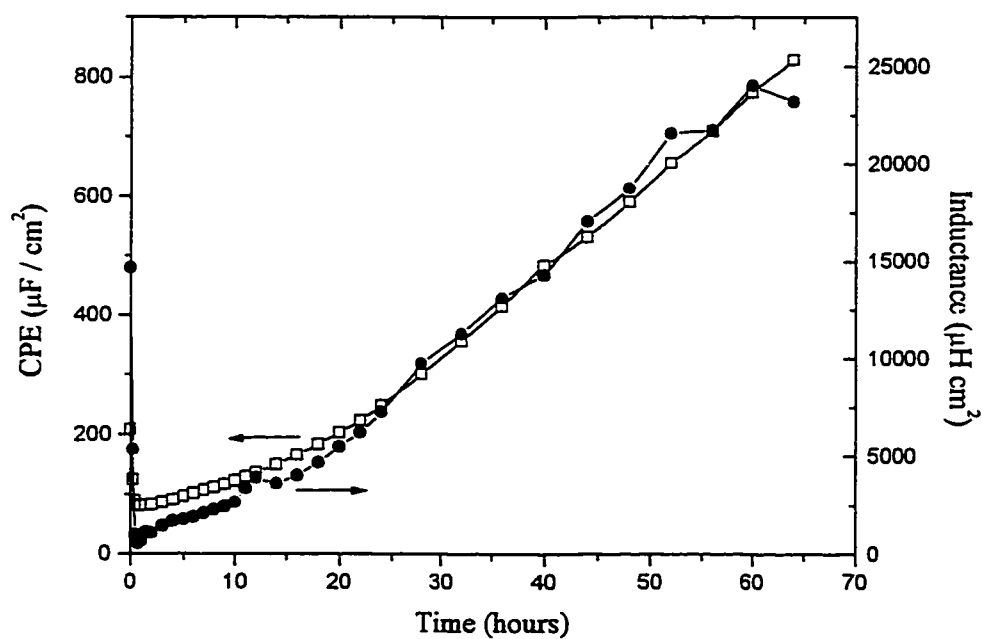


Figure 6-7. Change in the CPE and the inductance with immersion time in CO_2 saturated NACE brine solution with no added inhibitor.

The n values were 0.90 ± 0.02 , suggesting that the CPEs are non-ideal capacitors. After ca. 65 hours, this non-ideal capacitor reached a value of $> 800 \mu\text{F}/\text{cm}^2$, which seems very high for a double layer capacitance response. Therefore, it is possible that more than one time constant may exist in the system, but that the difference between the two time constants is too small (less than two orders of magnitude) for them to be separated from one another. Alternatively, the surface of the blank may become roughened with time of exposure to solution, so that the true value of the CPE would be lower. Interestingly, the change of the OCP of the system shows almost the opposite trend as does the change in resistance, as shown in Figure 6-8.

Generally, the change in impedance and OCP for the blanks can be seen to occur in three stages:

First stage (ca. 0 to 2 hrs): R increases and OCP shifts positively.

Second stage (ca. 2 to 20 hrs): R decreases and OCP shifts negatively.

Third stage (ca. 20 to > 60 hrs): R decreases and OCP shifts positively.

6.4.4 Corrosion mechanisms of steel in NACE brine solution without added inhibitor formulation

With the use of an Evans-Hoar diagram [102], one can gain information regarding corrosion mechanisms. A simplified representation of a corrosion process is illustrated in Figure 6-9. One can attempt to identify the rate determining step responsible for the change in the R and OCP values in the three stages observed in Section 6.4.3. For example, in the first stage, R increases, while the OCP shifts positively. The only way that

this can be achieved, as seen from the Evans diagram in Figure 6-10, is by a decrease in the rate of the anodic reaction (either by a change of the Tafel slope and/or exchange current density).

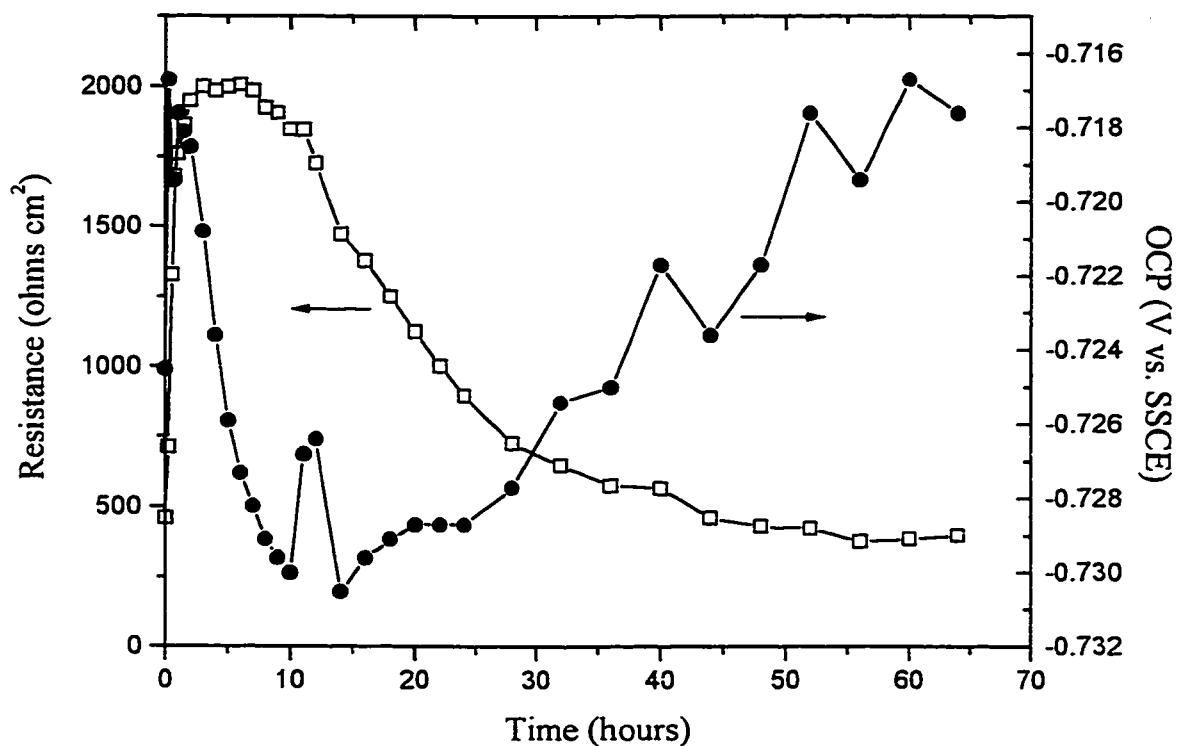


Figure 6-8. Change in the OCP and system resistance of a blank as a function of time.

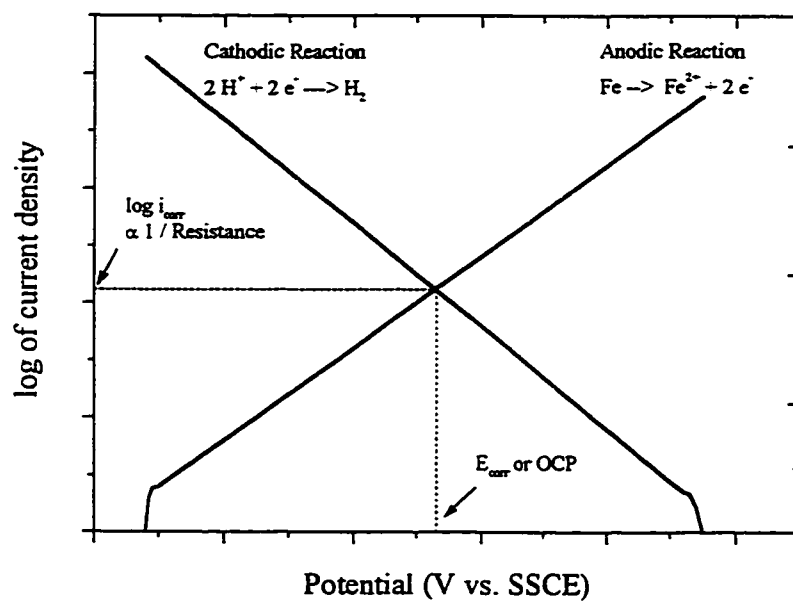


Figure 6-9. An illustration of an Evans diagram for a simple corrosion process.

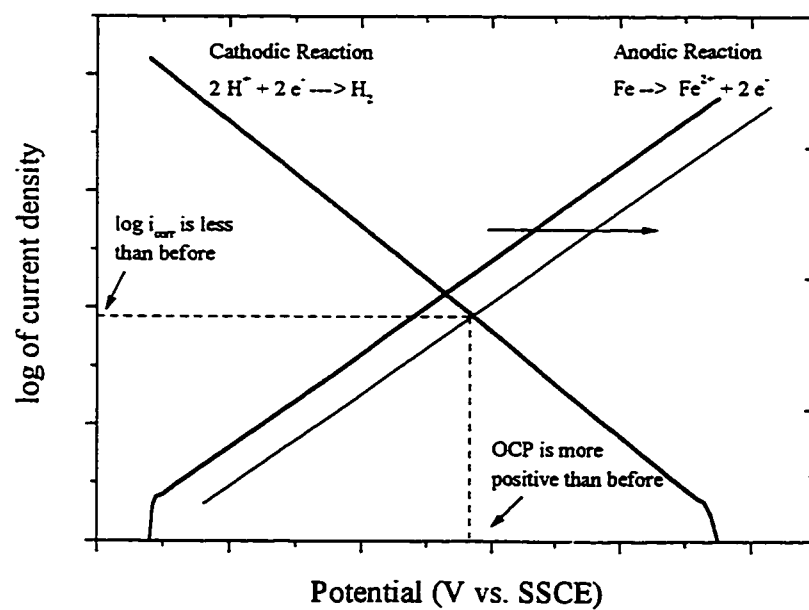


Figure 6-10. An illustration of the changes in an Evans diagram to fit the experimental observations.

Using similar logic, the three stages can be characterized as follows:

First stage: decrease of anodic reaction rate

It is possible that some corrosion product on the electrode surface formed at early times of immersion blocks some of the metal dissolution sites in this early stage and decreases the anodic reaction somewhat. The corrosion product was often seen as a black surface film, probably FeCO_3 and/or Fe_3O_4 [103].

Second stage: increase of anodic reaction rate

Since the thin film accumulated in the first stage may not be very protective in nature, it could break down, thus exposing the underlying metal surface with time, allowing it to dissolve. Another reason for this increase in the anodic reaction rate may be due to an initial delay in chloride ion penetration to the metal/oxide interface.

Third stage: increase of cathodic reaction rate

The thin film produced in the first stage not only can break down, but may also be thinned, which may increase the rate of the cathodic reaction by decreasing the electron transfer pathlength. Another explanation for this observation could be related to an increase in the amount of dissolved oxygen in the system after longer periods of experimentation, even though carbon dioxide was continuously purging the solution. Oxygen would also serve as an electron sink [eq. 2-2] and could therefore enhance the corrosion rate.

6.5 acZ Studies of Steel Specimen in NACE Brine Solution With Added Corrosion Inhibitor Formulation

The major differences between the acZ response of steel specimens in a NACE brine solution with and without the addition of formulated corrosion inhibitor (e.g., 50 μM Quat 7 with additives) were the development of a second time constant, the increase of the total system resistance and the absence of an inductance at low frequencies. The disappearance of an inductive loop at low frequencies with the addition of corrosion inhibitor has been reported by Altoé et al [2] in their work with carbon steel electrode in 1 % NaCl solution (see Section 2.1.4.1).

6.5.1 Development of two time constants

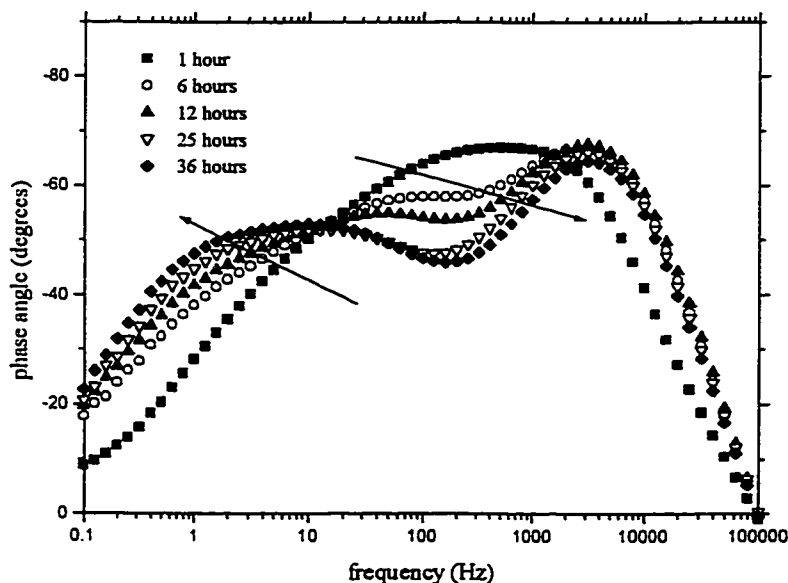


Figure 6-11. Typical set of impedance spectra observed for steel electrode as a function of time in CO_2 saturated NACE brine solution containing formulated corrosion inhibitors, ac V = ± 10 mV vs. OCP.

Figure 6-11 shows that two time constants were developed in the phase angle Bode plots as a function of electrode immersion time in inhibitor-containing solution. The presence of a second time constant required the use of a new equivalent circuit in order to fit the impedance data. A circuit involving two parallel R-CPE units in series did not seem to fit the data well. However, a modified Randles circuit, as shown in Figure 6-12, resulted in a good quality overlay of the experimental and calculated data. It should be noted that the addition of an inductor to the EC was no longer necessary to fit the data at low frequencies, suggesting that pitting was no longer a factor in this inhibitor-containing solution. However, despite the fact that the inductance at high frequencies could no longer be seen, the fit was much better when some of the high frequency data points (> 20 kHz) were removed (Figure 6-12). It should be noted that the cutting of high frequency data points did not cause any significant change in the values of the circuit elements. This implies that the instrumental artifact associated with high frequencies (as seen for the blanks) still existed, but to a much lesser extent in this higher resistance system. Nevertheless, the standard deviation of the fit in this particular data set ranged randomly from 0.65 to 1.3 % when the > 20 kHz data was taken out, signifying that the circuit shown in Figure 6-12 fit the data well throughout the time of experimentation.

6.5.2 Change in resistance with time

The solution resistance, R_s , remained at ca. 1Ω throughout this experiment (similar to the blanks, see Section 6.4.3). It should be noted that the total resistance, as

shown in Figure 6-13, is much higher than that of the blanks (Figure 6-6). Interestingly, Figure 6-13 shows that the change in film resistance, R_f (see the EC in Figure 6-12), with immersion time followed a very similar trend as did the change in the charge transfer resistance, R_{ct} , except that the R_f values were about 100x larger than R_{ct} . The sum of R_f and R_{ct} would be equivalent to R_p (see Section 2.2.1) in these experiments.

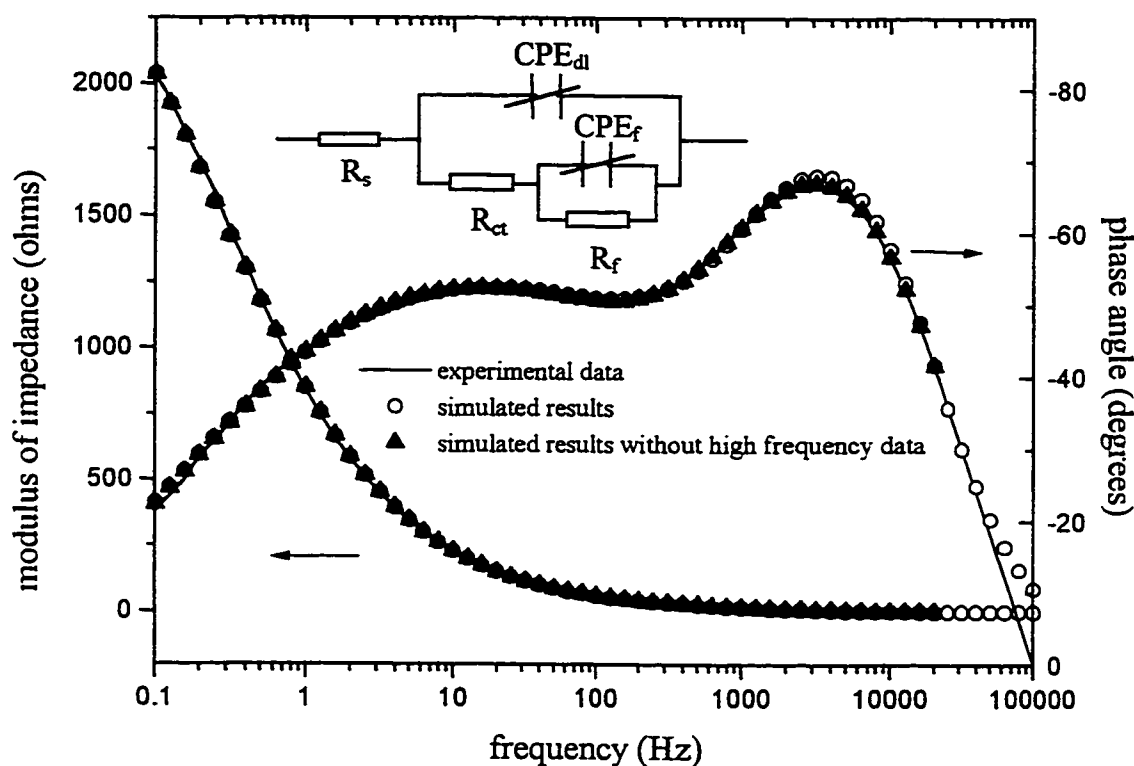


Figure 6-12. Overlay of acZ data of a steel specimen in CO_2 saturated NACE brine solution containing formulated inhibitor to a modified Randles circuit shown, ac $V = \pm 10$ mV vs. OCP.

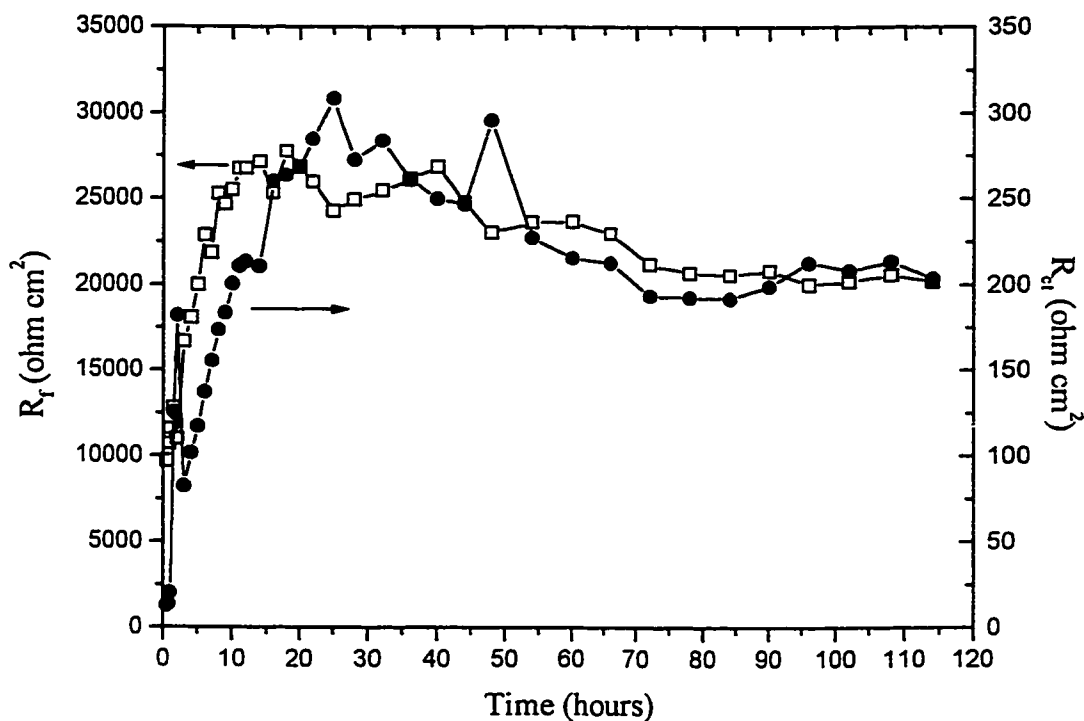


Figure 6-13. Change in the film and charge transfer resistance of a steel specimen in CO_2 saturated NACE brine solution containing formulated inhibitor as a function of time.

6.5.3 Change in CPEs with time

The CPE parallel to R_{ct} (see the EC in Figure 6-12) is termed the double layer capacitance, CPE_{dl} . The n value of this CPE was 0.96 ± 0.03 throughout the experiments, suggesting that it is close to an ideal capacitor. The changes in CPE_{dl} and its n values with immersion time are illustrated in Figure 6-14. It should be noted that the n value decreases with time, while the CPE_{dl} value increases. The decrease of the n value may indicate that the surface of the WE became less homogeneous with time [27], causing the

capacitor to deviate more from ideal ($n = 1$). The small value of CPE_{dl} probably implies that a relatively thick film is covering the electrode surface so that only a small area of metal is exposed to solution. The increase of CPE_{dl} with time suggests the penetration of the film to the metal via pores, which increase in size or number with time in solution.

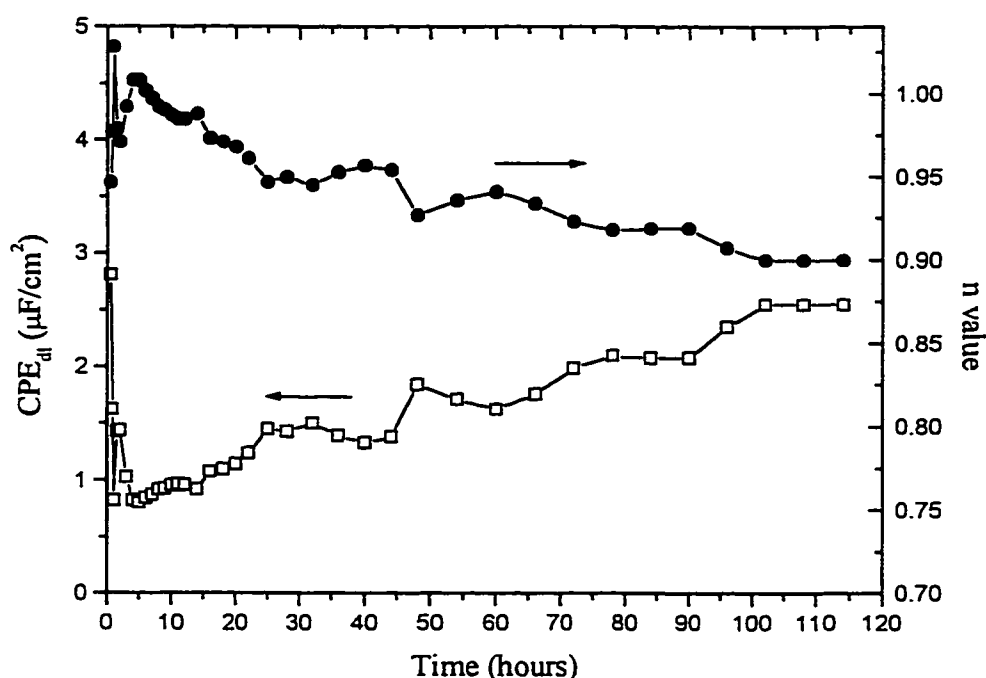


Figure 6-14. Change in CPE_{dl} and n value of a steel specimen in CO_2 saturated NACE brine solution containing formulated inhibitor as a function of time.

The n value of CPE_f was about 0.65 ± 0.05 , which is not uncommon for a CPE ascribed to a surface film [27]. The fact that the n value is much smaller than unity and close to 0.5 may suggest that a diffusion controlled process is involved in the reaction. It

should be noted that the impedance of a CPE is termed a Warburg impedance when the n value is equal to 0.5. It has been introduced to represent the impedance of a semi-infinite linear diffusion process, obeying Fick's law in the time regime [104]. The change in the CPE_f and its n value with immersion time is plotted in Figure 6-15. The fact that they both increase with time indicates that the system is becoming increasingly reactive. The values of this CPE should not be directly compared with capacitance values in this case, as the n values are significantly less than unity.

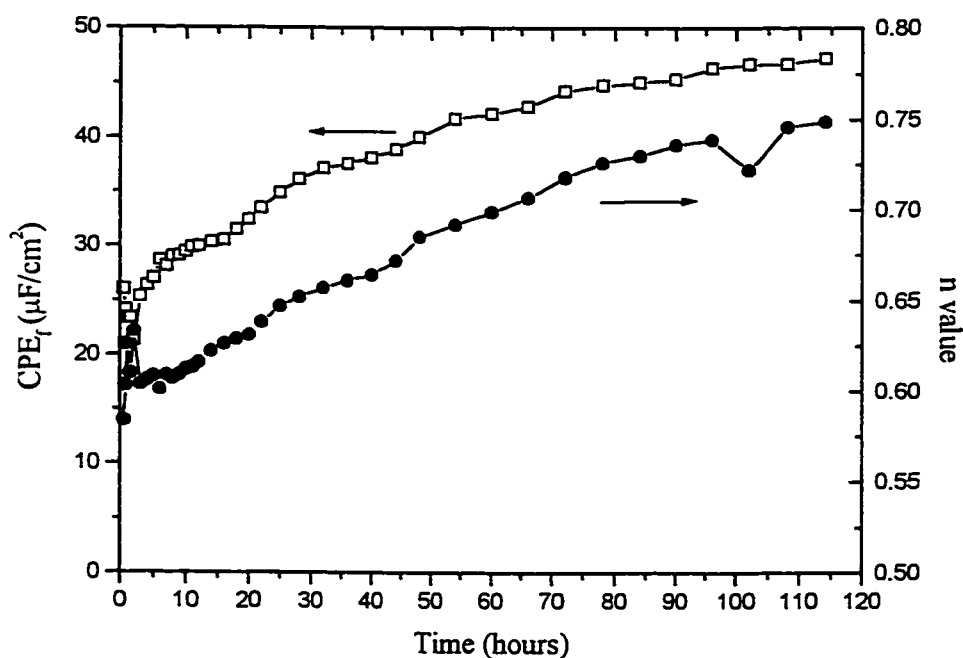


Figure 6-15. Change in CPE_f and its associated n value of a steel specimen in CO_2 saturated NACE brine solution containing formulated inhibitor as a function of time.

6.5.4 Change of OCP with time

Overall, the OCP shifted positively in the first hour, and then negatively with the passage of time when the electrode was exposed to the brine solution containing formulated corrosion inhibitor (50 μM Quat 7 with additives), as shown in Figure 6-16. In Figure 6-13, the total system resistance was seen to increase in the first 20 hours, and then decrease slightly. Therefore, three distinct stages of behaviour can be identified for these inhibitor- containing experiments:

First stage (ca. 0 to 1 hr) - R increases and OCP shifts positively.

Second stage (ca. 1 to 20 hrs) - R increases and OCP shifts negatively.

Third stage (ca. 20 to 120 hrs) - R decreases and OCP shifts negatively.

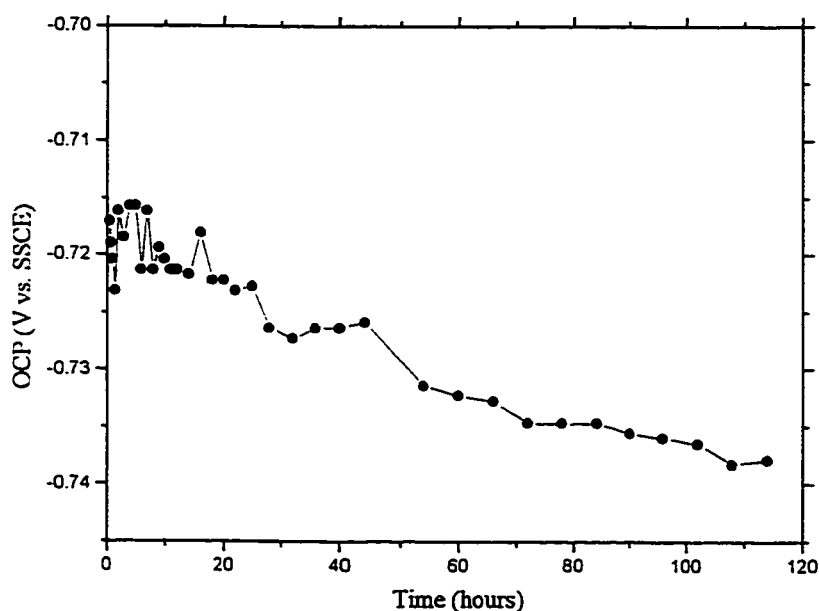


Figure 6-16. Change in the OCP of a steel specimen in CO_2 saturated NACE brine solution containing formulated inhibitor as a function of time.

6.5.5 Corrosion mechanisms of steel in NACE brine solution with added inhibitor formulation

An Evans diagram approach (Figures 6-9 and 6-10) was used again to analyze the impedance data and to attempt to establish a mechanism for the behaviour of steel in inhibitor-containing brine solution:

First stage: decrease of anodic reaction rate

The most likely dominating process at this stage is the adsorption of the inhibitor on the steel electrode surface. This blocks some of the surface sites and causes the rate of dissolution of Fe to decrease. Adsorption of inhibitor during this time is also supported by the decrease of CPE_{dl} .

Second stage: decrease of cathodic reaction rate

The Quats listed in Table 3-3 and studied in this chapter are commonly known as cathodic inhibitors. Their presence may increase the overpotential for the cathodic reaction and hence, lower the rate of the HER. The adsorption of the inhibitor during the first stage may also cause a decrease in the cathodic reaction rate in this stage by increasing the length of the pathway for electrons to react with protons or oxygen in solution.

Third stage: increase of anodic reaction rate

Since these Quats are normally added in a continuous mode in practice, their performance is expected to degrade with electrode immersion time in a corrosive environment. In this case, the increase of the anodic reaction rate at long times can be attributed to the increasing extent of breakdown of the inhibitor film with time of exposure to the brine solution.

6.5 Summary

The addition of individual components of the formulated corrosion inhibitor mixture showed that the additives increase the impedance (decreased the pitting current) of the carbon steel electrode to a much greater extent than did the addition of the Quats alone (even Quats 6 and 7) in sweet systems. These results led to the study of carbon steel electrodes in CO₂ saturated brine solution, with and without the addition of the complete inhibitor formulation, using CV and acZ methodologies.

The CV study of steel electrodes in brine solutions without added inhibitor formulation revealed a hysteresis response which is indicative of active pitting of the electrode surface. Correspondingly, the impedance measurements showed an inductive response at low frequencies. When a formulated corrosion inhibitor was added to solution, the hysteresis response and inductor disappeared, suggesting that pitting was prevented.

The analysis of the acZ data for the “blanks” suggests an initial buildup of corrosion product, possibly an iron carbonate and/or iron oxide film. With longer exposure times to solution, this film breaks down and the resistance of the system decreases. The impedance data was fitted using a $R_s (R_1 \text{ CPE } L)$ circuit.

The acZ study of systems containing the formulated corrosion inhibitor (e.g. 50 μM Quat 7 with additives) showed the rapid development of two time constants, an increase in the overall system resistance, and the absence of the low frequency inductor. Analysis of the acZ results suggests the initial adsorption of inhibitor on the electrode surface, which then inhibits the cathodic reaction of the corrosion process. This inhibitor film is relatively stable, but eventually breaks down with long times of exposure to the brine solution. These results suggest that Quats are cathodic inhibitors and that the mode of addition, in practice, should be continuous instead of batch.

VII. CONCLUSIONS AND RECOMMENDATIONS FOR FUTURE WORK

7.1 Conclusions

1. The eight Quats under study adsorb on Pt to differing extents, based on the degree of suppression of the Pt CV signal in 0.1 M NaOH solution, with all other variables kept constant. The results are consistent with parallel corrosion “wheel tests” using carbon steel specimens, carried out at Travis Chemicals Inc.
2. Quats 6 to 8, all containing a long hydrocarbon side chain at the *meta* position of the ring, show the highest degree of suppression of Pt electrochemistry. The extent of adsorption of Quat 6 or 8 is slightly greater than Quat 7 at Pt in phosphate buffer solution. The better adsorption may be caused by the electron-withdrawing amide functional group of Quats 6 and 8, which can make their pyridinium nitrogen slightly more electron deficient than that of Quat 7.
3. Based on concurrent CV and QCMB experiments in neutral phosphate buffer solution, the suppression of the Pt CV signal is shown conclusively to reflect the adsorption of Quat 7 on Pt. The electrode mass gain suggests that approximately one monolayer of adsorbed Quat 7 (3.0 to 3.8×10^{14} molecules cm^{-2}) is sufficient to block normal Pt electrochemistry. A further mass gain, which does not lead to any further suppression of the Pt CV signal, is seen with longer times. Based on

the mass gain with long time exposure to 40 μM Quat 7 containing solution, a bilayer structure of the adsorbed Quats is proposed.

4. All Quats are reducible at ca. -1.15 V vs. SSCE in neutral phosphate buffer solution and the reduced product deposits on Pt and GC electrode surfaces. A solution diffusion controlled process governs the rate of deposition in the early stage of the experiments. The reduced surface film can be oxidized at ca. -0.25 V vs. SSCE, with most of it re-dissolving into solution.
5. After holding at -1.5 V vs. SSCE for ca. 20 minutes, the high charge density ($4000\text{ }\mu\text{C}/\text{cm}^2$) in the oxidation peak suggests that approximately 25 monolayers of tightly packed product may be deposited on the GC electrode.
6. The reduction/oxidation of the Quats as a monomer is believed to be the dominant reaction from the study of Quat 6 at GC. However, other products may also form through dimerization and/or polymerization processes, especially at longer times of experimentation, when a non-oxidizable surface residue begins to form.
7. A study of the effect of the individual components of the formulated corrosion inhibitor mixture on carbon steel electrodes suggests that the additives (i.e., emulsifiers and surfactants) increase the impedance much more than do Quats alone in CO_2 saturated brine solution.

8. The acZ study of steel in the presence of formulated corrosion inhibitor in CO₂ saturated NACE brine solution shows that an adsorbed inhibitor film appears to deposit on the steel surface, as seen by the development of two time constants with time. The polarization resistance is about 50 times higher than that seen in the absence of corrosion inhibitor in the brine solution. The low frequency inductor and the hysteresis response of CV disappear when corrosion inhibitor formulation is added to the brine solution. The acZ analysis reveals that Quats are cathodic inhibitors and that the mode of addition should be continuous, in practice.
9. All Quats (other than Quats 6 to 8) show only weak adsorption at gold, platinum, glassy carbon and carbon steel electrodes. Based on the studies of the strongly adsorbed Quats on Pt, adsorption is preferred in basic > neutral > acidic solutions. Since adsorption appears to be independent of potential, it is not clear from this work if Quats prefer to adsorb on a metallic or an oxide-coated surface.

7.2 Recommendations For Future Work

1. Since Quats are believed to be cathodic inhibitors, the effect of the Quats on the rate of the hydrogen evolution reaction (HER) at various electrodes could also be used to study the coverage and strength of adhesion of these compounds in more detail.
2. The nature of the deposited products, which are formed primarily by the reduction of the Quats, should be examined using the QCMB technique. The products should also be analyzed using GC-MS and/or NMR to confirm their molecular structures.
3. An impedance study of carbon steel in H_2S saturated brine solution, with and without added Quats, may also show strong adsorption, possibly due to the interaction between the positively charged pyridinium nitrogen and the sulfur specie of the iron sulfide surface film.
4. The study of Quat adsorption at Pt or Au surfaces, at which a layer of sulfur or sulfide has been deposited, would also be of interest, as carbon steel, in practice, is expected to be coated with a FeS surface film in sour systems.

5. The use of scanning force/scanning tunneling microscopy at Pt, Au or GC electrode as a function of the nature of the Quat and its concentration, would also be of interest. It would be useful to establish whether Quats 6 and 7, in particular, adsorb preferentially at a metal, oxide-coated, sulfide-coated or carbon surface. Also, the orientation of the monolayer of Quats 6 and 7 should be established conclusively using this technique and/or with the aid of ellipsometry.
6. The adsorption process of the Quats at Pt could also be examined using optical second harmonic generation (SHG). An adsorption isotherm can be obtained, by varying the concentration of Quat in solution in separate experiments, so that the free energy of Quat adsorption can be determined. This technique may also reveal any dependency of adsorption with changing potential of the electrode.

REFERENCES

- 1 X. Mao, X. Liu and R.W. Reve, *Corrosion*. **50**, 9 (1994) 651.
- 2 P. Altoé, G. Pimenta, C.F. Moulin, S.L. Díaz and O.R. Mattos, *Electrochim. Acta*. **41** (1996) 1165.
- 3 S. M. Wilhelm and D. Abayarathna, *Corrosion*. **50**, 2 (1994) 152.
- 4 R.L. Martin and R.R. Annand, *Corrosion*. **36**, 5 (1981) 297.
- 5 A.S. Aricò, V. Antonucci, P.L. Antonucci, D.L. Cocke and N. Ciordano, *Electrochim. Acta*. **36** (1991) 581.
- 6 E.C. French, R.L. Martin and J.A. Dougherty, "Corrosion and its inhibition in oil and gas wells". *Corrosion /89*. Paper no. 435.
- 7 L.W. Jones, Corrosion and Water Technology for Petroleum Producers, OGCI Publications, Oklahoma, 1988.
- 8 P. Li, T.C. Tan and J.Y. Lee, *Corrosion*. **53** (1997) 186.
- 9 A. Srhiri, M. Etman and F. Dabosi, *Electrochim. Acta*. **41** (1996) 429.
- 10 P. Li, J.Y. Lin, K.L. Tan and J.Y. Lee, *Electrochim. Acta*. **42** (1997) 605.
- 11 R. Raicheff, I. Betova, M. Bojinov and E. Lazarova, *Modelling Aqueous Corrosion*. (1994) 89.
- 12 NACE Glossary of Corrosion Terms, *Materials Protection*. **4**, 1 (1965).
- 13 I. Betova, G. Neykov, R. Raicheff and E. Lazarova, *Langmuir*. **9** (1993) 3452.
- 14 J.M. West, Basic Corrosion and Oxidation, Ellis Horwood Limited, England, 1980.
- 15 R.A.D. Cintio and G.D. Carolis, *Corrosion prevention and control*. **40**, 5 (1993) 104.
- 16 B.G. Clublely, Chemical Inhibitors for Corrosion Control, Royal Society of Chemistry, 1990, p.2 to 5.
- 17 S. Ramachandran, B-L Tsai, M. Blanco, H. Chen, Y. Tang and W.A. Goddard, *Langmuir*. **12** (1996) 6419.
- 18 D.W. Hairston, *Chem. Eng.* **103**, 3 (1996) 65.
from ref. [17].
- 19 R. Zanneti, *Chem. Eng.* **97**, 5 (1990) 5.
from ref. [17].
- 20 ISSN 1091-8213. The 193rd meeting of the Electrochemical Society, Inc. Meeting Abstracts. Volume 98-1. Abstract 110, 111, 113 – 117, 1998.

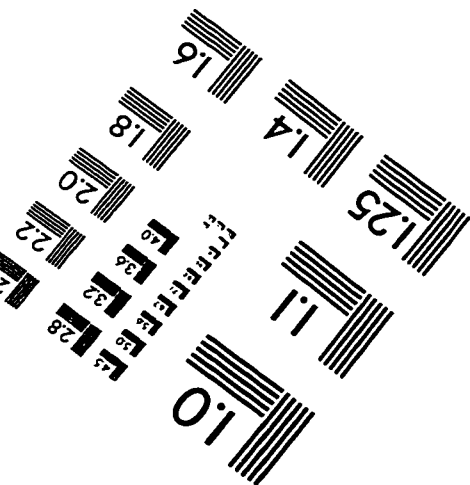
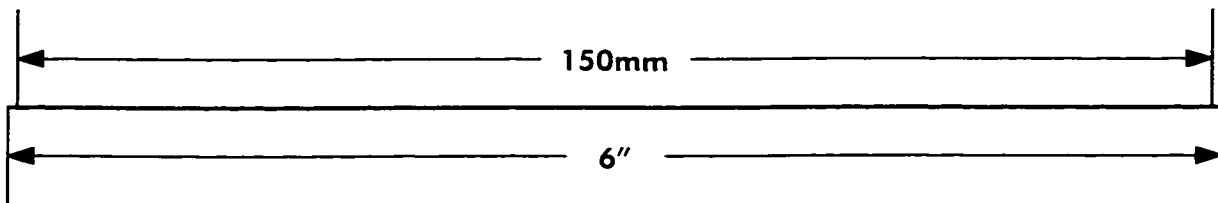
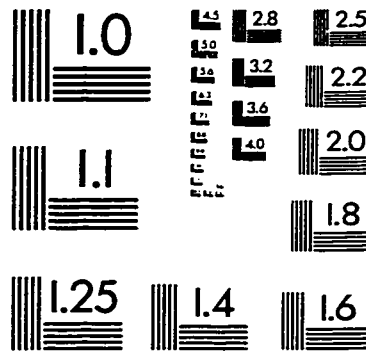
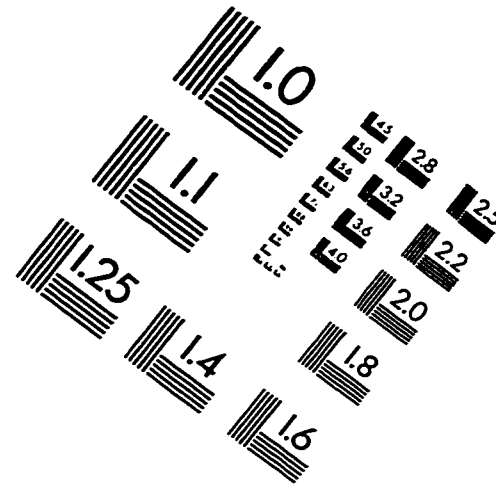
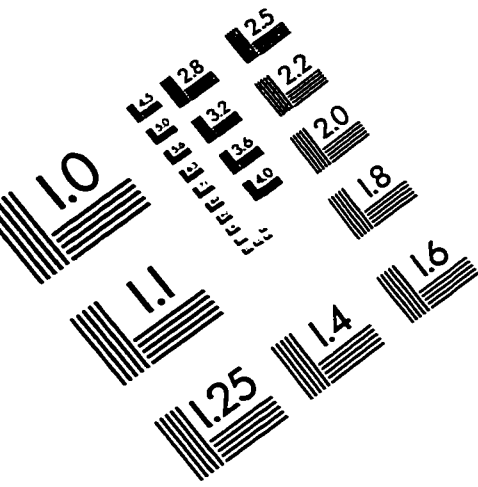
-
- 21 ISSN 1091-8213. The 193rd meeting of the Electrochemical Society, Inc. Meeting Abstracts. Volume 98-1. Abstract 118, 120 – 123, 1998.
 - 22 L.I. Antropov, I.S. Pogrebova and G. I. Dremova, *Prot. Met.* **7** (1971) 1.
 - 23 J. Cossar, Development of Chemical Inhibitors for Extremely Corrosive Environments, NRC/IRAP RDA Project Reference 25500U-D2-18, section 2, 1997.
 - 24 M. Elachouri, M.S. Hajji, S. Kertit, E.M. Essassi, M. Salem and R. Coudert, *Corrosion Science*. **37**, 3 (1995) 381.
 - 25 S. Kertit, J. Aride, A. Srhiri, A. Ben-Bachir and M. Etman, *J. Appl. Electrochem.* **23** (1993) 1132.
from ref. [24].
 - 26 H. Malik, *Corrosion*. **51**, 4 (1995) 321.
 - 27 A. Popova, S. Raicheva, E. Sokolova and M. Christov, *Langmuir*. **12** (1996) 2083.
 - 28 B. Yang, N. Smart and J. O'M. Bockris. *Electrochim. Acta*. **37**, 2 (1992) 317.
 - 29 J.O'M. Bockris and B. Yang, *Electrochim. Acta*. **36**, 8 (1991) 1333.
 - 30 G. Zilberman, V. Tsionsky and E. Gileadi, *Can. J. Chem.* **75** (1997) 1674.
 - 31 A. Czerwiński, S. Zamponi, J. Sobkowski and R. Marassi, *Electrochim. Acta*. **35**, 3 (1990) 591.
 - 32 C.P. Wilde and T. Ding, *J. Electroanal. Chem.* **327** (1992) 279.
 - 33 C.P. Wilde and D. Pisharodi, *J. Electroanal. Chem.* **398** (1995) 143.
 - 34 D. Kouznetsov, A. Sugier, F. Ropital and C. Fiaud, *Electrochim. Acta*. **40**, 10 (1995) 1513.
 - 35 J. Wang, M. Jiang and F. Lu, *J. Electroanal. Chem.* **444** (1998) 127.
 - 36 F. Kusu, K. Yuasa and K. Takamura, *Anal. Chem.* **9** (1993) 583.
 - 37 J. Volke, J. Urban and V. Volkeová, *Electrochim. Acta*. **39**, 13 (1994) 2049.
 - 38 J.O'M. Bockris, Surface Electrochemistry, Plenum, New York, 1993.
 - 39 M. Stern and A.L. Geary, *J. Electrochem. Soc.* **104** (1957) 56.
from ref. [38].
 - 40 C. Andrade, L. Soler, C. Alonso, X.R. Nóvoa and M. Keddam, *Corrosion Science*. **37**, 12 (1995) 2013.
 - 41 ZView for Windows, Operating Manual, version 2.0. Scribner Associates Inc. Virginia. 1997.
 - 42 P. Vanýsek, "Introduction to electrochemical impedance", an internal report from his sabbatical leave at the University of Calgary, 1994.

-
- 43 H. Dinh, Ph.D. Diss. The University of Calgary, September 1998.
- 44 C. Bock, Ph.D. Diss. The University of Calgary, April 1997.
- 45 J.E.B. Randles, *Trans. Faraday Soc.* **44** (1948) 327.
from ref. [42].
- 46 R. Yue, M.S. Thesis. The University of Calgary, April 1997.
- 47 D. Johnson's email, a response to technical questions of the ZView software, 1997.
- 48 J.S. Gordon, *J. Electroanal. Chem.* **365** (1994) 267.
- 49 G. Z. Sauerbrey, *Z. Phys.* **155** (1959) 206
from ref. [48].
- 50 M.M. Ficquelmont-Loizos, H. Takenouti and W. Kante, *J. Electroanal. Chem.* **428** (1997) 129-140.
- 51 A.M.O. Brett and F.M. Matysik, *J. Electroanal. Chem.* **429** (1997) 95-99.
- 52 D.R. Lide, *CRC Handbook of Chemistry and Physics*, 71st edition, CRC Press, Boca Raton, 1990.
- 53 *Annual Book of ASTM Standards*, section 11, Water and Environmental Technology, volume 11.02, 1993.
- 54 L. Stolberg, J. Richer, J. Lipkowski and D.E. Irish, *J. Electroanal. Chem.* **207** (1986) 213.
- 55 D. Bizzotto, A. McAlees, J. Lipkowski and R. McCrindle, *Langmuir* **11** (1995) 3243.
- 56 M.M. Gómez, M.P. García, J.S. Fabián, L. Vázquez, R.C. Salvarezza and A.J. Arvia, *Langmuir* **12** (1996) 818.
- 57 M.M. Gómez, M.P. García, J.S. Fabián, L. Vázquez, R.C. Salvarezza and A.J. Arvia, *Langmuir* **13** (1997) 1317.
- 58 K.L. Hanrahan, S.M. MacDonald and S.G. Roscoe, *Electrochim. Acta.* **41**, 15 (1996) 2469.
- 59 S.G. Roscoe, K.L. Fuller and G. Robitaille, *J. Colloid and Interface Science* **160** (1993) 243.
- 60 P. Zelenay and J. Sobkowski, *Electrochim. Acta.* **29**, 12 (1984) 1715.
- 61 J.F.E. Gootzen, W. Visscher and J.A.R. van Veen, *Langmuir* **12** (1996) 5076.
- 62 M.T.M. Koper, M. Hachkar and B. Beden, *J. Chem. Soc. Faraday Trans.* **92**, 20 (1996) 3975.
- 63 E.K. Krauskopf and A. Wieckowski, *J. Electroanal. Chem.* **271** (1989) 295.
- 64 J. Sobkowski, P. Waszczuk and P. Zelenay, *Russian Journal of Electrochemistry* **31**, 8 (1995) 850.

-
- 65 D.F. Yang, C.P. Wilde and M. Morin, *Langmuir* **12** (1996) 6570.
- 66 Y.J. Lee, I.C. Jeon, W. Paik and K. Kim, *Langmuir* **12** (1996) 5830.
- 67 M. Kunitake, Y. Narikiyo, O. Manabe and N. Nakashima, *J. Materials Science* **30** (1995) 2338.
- 68 I.O. Efimov and K.E. Heusler, *J. Electroanal. Chem.* **414** (1996) 75.
- 69 Y. Lim and E. Hwang, *Bull. Korean Chem. Soc.* **18**, 1 (1997) 6.
- 70 S. Morin, B.E. Conway, G.J. Edens and M.J. Weaver, *J. Electroanal. Chem.* **421** (1997) 213.
- 71 H. Angerstein-Kozłowska, B.E. Conway and W.B.A. Sharp, *Electroanalytical Chemistry and Interfacial Electrochemistry* **43** (1973) 9.
- 72 A. H. Lanyon and B.M.W. Trapnell, *Proc. Roy Soc.* **227A** (1995) 387.
from ref. [38].
- 73 A. K. Reddy, M.A. Genshaw and J.O. Bockris, *J. Chem. Phys.* **93** (1990) 8361.
from ref. [38].
- 74 T. Takamura and K. Takamura, *J. Electroanal. Chem.* **39** (1972) 478.
- 75 M. Weber and F.C. Nart, *Electrochim. Acta.* **41**, 5 (1996) 653.
- 76 A.J. Bard and L.R. Faulkner, Electrochemical Methods, Fundamentals and Applications, John Wiley & Sons Inc, N.Y. 1980.
- 77 S. Dong, Y. Zhu and G. Cheung, *Langmuir* **7** (1991) 389.
- 78 S.H. Pine, Organic Chemistry, 5th edition, McGraw-Hill Book company, N.Y. 1987.
- 79 Y. Wang, J. Zhang, G. Zhu and E. Wang, *J. Electroanal. Chem.* **419** (1996) 1-6.
- 80 R. L. McCreery, Carbon electrodes, editor A. J. Bard, Electroanalytical Chemistry, vol 17 (1991).
- 81 P. Heiduschka, A. W. Munz and W. Gopel, *Electrochim. Acta.* **39**, 14 (1994) 2207.
- 82 H.P. Dai and K.K. Shiu, *J. Electroanal. Chem.*, **419** (1996) 7-14.
- 83 M. T. McDermott, C. A. McDermott and R. L. McCreery, *Anal. Chem.* **65**, 7 (1993) 937.
- 84 V.I. Birss, S. Guha-Thakurta, C.E. McGarvey, S. Quach and P. Vanýsek, *J. Electroanal. Chem.* **423** (1997) 13.
- 85 D.C. Harris, Quantitative Chemical Analysis, 3rd edition, W.H. Freeman and Company, New York, 1991.
- 86 M.A. Rahman and A.K. Ghosh, *J. Colloid Interface Sci.* **77** (1980) 50.

-
- 87 B. Persson, Thesis, Lund, 1990.
from ref. [38].
- 88 S. Sampath and O. Lev, *J. Electroanal. Chem.* **446** (1998) 57.
- 89 J. Volke, L. Dunsch, V. Volkeová, A. Petr, and J. Urban, *Electrochim. Acta.* **42**, 12 (1997) 1771.
- 90 K. Dang, personal communication, The University of Calgary, July 1998.
- 91 E.A. Charles and R.N. Parkins, *Corrosion.* **51**, 7 (1995) 518.
- 92 A. Dugstad, L. Lunde and K. Videm, "Parametric study of CO₂ corrosion of carbon steel". Corrosion / 94. Paper no. 14.
- 93 A.K. Dunlop, H.L. Hassell and P.R. Rhodes, "Fundamental considerations in sweet gas well corrosion". Corrosion / 83. Paper no. 46.
- 94 L. Gray, "Effect of pH and temperature on the mechanism of carbon steel corrosion by aqueous carbon dioxide". Corrosion / 90. Paper no. 40.
- 95 N.N. Bich, "Electrochemical evaluation of corrosion inhibitors for sour gas and oil production and water injection", Materials performance: sulphur and energy, (1989) 17.
- 96 J.M. Blengino, M. Keddam, J.P. Labbe and L. Robbiola, *Corrosion science.* **37**, 4 (1995) 621.
- 97 M. Al-Sayed, Ph.D. Diss. Corrosion and Protection Centre, UMIST, 1989.
from ref. [26].
- 98 Z. Xia, C. Chou and Z. S. Smialowska, *Corrosion.* **45**, 8 (1989) 636.
from ref. [26].
- 99 K. Videm and A. Dugstad, "Corrosion of Carbon Steel in an Aqueous Carbon Dioxide Environment. Part 1: Solution Effects". Environment Treatment & Control. 1989.
- 100 J. R. Macdonald, editor, Impedance Spectroscopy Emphasizing Solid Materials and Systems, John Wiley & Sons, New York, 1987.
- 101 P. L. Bonora, F. Deflorian and L. Fedrizzi, *Electrochim. Acta.* **41** (1996) 1073.
- 102 U.R. Evans, An Introduction to Metallic Corrosion, Arnold, London, 1963.
from ref. [38].
- 103 U. Lotz, L. van Bodegon, and C. Ouwehand, *Corrosion.* **47** (1991) 635.
from ref. [2].
- 104 E. Warburg, *Ann. Phys. Chem.* **67** (1899) 493.
from ref. [42].

IMAGE EVALUATION TEST TARGET (QA-3)



APPLIED IMAGE, Inc.
1653 East Main Street
Rochester, NY 14609 USA
Phone: 716/482-0300
Fax: 716/288-5989

© 1993, Applied Image, Inc., All Rights Reserved

